DALIA BUIVYDIENĖ

FORMATION OF FIBROUS MATERIALS FOR AIR FILTRATION APPLICATIONS VIA MELT ELECTROSPINNING

DOCTORAL DISSERTATION

Kaunas
2020

KAUNAS UNIVERSITY OF TECHNOLOGY

DALIA BUIVYDIENĖ

FORMATION OF FIBROUS MATERIALS FOR AIR FILTRATION APPLICATIONS VIA MELT ELECTROSPINNING

Doctoral Dissertation
Technological Sciences, Environmental Engineering (T 004)

2020, Kaunas

This doctoral dissertation was prepared at Kaunas University of Technology, Faculty of Chemical Technology, Department of Environmental Technology, during the period of 2015–2019. The studies were supported by the Research Council of Lithuania.

Scientific Supervisor:

Prof. dr. Linas KLIUČININKAS (Kaunas University of Technology, Technological Sciences, Environmental Engineering, T 004).

This doctoral dissertation has been published at:
http://ktu.edu

Editor:

Armandas Rumšas (Publishing Office “Technologija”)

KAUNO TECHNOLOGIJOS UNIVERSITETAS

DALIA BUIVYDIENĖ

PLUOŠTINIŲ MEDŽIAGŲ FORMAVIMAS LYDALO ELEKTROVERPIMO METODU IR JŲ TAIKYMAS ORO FILTRAVIMUI

Daktaro disertacija
Technologijos mokslai, Aplinkos inžinerija (T 004)

2020, Kaunas

Disertacija rengta 2015-2019 metais Kauno technologijos universitete, Cheminės technologijos fakultete, Aplinkosaugos technologijos katedroje. Mokslinius tyrimus rėmė Lietuvos mokslo taryba.

Mokslinis vadovas:

Prof. dr. Linas KLIUČININKAS (Kauno technologijos universitetas, technologijos mokslai, aplinkos inžinerija, T 004).

Interneto svetainės, kurioje skelbiama disertacija, adresas:
http://ktu.edu

Redagavo:

Armandas Rumšas (Leidykla „Technologija“)

ACKNOWLEDGEMENTS

To my husband and son. Without you, it probably would've been faster, but not as fun.

To my huge extended family and friends. Thank you for challenging me and being there whenever I needed you.

You all helped me to grow.

Table of Contents

List of Tables 8
List of Figures 9
List of Appendices 11
List of Abbreviations 12
Introduction 13
1. LITERATURE REVIEW 16
1.1. Air pollution 16
1.1.1. Current situation and problems 16
1.1.2. Particulate matter 19
1.2. Theoretical background of air filtration 20
1.2.1. Parameters of non-woven fibrous filters 22
1.2.2. Standardization of filter efficiency 23
1.3. Fibrous filters 24
1.3.1. Microfibre filters 25
1.3.2. Nanofibrous filters 26
1.3.3. Hierarchically structured/mixed media filters 26
1.4. Introduction to electrospinning 27
1.4.1. Basic principle 28
1.4.2. Solution electrospinning 30
1.4.3. Melt electrospinning 30
1.4.4. Electrospinning for filtration applications 34
1.5. Summary of literature review 35
2. METHODS AND MEASUREMENTS 36
2.1. Preparation of Fibrous Material 36
2.1.1. Materials in Use 36
2.1.2. Melt electrospinning 37
2.1.3. Combined electrospinning 38
2.1.4. Experiment I 39
2.1.5. Experiment II 40
2.1.6. Experiment III 40
2.2. Mat characterization 42

2.3. Testing of filtration efficiency 43
2.3.1. Experiment II 43
2.3.2. Experiment III 44
2.4. Characterization of filter media 45
2.5. Quality assurance 45
3. RESULTS AND DISCUSSION 46
3.1. Primary Melt Electrospinning Parameter Testing (Experiment I) 46
3.1.1. Fibre formation by customized electrospinning setup 46
3.1.2. Distribution of fibre diameter 47
3.1.3. Impact of process parameters on fibre diameter 49
3.1.4. Optimization of melt electrospinning parameters 51
3.2. Characterization of air filter material printed by melt electrospinning (Experiment II) 53
3.2.1. Morphology of filter mats 53
3.2.2. Fibre diameter distribution 56
3.2.3. Effects of process parameters on fibre diameter 57
3.2.4. Filtration performance 58
3.3. Multi-layered air filter formation: melt/solution electrospinning for micro/nano fibrous material (Experiment III) 64
3.3.1. Mat morphology and characterization 64
3.3.2. Filtration efficiency and quality factor 67
4. Conclusions 74
5. References 76

List of Tables

Table 1. Health effects associated with indoor air pollutants 17
Table 2. Summary of research on melt electrospinning 32
Table 3. List of polymers used for melt electrospinning 36
Table 4. Electrospinning parameters and process combinations for combined electrospinning 41
Table 5. Experimental process parameters and obtained fibre diameter values 48
Table 6. Input process parameters and obtained fibre diameter values of the reproduced screening experiment 51
Table 7. Summary of filtration performance data of polymer A mats passing ePM1, min ≥ 50% 59
Table 8. Parameters of formed fibre mats 66
Table 9. Filtration efficiencies for different PM fractions for the produced fibre mats based on different methods 69
Table 10. Pressure drop, average filtration efficiencies and quality factors for tested mats 72

List of Figures

Figure 1. A hypothetical mixed particle distribution [4] 19
Figure 2. Main fibrous filters air filtration mechanisms: a) The main filter mechanisms of fibre material [54]; b) Filtration efficiency for individual single-fibre mechanisms and total efficiency. c) Different filtering effects on the particle size [55] 20
Figure 3. Basic scheme of electrospinning.....28
Figure 4. Schematics of fibre printing melt electrospinning apparatus.....38
Figure 5. Schematics of combined melt electrospinning and solution electrospinning apparatus 39
Figure 6. Schematic of fibre count 42
Figure 7. experimental set-up for filtration efficiency and pressure drop measurements 43
Figure 8. The experimental set-ups for filtration efficiency and pressure drop measurements (S1 – small NaCl particles; S2 – large KCl particles) 45
Figure 9. Microscopic pictures of the produced fibre membranes (scale bar – 5mm): 47
Figure 10. Stereomicroscopy images and fibre diameter histograms (magnification ×1000): A – N6; B – N1; C – N16; D – N10 49
Figure 11. Different parameter effect on fibre diameter (A – Tip to Collector distance; B – Voltage; C – Temperature 50
Figure 12. Response-surface plot of process parameters for production of fibres with the desired fibre diameters (fibre diameter, μm, is represented by different colours).....51
Figure 13. SEM images of repeated samples with rotating drum (A – N8_II; B – N11_II; C – N12_II; D – N14_II) 52
Figure 14. SEM image of polymer mat prepared with optimized conditions .53
Figure 15. SEM images of typical morphologies (A - disperse (N9D); B - ribbon (N7B); C - parallel (N25E); D - normal (N4A); E - supressed whipping (N8A); F - glued (N3C).....54
Figure 16. Fibre diameter distributions of melt electrospun mats obtained from various polymers (A - Vestamid™ L 1600; B - Vestamid™ L 1901; C - Arnitel® 3106; D - Rilsamid® AMN 0 TLD; E - Pebax® 35R53 SP 01) 56
Figure 17. Effects of melt electrospinning parameters on the fibre diameter, μm (A - median; B - IQR) 58
Figure 18. Filtration efficiencies for N4A and N5A filter media compared to F7 filter (positive error bar indicates initial efficiency, negative indicates minimum efficiency after charge neutralization).....60
Figure 19. ePM1 dependency on fibre diameter (A - median; B - IQR).....61
Figure 20. Effects of base mass (A) and packing density (B) on ePM1.....62
Figure 21. Effects of IQR of fibre diameter (A) and packing density (B) on pressure drop 63

Figure 22. Relationship between filtration efficiency (ePM1) and pressure drop 63
Figure 23. SEM images of fibre surfaces with different process combinations at magnification x1000 (A – M; B – M_MS_M; C – MS; D – S).....65
Figure 24. Cross sections of fibre mats (without supporting layer): (I) feed rate – 0.6 g/h, tip to collector distance – 50 mm; (II) feed rate – 1.8 g/h, tip to collector distance – 50 mm; (III) feed rate – 0.6 g/h, tip to collector distance – 70 mm.....67
Figure 25. Particle trapping efficiencies of fibre mats fabricated by various formation methods (dotted line represents solution electrospinning filtration efficiency).....68
Figure 26. Filtration efficiencies of "without discharge" and "discharged" fibrous mats at Most Penetrating Particle Size.....71
Figure 27. The relationship between porosity and pressure drop of tested mats 72
Figure 28. The relationship between filtration efficiency (ePM_1) and pressure drop of mats.....73
Figure 29. Fibre ratio (sub- vs super- micrometre as nm:μm) effect on filtration efficiency.....74

List of Appendices

Appendix 1. Technical properties of polymers used in melt electrospinning ..93
Appendix 2. Fibre size parameters and morphologies of formed mats. 96
Appendix 3. List of scientific publications 99

List of Abbreviations

AED – aerodynamic equivalent diameter
ePM_x – filtration efficiency for a certain size of particle material
ESPs – electrostatic precipitators
HEPA – high efficiency particulate air filters
HVAC – heating, ventilating, and air-conditioning system
IQR – interquartile range
ME – Melt Electrospinning
MFR – Melt Flow Rate
MPPS – most penetrating particle size
OPS – Optical Particle Sizer
PCL – polycaprolactone
PEEK – poly(ether ether ketone)
PEG_{47}-b-PCL_{95} – poly(ethylene glycol)-block-poly(3-caprolactone)
PHB – polyhydroxybutyrate
PLLA – poly(L-lactic acid)
PM – particulate matter
PMIA – poly(m-phenylene isophthalamide)
PP - polypropylene
QF – quality factor
SE – solution electrospinning
SMPS – Scanning Mobility Particle Sizer
SrBG – strontium-substituted bio-active glass
TtCD – Tip-to-Collector Distance
VOCs – volatile organic compounds
WHO – World Health Organization

Introduction

The association between the concentration of the airborne particulate matter (PM) and its adverse effects on human health has been thoroughly established in the recent decades [1–4]. The size of particles is of importance, thus, size classes of PM_{10}, $PM_{2.5}$, and PM_1 have been established in order to reflect the negative effects on health. Smaller particles are associated with more pronounced adverse health effects owing to their higher penetration and deposition efficiencies in lung alveoli and their overall higher toxicity [5–9]. Not only the respiratory system but also skin contact [10–13] might be a pathway for nanoparticles to an organism. Because of that, it is important to look for solutions regarding particle removal in order to avoid potential health risks.

Air filters serve as the most robust and well-established technology for removing particles from air. Filters are installed as standard equipment for use in heating, ventilating and air-conditioning systems in order to improve the indoor air quality by controlling indoor particulate matter from both indoor and outdoor sources [4,5,8,14–16].

Non-woven fibrous media have been extensively used in air filtration applications. This type of filter manufacturing technology includes the synthesis of the filter material by means of melt-blown, melt-spun, wet-laid, and various other techniques. Electrospun filtration materials are relatively new, but they are being considered as a promising alternative to the currently well-established technologies owing to their high filtration efficiency at a relatively low basic weight compared to the traditional air filtration media because of their small fibre diameters, which results in a high surface area-to-volume ratio, high porosity, an interconnected pore structure, and a controllable fibre diameter [5,17–19].

Melt electrospinning is an emerging technique that is capable of spinning polymers from their melts thus avoiding the undesirable consequences of solvent use. Moreover, applications in filter material manufacturing are still limited at present, mostly owing to the insufficient capability of producing small-diameter fibres compared to solution electrospinning [5,20,21].

Mixed micro and sub-micro-sized fibre materials are gaining attention in the fields of energy and the environment, particularly for air filter and fluid membrane applications [22–24]. High-durability filters or membranes with a high surface area and a low pressure drop are essential for such applications. Synthesizing nanofibres is one of the methods used to address these issues, which is becoming increasingly common. This strategy has been proven to increase the performance of the air filter by allowing a higher surface area in order to trap more dust particles and by introducing the presence of the slip flow at the same time [18,23,25]. As nanofibres create high-density filters, the pressure drop may increase rapidly even despite the presence of the slip flow phenomena. The combination of submicron-sized fibres and nanofibres should decrease the density of fibrous media [23,26].

While information on the mixed nano-submicron and supermicron media filters is quite limited, we believe that it is a promising path for the further development of air filtration. For that reason, we have created a novel technique of combined

electrospinning which utilizes both solution and melt electrospinning. Such a method allows simultaneous formation of nano-submicron and supermicron-sized fibres and could be a new direction on the way to achieve high filtration efficiency with a low air pressure drop.

Aim of the doctoral thesis

To develop novel melt electrospun fibrous structures, test their suitability for air filtration applications, and optimize the process parameters.

Objectives

- To determine the main variables affecting the process of melt electrospun fibre formation and optimize the fibre formation parameters.
- To form melt electrospun fibrous materials and test the filtration properties of the produced fibre mats.
- To design a prototype fibre formation apparatus based on combined melt and solution electrospinning principles.
- To manufacture fibrous materials by combining melt and solution electrospinning, to compare the morphology and filtration efficiencies of the produced structures.
- To determine the pressure drop and estimate the filtration quality factors for the produced fibrous mats.

Scientific novelty

A novel method for fibrous media formation when melt and solution electrospinning are being simultaneously applied with an objective to form mixed size fibres has been developed. The filtration properties of these novel structures for different PM size classes in several model systems have been tested thus providing new knowledge on the filtration properties of such filter media.

Structure of the dissertation

This doctoral thesis consists of the following chapters: introduction, literature review, materials and methods, results and discussion, conclusions, reference list, publication list, and three appendices. The thesis comprises 103 pages, including 29 figures, 10 tables, and 3 appendices.

Publication of the research results

Two original research articles based on the research presented in this thesis have been published in international journals registered in the *CA Web of Science* database. One more manuscript has been submitted. The experimental results have been presented at five international conferences.

Practical value of the work

The novel morphology of a composite supermicron and nano-submicron structured fibrous material provides technologically and environmentally favorable opportunities to achieve superior air filtration properties. The presented work is aimed at the demonstration of the technological feasibility of the developed fibrous materials. This research corresponds to level 3 of the *Technology Readiness Level*. Small-scale production can already be applied in personalized, low-capacity treatment plants for air quality improvement. Nevertheless, the scaling-up of the production of such filter media still poses a major research challenge. Possible applications of this research are being discussed with air filter manufacturers.

Author's contribution

The data and results presented and discussed in the third chapter of this doctoral thesis were originally obtained and analyzed by the author. The research was carried out in 3 consecutive experiments resulting in three research articles.

In Experiment #1, optimization (D-optimal) of melt electrospinning parameters was performed. The author designed and conducted all the fibre formation experiments, performed data analysis, and prepared the manuscript for publication.

In Experiment #2, optimization (D-optimal-interaction) was performed for the parameters left out in Experiment #1. In order to select the most suitable air filtration parameters, four additional polymers for fibre formation were introduced. In the second set of experiments, the author conducted the formation of melt electrospun fibrous materials, performed hot-pressing, applied the electrostatic discharge, and tested the filtration efficiency as well as the pressure drop. Based on the analysis of the experimental data, the author prepared the manuscript for publication.

In Experiment #3, combined melt and solution electrospinning methods were applied thus providing fibre mats with mixed nano-, sub- and super- micron structures. The author designed the system for combined electrospinning, designed and conducted mat formation experiments, tested the filtration efficiency as well as the pressure drop, performed data analysis and prepared the manuscript for publication. The filtration efficiency and pressure drop testing was performed by the author at the *Institute for Energy and Environmental Technology* (IUTA), Duisburg, Germany.

The published manuscripts of the research articles were prepared by the author under professional guidance of the supervisor and the co-authors.

1. LITERATURE REVIEW

1.1. Air pollution

Pollution is one of the most significant environmental causes of disease and premature death in the world today. Diseases caused by pollution were responsible for an estimated 9 million premature deaths in 2015 – 16% of all the deaths worldwide, which is three times more deaths than from AIDS, tuberculosis, and malaria combined and 15 times more than from all the wars and other forms of violence. In the most severely affected countries, pollution-related disease is responsible for more than one death in four [27]. Air pollution not only endangers health, but also causes economic loss, which eventually leads to a number of social problems [28,29]. As attention to the pollution problem has been rising, more and more researchers are focusing their attention not only on the pollution sources and health effects, but also on innovative solutions how to reduce these risks.

1.1.1. Current situation and problems

Health effects of air pollution from particulate matter are well known, and worldwide efforts are being made to reduce both air pollution peaks and long-term exposure to harmful levels. However, air pollution episodes and sustained high levels still occur in various parts of the world. The *World Health Organization* (WHO) states that 91% of the world's population lives in places where air quality exceeds WHO guideline limits, which results in 4.2 million deaths due to the exposure to the ambience, and 3.8 million deaths are due to indoor air pollution [30].

Indoor air pollution causes deaths resulting from pneumonia (12%), stroke (34%), ischemic heart diseases (26%), chronic obstructive pulmonary diseases (22%), and lung cancer (6%) [29,31,32]. As shown in Table 1, indoor air pollution has been extensively studied in homes [33,34], schools [35,36], hospitals [37–40], offices [2,41] and restaurants [42,43]. However, indoor air pollution continues to be a global problem, especially in the developing countries.

Recent studies have shown that about 90% of the population's time is being spent in the indoor environments: homes, schools, offices, etc. This is much higher than the average time spent in the outdoor environments, which indicates the enormity of human health risk posed by indoor air pollutants [27,32,44–46].

Table 1. Health effects associated with indoor air pollutants

Health effect	Environment	Country	Pollutants	Key findings	References
Influenza-like illness (ILI)	Home	China	Not specified	Frequent cooking in the kitchen with coal as the primary fuel and less ventilation in the living room or bedroom with a coal-fuelled stove for heating during the heating season were two important risk factors to frequent ILI for housewives.	Wang, Liu, Li, & Li, 2016
Pneumonia	Indoor and outdoor pollutants	China	NO_2, SO_2 and particulate matter PM_{10}	Pneumonia in children was associated with postnatal exposure to indoor renovation, new furniture and redecoration. Combined exposure to outdoor high PM_{10} and indoor renovation significantly increased pneumonia risks.	Jiang *et al.*, 2018
Leukocyte telomere length (LTL) dysfunction	Home	China (Beijing)	Not specified	LTL is associated with the decades of using solid fuel for cooking. TLs were also observed in the population in certain occupations, such as farmers and workers, who are exposed to higher indoor air pollution levels. It is concluded that the accumulated burden of indoor air pollution exposure over decades, particularly solid fuel combustion, has a significant effect on telomere dysfunction	Lin *et al.*, 2017
Non-communicable diseases (NCDs) and lower respiratory infections (LRIs)	Ambient air	Iran (Tehran)	$PM_{2.5}$	With annual mean $PM_{2.5}$ concentration of 2.4 $\mu g/m^3$, it was estimated that 7146 premature deaths among adults could be avoided.	Bayat *et al.*, 2019
Respiratory health	Urban air	Finland (Helsinki)	Particulate matter PM_{10}, $PM_{2.5}$ and $PM_{1;}$ CO, NO, NO_2	The present results show that particle number concentrations in the ambient air, especially in the ultrafine range, are negatively associated with the respiratory health of adult asthmatics.	Penttinen *et al.*, 2001

Health effect	Environment	Country	Pollutants	Key findings	References
Cardiovascular and respiratory health	Homes	Nepal	PM_{10}, $PM_{2.5}$ and black carbon	A non-reversible bronchial obstruction was found in 18% of subjects, for 54% of subjects, which is suggestive of early respiratory impairment being diagnosed. Indoor pollution exposure was associated to early pulmonary and cardiovascular damages, which is more evident for longer duration and higher intensity exposure.	Pratali *et al.*, 2019
Headaches, skin reactions and respiratory systems	Hospital	Finland	VOCs	It was found that over 40% of the staff suffered from skin reactions, over 50% had upper respiratory tract symptoms, and 25% suffered headaches. It was determined that these effects were due to the VOCs in the hospital air	Rautiainen *et al.*, 2018

1.1.2. Particulate matter

Particulate matter (PM) is the segment of air pollution that is made up of extremely small particles and liquid droplets containing acids, organic chemicals, metals, and soil or dust particles. PM can be described by its aerodynamic equivalent diameter (AED). Particles of the same AED tend to exhibit the same settling velocity. Researchers traditionally subdivide particles into AED fractions based on how the particles are generated and where they deposit in human airways: <10, <2.5, and <0.1 μm (PM_{10}, $PM_{2.5}$, and $PM_{0.1}$, respectively).

Particles with a diameter greater than 10 μm have a relatively small suspension half-life and are largely filtered out by the nose and the upper airway. Researchers define a diameter between 2.5 and 10 μm ($PM_{2.5–10}$) as 'coarse', less than 2.5 μm as 'fine', and less than 0.1 μm as 'ultrafine' particles. When interpreting this PM research, it is important to appreciate that PM_{10} contains ultrafine ($PM_{0.1}$), fine ($PM_{0.1–2.5}$), and coarse ($PM_{2.5–10}$) fractions. In a mixed environmental sample, the total number and the total surface area of these particles increases exponentially as the diameter of the particles decreases. However, the total particulate mass of a substance generally decreases exponentially with the decreasing particle diameter. For example, in a sample of PM_{10}, the numerical majority of particles would be ultrafine, but these particles would make up a negligible portion of the sample's total particulate mass [4]. A hypothetical mixed particle distribution is shown in Figure 1.

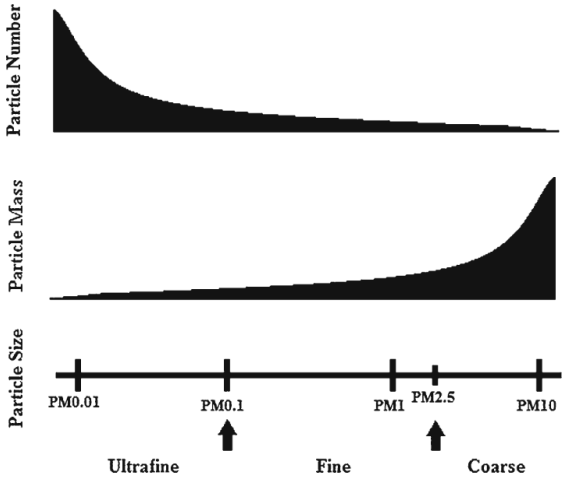

Figure 1. Hypothetical mixed particle distribution [4]

Particulate matter is thought to contribute to cardiovascular and cerebrovascular disease by the mechanisms of systemic inflammation, direct and indirect coagulation activation, and direct translocation into systemic circulation [46,51,52]. The data demonstrating PM's effect on the cardiovascular system is well-grounded. Populations subjected to long-term exposure to PM have a significantly higher cardiovascular incident and mortality rate [4,15,32]. Short-term acute exposures prominently increase the rate of cardiovascular events within days of a pollution spike.

Respiratory diseases are also exacerbated by exposure to PM, such as respiratory morbidity and mortality by creating oxidative stress and inflammation, which leads to pulmonary anatomic and physiologic remodeling. Literature shows that PM causes worsening of respiratory symptoms, triggers more frequent medication use, decreased lung function, recurrent health care utilization, and the subsequent increased mortality [4,6,32].

These consistent results were obtained by multiple studies with varying populations, protocols, and regions. The data demonstrates a dose-dependent relationship between PM and human disease, and shows that removal from a PM-rich environment decreases the prevalence of these diseases. Indoor PM exposure can be reduced by the usage of air conditioning and particulate filters, decreasing indoor combustion for heating and cooking, and smoking cessation. Susceptible populations, such as the elderly or asthmatics, may benefit from limiting their outdoor activity during peak traffic periods or on poor air quality days. These simple changes may benefit individual patients in both short-term symptomatic control and long-term cardiovascular and respiratory complications [4].

1.2. Theoretical background of air filtration

Air filters are the most common air purification systems due to the low cost, application simplicity, and a wide variety of suitable materials. Extensive theoretical investigations of filtration mechanisms have been conducted since 1943. The mechanical collection mechanisms of air filters are Brownian diffusion, inertia, interception, and gravity [53]. The main filter mechanisms of fibre material, filtration efficiency for individual single-fibre mechanisms, and the total efficiency and different filtering effects on the particle size are represented in Figure 2.

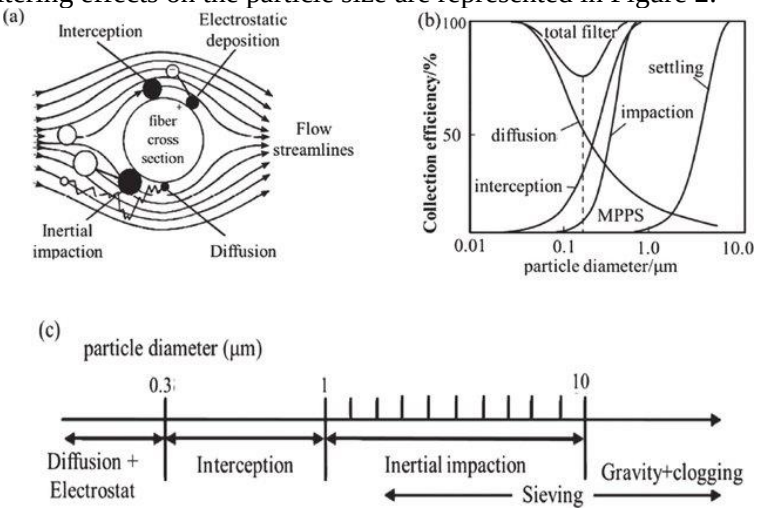

Figure 2. Main fibrous filters air filtration mechanisms: a) Main filter mechanisms of fibre material [54]; b) Filtration efficiency for individual single-fibre mechanisms and total efficiency. c) Different filtering effects on the particle size [55]

The interception capture mechanism occurs when particles move with the airflow as the distance between the streamline of the particle's centreline and the streamline of the fibre centreline is less than or equal to the sum of the fibre radius and the particle radius. Interception efficiency is affected by Reynolds number (*Re*) and the intercept coefficient [56].

The diffusion capture mechanism is observed when small-sized particles are captured by the fibre surface with gas molecule collisions and random movement. The diffusion capture mechanism is a function of Reynolds number (*Re*) and Peclet number (*Pe*). This mechanism is most significant for the particles smaller than 1 μm. The smaller is the particle size, the more intense is the random movement, and the more obvious is the diffusion efficiency. Research shows that the theoretical calculation value of the diffusion capture efficiency becomes greater than 80% when the particle size is less than 0.1 μm. Under these circumstances, any other capture efficiency can be ignored [57].

One of the simplest ways to combine the diffusion and the interception mechanisms with a reasonable accuracy is to add the two individual efficiencies so that to obtain the combined efficiency. This practice assumes that only one mechanism is predominant, with the contribution made by the other mechanism being small. This assumption has been found to be adequate for combining the diffusion and the interception mechanisms. The efficiency due to diffusion decreases with the increasing particle size, whereas the efficiency due to interception increases rapidly with the increasing particle size [57].

The inertia capture mechanism is closely related to the mass of the particles. The inertia effect occurs when particles move with the airflow. Particulate matter that is not within the airflow streamline will be arrested by the fibre surface when the flow changes. The inertial capture efficiency is greatly influenced by the speed of the air stream, as it is the function of Stokes parameter (*St*) and Reynolds number (Re_f). The bigger is the particle size, the greater is the inertia, and the higher the inertia efficiency will be [58].

Electrostatic capture efficiency refers to the collection efficiency of particles or fibres in the electric field formed by the opposite charged Coulomb force, the image force, and the polarization force of the electric field emission. Electrostatic effects are generally present in filtration processes because particles and fibres are charged to some extent. However, the effects are insignificant unless the particles or fibres are highly charged [59].

While filters composed of fibres remove particles mainly by the above mentioned mechanisms, the collection efficiency is affected by the internal structure of the filter, such as the variance of the fibre diameter, the inhomogeneity factor, and the packing density. The relative contribution of each collection mechanism to the particle depends on the physical properties of the filter (the fibre diameter, the packing density, the orientation of fibres, and the internal structure of the filter), and the particle properties (their diameter, density, and shape) as well as the filtration conditions (filtration velocity, pressure, and temperature).

1.2.1. Parameters of non-woven fibrous filters

Fibrous filters aim to minimize both the particle penetration (P) and the pressure drop (Pd) across the filter. Particle penetration is defined as the ratio of the particle number concentration downstream to that upstream of the filter. The overall performance of the filter is often evaluated by using the quality factor. From the application point of view, the deposited mass of the particles at which a filter clogs is also fundamentally important (Chattopadhyay, Hatton, & Rutledge, 2015).

The filtration efficiency of a clean non-woven fibrous filter can be approximated by an idealized structure of fibres, for which, the filtration efficiency (η, %), fibre packing density (α, g/cm^3), single fibre efficiency (η_f, %), filter thickness (Z, cm), and the mean fibre diameter (d_f, cm) are all related as follows [25,60]:

$$\eta = 1 - \exp\left[-\frac{4\alpha\eta_f Z}{\pi(1-\alpha)d_f}\right] \quad \textbf{Eq. 1}$$

When the slip effect is taken into account, it shows good results for the particle size from 80 to 400 nm and the fibre diameter at 1 μm. For nanofibre filters, the interaction of diffusion and interception is more significant than the inertial impaction, hence:

$$\eta_f = \eta_D + \eta_R \quad \textbf{Eq. 2}$$

where η_D and η_R are the single fibre efficiencies due to diffusion and interception, respectively, and are expressed in Eqs. 3 and 8 accordingly:

$$\eta_D = 1.6\left(\frac{1-\alpha}{Ku}\right)^{1/3} Pe^{-2/3} C_1 C_2 \quad \textbf{Eq. 3}$$

$$C_1 = 1 + hKn_f\left[\frac{(1\alpha)Pe}{Ku}\right]^{1/3} \quad \textbf{Eq. 4}$$

$$C_2 = \frac{1}{1+1.6[(1-\alpha)/Ku]^{1/3}Pe^{-2/3}C_1} \quad \textbf{Eq. 5}$$

where $Ku = -(\ln\alpha)/2 + \alpha - \alpha^2/4 - 3/4$ is Kuwabara hydrodynamic factor, $Pe = U_0\, d_f/D$ is Peclet number with U_0 as the face velocity (m/s), $D = k_B T C_S/3\pi\mu D_p$ is the diffusion coefficient (m^2/s), k_B is Bolzmann constant (J/K), T is the absolute temperature (K), μ is the air dynamic viscosity (Pa·s), D_p is the aerosol size (μm), $C_S = 1 + Kn[1.207 + 0.44\exp(-0.78/Kn)]$ is Cunningham slip correction factor [61,62] with $Kn = 2\lambda/D_p$ as Knudsen number based on the aerosol size, $Kn_f = 2\lambda/d_f$ as Knudsen number based on the fibre diameter, and h is a constant that equals to 0.388 in Payet's correlation [62].

$$\eta_R = 0.6\left(\frac{1-\alpha}{Ku}\right)\left(1 + \frac{Kn_f}{D_p/d_f}\right)\left(\frac{D_p^2/d_f^2}{1+D_p/d_f}\right) \quad \textbf{Eq. 6}$$

where D_p/d_f is sometimes referred to as the interception ratio.

There are two ways to improve the filter quality. The first strategy is to make it more efficient in filtering out particles in order to increase the filtration efficiency, and the other method is to make it more permeable in order to reduce the pressure drop [38,62].

Forchheimer's equation is used to evaluate the fluid flow in porous media. The first term of this equation refers to purely viscous effects, whereas the second term refers to the inertial effects, according to Equation 7:

$$\frac{\Delta P}{L} = \frac{\mu}{k_1} \cdot v_s + \frac{\rho_g}{k_2} v_s^2 \qquad \textbf{Eq. 7}$$

where L represents the thickness of the filter media (cm), μ is the viscosity of the fluid (Pa·s), k_1 and k_2 are constants of the permeability of the filter media, ρ_g represents the density of the gas (kg/m^3), and v_s is the superficial velocity (m/s). ΔP is the pressure drop (Pa) that is the difference between the inlet and the outlet pressure of the filter during the passage of the air stream [38].

When a low filtration velocity is being used, the second term of Eq. 7 can be neglected, and thus Eq. 8 may be used:

$$\frac{\Delta P}{L} = \frac{\mu}{k_1} \cdot v_s \qquad \textbf{Eq. 8}$$

Thus, the permeability of the porous filter media can be obtained by Darcy's equation. This equation evaluates the flow of fluids in porous filter media relating the pressure drop values with the superficial velocity [38].

As it was mentioned in the previous chapter, filtration efficiency is not a sufficient parameter for filter quality evaluation. Fibrous filters could be described by the packing density and porosity of mats, which could be estimated by the following equations:

$$\alpha = W/Z \times \rho \qquad \textbf{Eq. 9}$$

$$\varepsilon = (1 - m/z \times A \times \rho) \times 100\% \qquad \textbf{Eq. 10}$$

where α is the packing density (g/cm^3) and ε is porosity (%), ρ is the fibre matter density (g/cm^3), Z is the filter matt thickness (cm), W is the filter area density (g/cm^2) [22], m is the filter mass (g), and A is the area of the filter (cm^2).

The optimal formulation for air filtration performance is defined by the quality factor (QF; Pa^{-1})[17,63] which balances the filtration efficiency and the pressure drop:

$$QF = -(ln(1 - \eta)/\Delta P) \qquad \textbf{Eq. 11}$$

where η is the filtration efficiency (%), and ΔP is the pressure drop (Pa).

1.2.2. Standardization of filter efficiency

High efficiency particle air filters are increasingly being recommended for use in heating, ventilating, and air-conditioning (HVAC) systems in order to improve the indoor air quality. ISO Standard 16890-2016 provides a methodology for approximating mass-based particle removal efficiencies for PM_1, $PM_{2.5}$, and PM_{10} by

using size-resolved removal efficiency measurements 0.3–1 μm for ePM_1, 0.3–2.5 μm for $ePM_{2.5}$, and 0.3–10 μm for ePM_{10} particles [64]. The fraction of particles that the test device removes from the air passing through was referred to as the particle penetration and was calculated from the amount of the particulate that penetrated the test device during the test:

$$P = C_{downstream}/C_{upstream} \quad \textbf{Eq. 12}$$

$$E_{ps} = (1 - P_{ps}) \times 100 \quad \textbf{Eq. 13}$$

where $C_{downstream}$ and $C_{upstream}$ is the particle mass concentration downstream and upstream of the test device, respectively; E_{ps} is the particle fractional efficiency at the particle size, *ps*, %; P_{ps} is the particle penetration at the particle size, *ps*.

The average fractional efficiency $E_{A,i}$ resulting from the averaging efficiencies of an electrostatically charged and discharged filter was calculated as follows (Eq. 14):

$$E_{A,i} = 0.5 \cdot (E_i + E_{D,i}) \quad \textbf{Eq. 14}$$

where E_i is the initial fractional efficiency of the particle size range, *i*, of the untreated and unloaded filter element, % (it equals to the efficiency values E_{ps} of the filter element taken from ISO 1689-2), and $E_{D,I}$ is the fractional efficiency of the particle size range, i, of the filter element after the artificial conditioning step, % (it equals to the efficiency values E_{ps} of the filter element taken from ISO 1689-2 after the conditioning step has been carried out according to ISO 16890-4)

The particulate matter efficiency of ePM_1 (Urban size distribution) (Eq. 15) was calculated from the average fractional efficiency $E_{A,i}$, $E_{A,i}=0.5\cdot(E_i+E_{D,i})$, and the standardized particle size distribution is defined in ISO 1689.

$$ePM_1 = \sum_{i=1}^{n} E_{A,i} \cdot q_{3u}\left(\bar{d}_i\right) \cdot \Delta \ln d_i / \sum_{i=1}^{n} q_{3u}\left(\bar{d}_i\right) \cdot \Delta \ln d_i \quad \textbf{Eq. 15}$$

where $\bar{d}_i = \sqrt{d_i \cdot d_{i+1}}$ is the geometric mean diameter, and $\Delta \ln d_i = \ln d_{i+1} - \ln d_i = \ln(d_{i+1}/d_i)$. In the formula $ePM_1=i=\ln E_{A,i}\cdot q_{3u}di\cdot\Delta\ln d_i i=1n q_{3u}di\cdot\Delta\ln di$, *i* is the number of the channel (size range) of the particle counter under consideration, and *n* is the number of the channel (the size range) which includes the particle size, x ($d_n < x \leq d_{n+1}$), where x = 1 μm for ePM_1, and the lower size limit of the smallest channel of the particle counter taken into account for the calculation of the efficiency values is equal to 0.3 μm (d_1=0.3 μm). The same principle is used for the calculation of $ePM_{2.5}$ and ePM_{10}, by changing x to 2.5 and 10, respectively.

Additionally, the minimum efficiency ePM_{min} could be calculated by using Eq. 15, by replacing $E_{A,i}$ to $E_{D,I}$ in the calculations. The initial efficiency (E_i), efficiency ($E_{A,I}$) and the minimum efficiency ($E_{D,i}$) values were used to classify the filter material.

1.3. Fibrous filters

Fibrous filters are the most commonly used separation systems in airborne particle filtration because they may offer a high filter efficiency while maintaining an acceptable pressure drop. Because of their numerous manufacturing processes, they

may exhibit very different characteristics in terms of the packing density, thickness or the fibre size distribution [65].

Currently, air filtration is still the most promising technique for air purification. Filtering exhibits the advantages of high purification efficiency and outstanding performance stability in a variety of applications. Additionally, the emergence of new materials with excellent physical and chemical properties further promotes the development of the filtration technology, along with the ongoing progress in the field of membrane materials science and technology [66].

1.3.1. Microfibre filters

The traditional air filtration media (micrometre-scale fibres), such as glass fibres, spun-bonded fibres, and melt-blown fibres usually show low filtration efficiency for fine airborne nanoparticles (0.1–0.5 μm) because the pore size formed with the micrometre-scale fibres is fairly large. Although some nonwoven filtration materials exhibit good filtering performance for micrometre-level particles, their performance is still far from satisfactory for sub-micrometre PM and for bacterial filtration. To improve the filtration efficiency of the traditional filter media, it is necessary to create thicker media. However, a thicker filter medium can be difficult to use due to a higher pressure drop and increased energy costs [66].

Chattopadhyay, Hatton and Rutledge (2015) analyzed the performance of microfibre filters with a diameter of 0.1–24 μm. By using analysis based on blocking filtration laws, they concluded that filters with a larger fibre diameter showed a transition in mechanisms from the initial regime characterized by pore blocking to a later regime characterized by cake formation [67]. Chen *et al*. (2017) experimented with a microfibre filter by loading it with PM from a gasoline direct injection engine. The experiment results showed that the filtration efficiency in terms of PM mass and number increased over time. A small fraction of the accumulation mode particles with a size between 70 nm to 500 nm penetrated the filters, while virtually all the nucleation mode particles with a size below 50 nm were captured by the filters.

Leung and Hung (2008) investigated the effects of particle loading on the filtration efficiency and pressure drop for three nanofibre filters and one microfibre filter at a face velocity of 0.05 ms^{-1}. The filters were made of fibres 0.3 and 1.8 μm in diameter, respectively. The thickness and the packing density of the microfibre filter were 0.1 mm and 0.04845, respectively. Monosized NaCl particles were used as the test particles. They found that the filtration efficiencies of clean nano- and micro-fibrous filters for particles smaller than 70 nm were in good agreement with the theoretical calculations. The most penetrating particle size (MPPS) was 103 and 203 nm, respectively, for nano- and micro- fibrous filters before they were loaded with particles. Particle loading led to a decrease in MPPSs for both types of filters, and the decrease was larger for nanofibre filters than for microfibre filters. An increase in the pressure drop across the nanofibre filter approximately followed a third degree polynomial function of the specific deposit. Under continuous loading conditions, the rate of an increase in the pressure drop was lower for the microfibre filter than for the nanofibre filter [69]. This shows that, besides a lower filtration efficiency in microfibre

filters, certain aspects, such as a lower pressure drop, are more prominent in micro structured fibre filters.

1.3.2. Nanofibrous filters

Nanofibre filters have been extensively studied in recent years. Nanofibre membranes are usually made of organic or inorganic polymers with fibre diameters ranging between 100–500 nm, and pore sizes ranging between 0.2–5μm [66,70–72].

Air filtration by using the nanofibrous structures is one of the more promising and interesting research areas [72–75]. The main purpose of developing nanofibrous filters is to create filters with a higher efficiency, a lower energy consumption, a longer lifetime, and easier maintenance. So far, several methods have been proposed for the production of nanofibres. In the meantime, the electrospinning process has been receiving much attention in the recent years due to its simplicity and its capacity to work with various mechanisms for the production of fibres. Electrospun nanofibrous mats, as one of the utmost promising and versatile filter media for fine particle filtration, are denoted by several fascinating features, such as a large specific surface area, high open porosity, controllable pore size distribution, and an interconnected porous structure [76–80].

The interactions between the fibrous media, the aerosol, and the operating conditions (filtration velocity, humidity, temperature, etc.) exert a significant impact on the deposit structure, the efficiency, and the energy expenditure. Typically, aerosols are first collected within the filter (depth-filtration). Then, the filtration mode changes from depth to surface filtration with the formation of a cake on the filter surface. During the transition between these two filtration modes, airborne particles may be collected by either the growing cake, or by the filter fibres. During filtration, the pressure drop and the collection efficiency evolve over time [81].

With high aerosol loading, the aerosols that get trapped by the nanofibre filter can reduce its flowable pores. Furthermore, the region near the upstream end of the filter which faces the challenging aerosol stream tends to trap more aerosols not only just from the fibres of the filter, but also from the trapped aerosols themselves thus producing the avalanche/domino effect. This region is known as the ‘cake’ layer [81–83] with the majority of the aerosol getting trapped tightly there; it also accounts for a large percentage of the pressure drop across the filter. Due to that, the filter pressure drop might reach an unacceptable level [83–85]. As both nanofibre and microfibre filters suffer from their own disadvantages, in the recent years, a new form of advanced filters came into the centre of attention in the scientific community. *Mixed media* or *Hierarchically structured* filters offer combinations of different-sized fibres and different materials so that the best quality filters could be developed.

1.3.3. Hierarchically structured/mixed media filters

Nano-micro fibrous membranes are seen as promising regarding their application as the filter media as they are denoted by an extremely high filtration efficiency for ultrafine to fine particles and a relatively low pressure drop due to their unique structure [22,86–89] Fibrous filters containing nanofibres are often produced as

multi-layered filters which consist of a nanoweb and a resistant substrate which provide physical and mechanical properties required for the filter [90–92].

By layering materials of differing fibre sizes [22,93,94] and/or different properties [87,95–97], a new generation of high performance air filters could be developed. These new structures promise high air filter efficiency without sacrificing the low air pressure drop or including the sorption of volatile organic compounds (VOCs) in the otherwise conventional filtration systems.

In their work, Zhong *et al*. (2018) fabricated a double-network membrane for efficient filtration of fine PM particles. The membrane was composed of binary hierarchical structures including scaffold poly(m-phenylene isophthalamide) (PMIA) nanofibres and intertwined ultra-fine SiO_2 nanofilaments on its surface. The presence of SiO_2 nanofilaments notably changed the morphology, the specific surface area and the porosity of the pristine PMIA nanofibres without reducing the mechanical strength. PM capture measurement demonstrates that the hybrid membrane exhibited a significantly better PM capture score than the bare PMIA membrane, and the removal efficiencies of $PM_{2.5}$ and PM_{10} were 97.33% and 98.48%, respectively.

Zhu *et al*. (2018a) created multifunctional poly(vinyl alcohol)/poly(acrylic acid) (PVA-PAA) composite membranes via electrospinning and thermal crosslinking. Superhydrophobic silica nanoparticles were then incorporated into the fibres thus resulting in a rough surface, after which, $AgNO_3$ was introduced, which resulted in the formation of Ag nanoparticles through UV reduction. The PVA-PAA-SiO_2-Ag NPs membranes were found to possess high air filtration performance (with >98% filtration efficiency for $PM_{2.5}$) as well as potent antibacterial and antiviral activities. These newly designed PVA-PAA-SiO2 NPs-Ag NPs nanofibrous membranes with many superior features (e.g., high filtration efficiency, high tensile strength, biological compatibility, and antibacterial properties) have a great potential in future applications.

1.4. Introduction to electrospinning

Almost all fibre barrier membranes used in the industry of nonwovens are based on the melt blowing technology as melt spinning processes are used to produce microfibres by injecting molten polymer streams into high velocity gas/air jets that form a self-bonded web when collected on a moving surface[100]. High-velocity air jets impinge upon the polymer as it emerges from the spinneret. The drag force caused by the air attenuates the fibre rapidly and reduces its diameter by as much as one hundred times in comparison to that of the nozzle diameter. The typical melt blown membranes feature fibre sizes ranging from 0.5 to 10 mm with an average fibre diameter of 1–2 mm. Melt blown webs are known for their high surface area per unit weight, a high insulation value, and high barrier properties. These properties make them excellent candidates for making high quality filters, surgical drapes and gowns, diaper leg cuff, and protective apparel, where a barrier to fluids and breathability are essential features [100–102].

Electrospun nanofibre membranes are a promising technology to address the three primary barriers associated with membrane filtration: high capital cost, low flux,

and severe fouling. The nanofibre morphology of electrospun membranes results in a higher flux than the conventional polymer membranes due to the improved effective porosity while retaining high selectivity in microfiltration applications. Furthermore, nanofibre membranes are denoted by lower production costs than the conventional membranes, which results in a significantly lower capital cost of the membrane systems. As a result, electrospun microfiltration membrane fabrication is a promising area of research [62,103–106].

1.4.1. Basic principle

Electrospinning is a fibre formation technique that was firstly described in 1902 by Cooley and by Morton. This started the long process of innovations and scientific analysis. Throughout the 20th century, the basic technique of electrospinning was laid down, but the present understanding of the process is mainly more recent research [107].

The formation of fibres through electrospinning is based on the stretching of a viscoelastic liquid due to the difference of the potentials between the positively charged electrode and the negatively charged collector. In order to understand and assess the process that enables the formation of various fibre assemblies, the principles of electrospinning and the different parameters that affect the process must be considered (Teo & Ramakrishna, 2006). Unlike the conventional fibre spinning methods, such as dry-spinning and melt-spinning, electrospinning makes use of electrostatic forces in order to stretch the solution or melt as it solidifies. Similarly to the conventional fibre spinning methods, the drawing of the solution in order to form the fibre will continue as long as there is enough material to feed the electrospinning jet. Thus, without any disruption to the electrospinning jet, the formation of the fibre will be continuous (Chronakis, 2005; Huang, Zhang, Kotaki, & Ramakrishna, 2003; Teo & Ramakrishna, 2006).

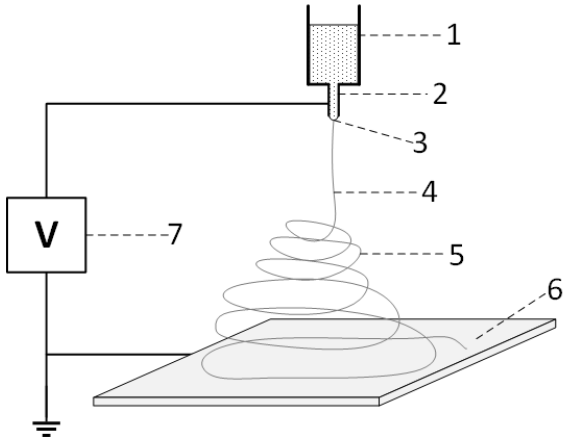

1 – Polymer solution or melt
2 – Needle
3 – Taylor cone
4 – Electrospinning jet
5 – Bending instability
6 – Collector
7 – High voltage power supply

Figure 3. Basic scheme of electrospinning

Electrospinning depends on the complex interactions between the surfaces, shapes, rheology, and electrical charge. These phenomena cooperate to create

electrified jets of polymer solutions, and polymer melts [108]. A basic scheme of electrospinning is shown in Figure 2. When an electric field is applied, charges accumulate on the surface of the polymer droplet formed at the tip of the needle and create instability that deforms the hemispherical droplet into a conical shape, referred to as the *Taylor cone*. Due to that, a competition develops between the Coulombic repulsion of charges favoring droplet distortion and the surface tension opposing droplet division. When the applied electric field strength is sufficiently high, a jet is continuously ejected from the apex of the cone and travels towards the grounded plate as a fibre. The high charge density on the surface of the fine jet leads to electrical instability, making it whip around rapidly. The jet diameter decreases due to stretching (whipping) and evaporation of the solvent if the solution of the polymer is being used [108–110].

During the deposition process, fibres with a small amount of the preserved residual Coulombic charge are repelled away from the previously deposited fibres. According to Brown *et al*., charge storage is dependent on the crystallinity, polymer structure and the presence of additives in the electrospun jet. Charges may trap at the interface of crystals and amorphous regions, as well as in the inner regions of spherulites. Hence, surface free charges may exist [111].

The results of numerous studies show that the final morphology of the fibre is highly influenced by the physical properties of the polymer precursor. Appropriate adjustment of the precursor's electrical conductivity and viscosity may be the most important factor in fine-tuning the morphology of the prepared fibres [112–115].

In the research by Balgis *et al*. (2017), due to the high viscosity of the cellulose nano fibre gel that the researchers were using for electrospinning, a medium concentration PVP of 8 wt. % was selected for fabricating the nanofibre composite in order to keep the diameter of the nanofibre composite as small as possible. The obtained results showed that the final morphology of the fibre is highly influenced by the physical properties of the polymer precursor. Appropriate adjustment of the precursor's electrical conductivity and viscosity may be the most important factor in fine-tuning the morphology of the prepared fibres [23].

The morphology of the out-coming fibres or mats will depend on several experimental conditions including the viscosity of the solution, the applied electric field (the applied voltage/the needle-to-collector distance), the pump rate, the temperature and pressure, the solvent vapor pressure (the evaporation rate), and the collection time. Another method employed to control the fibre morphology (alignment) during electrospinning is the use of a rotating collector or an oscillating needle [116–118]. This makes electrospinning serve as a good tool to produce mats with a better-controlled morphology. A common morphological feature in the electrostatically deposited fibres and mats is the formation of beads or beading. This particular feature involves the formation of random beads, preferentially where fibres intercrossing each other, often due to the viscoelastic nature of the electrospun precursor fluids or fluctuations in the deposition parameters. The permeability of mats is a function of the distribution of pore dimensions. These dimensions are statistically distributed, and they tend to correlate inversely with the mat thickness or the electro-

spinning deposition time. The dimensions of most pores for reasonable deposition times (a few hours or less) lie within the range between micro and nano-metres, as evidenced by SEM micrographs [119].

1.4.2. Solution electrospinning

Electrospinning is a fast-emerging technique intended to produce fine and ultrafine fibres from a wide range of polymers. This technique can be used with both solution and melt phases of polymers depending on the application. Solution electrospinning has been widely used due to the low cost and simplicity of the device, as well as because of the ease of adaptation to a wide variety of polymers. In the conventional electrospinning processes, polymer solutions turn into continuous polymer jets in the presence of an electric field applied between the nozzle and the collector [10,120]. However, the major drawbacks of this technique are related to the uncontrollable nature of the spun fibres and the use of toxic solvents which may not evaporate completely during the process [121–123]. Studies with solution electrospinning show that the final morphology of the fibre is highly influenced by the physical properties of the polymer precursor [10,23]. This complicates the selection of polymer solution electrospinning and may lead to the usage of hazardous solvents and additives, which will restrict any further usage of the product.

To address these challenges, some innovative approaches, such as the focused electrical field [124], nearfield electrospinning [109], and direct-write electrospinning [125,126] have been used in order to produce structures with more controlled features. However, these methods still require solvents throughout the process. In contrast, melt electrospinning is an alternative technique which does not rely on any solvents and can deliver highly ordered fibre depositions. Moreover, polymer melts usually feature a higher viscosity than solutions, which results in the formation of more stable polymer jets denoted by a better control and higher precision [10,127–131].

1.4.3. Melt electrospinning

The idea of melt electrospinning originated from the work of Norton in 1936 while its importance was truly realized by Kim and Lee in 2000 [132]. Since then, the electrodynamics of nonisothermal polymer jets as well as the polymer structures has been extensively studied both experimentally and theoretically [133–136]. Different setups as well as polymers have tested throughout recent years [137–143] Inspiring work was conducted by Dalton and Hutmacher [126,135,137,144–146]. The technique of 3D printing was embedded into melt electrospinning, which was termed as melt electrowriting [144], by which, nontoxic and micro-scaled scaffolds with various structures can be easily printed out for cell culture and drug releasing.

Previous studies demonstrated that it is possible for melt electrospinning to obtain fibres with sub-micron diameters [133,147,148]. It was reported that the diameter of fibres decreases when increasing the applied voltage and the melt temperature. Lyons *et al*. found that fibres of polypropylene and poly(ethylene terephthalate) electrospun by melt electrospinning could be obtained with diameters ranging from hundreds of nanometres to hundreds of micrometres via a modified device design [133]. While it

seems that modified melt electrospinning can produce finer fibres, more data is still needed.

Melt electrospun fibres have been produced by adding a plasticizer [149], with a CO_2 laser heated melt electrospinning device [143], or by employing the airflow assistance technology [139,150,151], coaxial [152] and other modifications; these efforts produced different results which are suitable for a variety of applications.

The solvent-free feature of melt electrospinning has shown great potential in the fields of air purification[5,26], tissue engineering [138], biomedical engineering [153–156], biosensors [155], etc.

The main effective parameters of melt electrospinning are the collector speed, the polymer feed rate, the tip-to-collector distance, the temperature of melt, and the applied voltage. In the literature, there are a number of studies considering the effects of different process parameters on the fibre diameter and the shape fidelity of electrospun structures [157–159]; however, a few works also explored their counter-influence and interactions [120]. Because of that, determining the influence of process parameters on the shape and the diameter of the deposited fibres is crucial in predicting the relevant set of the process parameters in order to achieve the desired fibre diameter.

While melt electrospinning offers some advantages for air filtration application, the process of fibre formation is usually overlooked due to the comparatively large fibre diameter. That being said, numerous researches on melt electrospinning analyze its suitability for other applications, such as scaffolds, drug delivery, etc. Such interest in this method results in introducing new materials and offers deeper knowledge on the process. The research analysis on melt electrospinning (polymers, conditions, fibre diameters and potential applications) is presented in Table 2.

Table 2. Summary of research on melt electrospinning

Polymer	Electrospinning conditions	Fibre diameters	Potential applications	Key findings	References
PP	Temperature of melt – 240 °C; feed rate – 15 g/h; collector speed – 1400 rpm; TtCD – variable (2 cm); Voltage – variable (20–55 kV)	2.23–6.48 μm	Water filtration	Experimental results demonstrated that electrospun oriented membranes showed higher efficiency in rejecting 0.5 μm particles with a diameter of 2.49 ± 0.418 μm and still maintained nearly the same permeate flux as that of the native membrane.	[160]
PLLA /PHB	Temperature of melt – 220 °C and 170 °C; TtCD – 7 cm Voltage – 35 kV	10.69–22.53 μm	Drug delivery	The crystallinity of PLLA slightly decreased as PHB was incorporated, and the addition of the drug significantly reduced the melting temperature of the composite. The interactions between PLLA and PHB mainly occurred at a proportion of 7:3, and drug encapsulation in the fibres was verified. The kinetic profiles of drug release demonstrated the predominant multiple patterns involving a diffusional stage in the short-term mode of release and kinetic process related to the hydrolysis of the biopolymers.	[161]
PEEK	Temperature of melt – 350 °C TtCD – 3.6 cm electric field strength – 2–5×10^5 V/m needle gauge – 22G	1–4 μm	Not specified	Dynamic fragilities of melt electrospun oriented amorphous PEEK fibres and amorphous PEEK quenched from the molten state were evaluated according to Moynihan's method of cooling at variable rates and then reheating at a fixed rate which were found to be 200 ± 5 and 150 ± 5, respectively. These results suggest that orientation in the amorphous state of electrospun fibres plays a role in the dynamics of glass formation.	[162]
PCL-SrBG	Temperature of melt –80–85 °C feed rate – 20 μl/h TtCD – 4–6 cm Voltage – 7 kV Needle gauge – 19–21 G	30.6–46.1 μm	Scaffolds	The produced composite scaffolds facilitated cellular attachment and proliferation, and possessed enhanced osteogenic potential compared to PCL scaffolds alone. The activity of cells cultured on these composite scaffolds was enhanced, and increased osteoblast differentiation was observed through the upregulation of gene expression *in vitro*. The composite scaffolds also enhanced collagen deposition.	[163]

PCL	Temperature of melt – 90 °C feed rate – 1.5 ml/h TtCD – 15 cm Voltage – 30 kV	2.48–2.51 μm	Tumor therapy	The inhibition ratios of HeLa and glioma cells following treatment with membranes prepared with 1, 5, and 10 wt.% daunorubicin hydrochloride were 62.69%, 76.12%, and 85.07% and 62.50%, 77.27%, and 84.66%, respectively. Therefore, PCL melt electrospun fibrous membranes loaded with daunorubicin hydrochloride may be used in the local administration of oncotherapy.	[164]
PEG_{47}-b-PCL_{95}; PLC	Temperature of melt – 90–320 °C feed rate – 0.02–0.3 mL/h TtCD – 4 and 10 cm Voltage – 20 kV	100 nm – 2.0 μm	Material science (not specified)	The focused deposition of melt electrospun fibres was maintained when multiple jets were observed with the collections from multiple jets separated by 3.8 ± 0.5 mm for a 5 cm collector gap. The frequent fusion points between melt electrospun fibres, and a reduction in the diameter for the gap method of alignment, indicated that the melt electrospun fibres are still slightly molten at collection.	[135]
PLC	Laser current – 4–12 mA TtCD – 12–20 cm Voltage – 5–20 kV	3–12 μm	Material science (not specified)	It was found that the fibre diameter tended to decrease as the laser current increased, while the applied voltage and the collection distance did not have a statistically significant effect on the fibre's diameter. It can be adjusted with the laser current for various fibre diameters, which could be useful for scaffold applications. In addition, it should be noted that the effect of laser heating on the molecular degradation of PCL fibres is especially useful for mechanical materials.	[142]
PLC	Temperature of melt – 65–73 °C dispensing pressure – 100 – 135 kPa TtCD – 1.2 mm Voltage – 2 kV	13–17 μm	Scaffolds	This research presented an experimental approach called the beam bridge test in order to identify the sagging behavior of melt-electrospun microfibres for preparing 3D lattice structures with a controllable architecture and well-defined pores in the transverse direction. Consequently, the sagging behavior of melt-electrospun microfibres could be identified in a systematic manner. The cell culture results indicated that the cell growth was considerably influenced by microfibre sagging and the grid size of the lattice structures.	[165]

1.4.4. Electrospinning for filtration applications

The recent progress in the manufacturing technology of polymer fibres enables us to produce nanofibres in large quantities at a relatively low cost. Air filters made of nanofibres featuring a diameter of less than 1 μm have been attracting great attention because they may attain a high collection efficiency with a low pressure drop at the same time. Various manufacturing methods, e.g., melt-blown, electrospinning and stretching of polymer films, have been developed to obtain fine fibres [65,85,135,166,167]. Particularly, electrospinning is the most popular method because it is simple and offers the possibility to fabricate nanofibres of various polymers.

Sun *et al*. (2014) studied the collection efficiency of nanofibre filters laminated on a base filter by using a theoretical 3-D model and showed that the reduction in the fibre diameter was effective for increasing the collection efficiency. Matulevicius *et al*. (2016) experimentally measured the collection performance of nanofibre filter media fabricated by electrospinning of polyamide and reported that the filter with finer fibres had a high collection efficiency and a high quality factor.

Electrospinning is mostly associated with the spinning of fibres from polymer solutions. Numerous studies on solution electrospinning for air filter media formation (Al-Attabi, Dumée, Schütz, & Morsi, 2018; Balgis *et al*., 2017; Chattopadhyay, Hatton, & Rutledge, 2015; Matulevicius *et al*., 2016; Zhang, Liu, Zuo, *et al*., 2017; Zhang, Liu, Yin, Yu, & Ding, 2016; Zhang, Liu, Yu, Luo, & Ding, 2016; Zhu *et al*., 2018) have highlighted process advances in aerosol separation. Furthermore, this process is associated with adverse environmental impacts owing to the potential evaporation of solvents, and thus with increased production costs. Another disadvantage of uniform nanofibrous matrices includes the high pressure drop as a result of the small interfibre pore sizes, thereby leading to high energy consumption in ventilation systems containing such filter products [5].

Melt electrospinning is an emerging technique that is capable of spinning polymers from their melts thus avoiding the undesirable consequences of solvent use. Moreover, applications in the filter material manufacturing are still limited at present, mostly owing to the insufficient capability of producing small-diameter fibres as compared to solution electrospinning [5,20,21].

Additive printing (sometimes referred to as additive manufacturing) is a technique for fabricating a wide range of structures and complex geometries from three-dimensional model data. The merging of such an approach and melt electrospinning may yield several interesting developments in the additive production of fibrous materials and products. Within such a process, successive layers of materials are printed on top of one another. A combination of both techniques allows for a more controllable deposition and layering of the fibre mat, and, thus, offers an improved quality of the filter media [5,171].

Combined melt electrospinning and hot pressing with an objective to produce mats containing fibres with an average diameter ranging between 6.18 and 13.92 μm. The mats with a thickness of 0.42 mm achieved > 95% filtration efficiency with oil particles of approximately 2.0 μm in diameter, while the air permeability and pressure

drop were 54.69 mm/s and 18.13 Pa, as opposed to the stock filter material resulting in 10.02 mm/s and 38.67 Pa, respectively. Zhou and Joo [134] directly melt electrospun polylactic acid fibres onto the cellulose filter media, which resulted in a substantial enhancement in the collection efficiency of sub-micrometre-sized dust particles. Despite the increase in the pressure drop by 11.1%, the filtration efficiency increased by 15% to 40% compared to the initial material [5].

Other interesting applications of melt electrospun fibres were observed in water filtration and air purification by catalysis. Electrospun-oriented fibre membranes with a diameter of 2.49 ± 0.418 μm exhibited a higher efficiency in removing 0.5 μm particles from water, and maintained nearly the same permeate flux as that of the conventional membrane [160]. Melt electrospun microfibre from polyamide 12 polymer has been demonstrated as an efficient support for nanofibrous TiO_2 catalysts [173]. Such a composite material is denoted by favorable structural properties and increased catalytic activity, which results in a high degradation efficiency of organic pollutants. The above listed applications indicate the high potential of melt electrospinning for filtration/purification applications, however, the data relating to such applications still remains sparse [5].

1.5. Summary of literature review

While solution electrospinning is a widely used technique for fibre formation, the limited control on the fibre placement and the toxic solvents that are usually used during the process limit the use of products and raise concern for the environment. For these reasons, more and more researchers are moving away from the conventional electrospinning and are shifting their research towards melt electrospinning. Both processes use the same principles, but fibre formation from melt eliminates all the concerns related to solvents being not only cheaper but also more sustainable. Despite the growing interest and the ever increasing amount of publications, there still is a lot of room for further improvements.

Hierarchically structured nanofibres are gaining attention in the fields of energy and environment, particularly for air filter and fluid membrane applications [71,91,174]. High-durability filters or membranes with a high surface area and a low pressure drop are essential for such applications. Synthesizing nanofibres with diameters less than 100 nm is one of the methods used to address these issues that are becoming increasingly common. This strategy has been proven to increase the performance of the air filter by allowing a higher surface area to trap more dust particles and introducing the presence of the slip flow at the same time [175,176]. However, the durability is still questionable because, in general, nanofibres create high-density filters, in which, the pressure drop may increase rapidly, even with the presence of the slip flow phenomena. The addition of either beads or submicron-size fibres among the nanofibres is a promising way to decrease the density of the nanofibre layers [23].

The presence of beads or microfibres creates a space or pores on the filter mat, which will maintain the pressure drop of the filter. However, the presence of these pores decreases the particle collection ability of the filter, while the addition of submicron-sized fibres to nanofibre mats promises a better filter performance and a

lower pressure drop. The two-step electro spinning is a common method used to obtain these dual-sized fibres. Typically, submicron-size fibres are spun on the surface of previously spun nanofibres [23]. Therefore, this process is time-consuming, and it is also difficult to obtain a good and random mixture of nano- and submicron-sized fibres. An appropriate filter design to obtain high particle collection while maintaining the pressure drop at a low level remains a great challenge. Furthermore, a facile method to obtain the optimum morphology is also necessary [23].

For these reasons, we decided to look into the suitability of melt electrospinning for air filtration applications by optimizing the process in order to generate fibres with our preferred qualities. In order to further improve the filtration efficiency, the technique for simultaneous melt/solution electrospinning was developed. Such a technique offers one step creation of mixed size (submicro-/supermicro-) fibrous mat maximizing filtration efficiency with a relatively low air pressure drop.

2. METHODS AND MEASUREMENTS

2.1. Preparation of Fibrous Material

2.1.1. Materials in Use

Five commercially available polymers representing polyester, polyether block amide, and polyamide classes (Table 3) were selected for the melt electrospinning based on their favorable melt viscosity and flow rate as the most important parameters for a stable melt electrospinning process [153]. More detailed characteristics of each polymer used for melt electrospinning are shown in Supplemented materials (Appendix 1) [5].

Table 3. List of polymers used for melt electrospinning

Supplier	Product Brand name	Product Code	Not.	Core Chemical structure	Melt Flow rate*; g/10 min	Melting point, (°C)**	Beginning of thermal degradation (°C)*
Evonik Industries AG	Vestamid ™	L 1600	A	Polyamide 12	132	178	382
		L 1901	B	Polyamide 12	15	178	332
DSM N.V.	Arnitel®	3106	C	Co-polyester	28	185	322
Arkema Group	Rilsamid ®	AMN 0 TLD	D	Polyamide 12	44	178	254
	Pebax®	35R53 SP 01	E	Block Polyether Amide	25	135	317

*Determined by the researcher; (2.16 kg; 230 °C), ** Declared by manufacturers

Both in Experiment I and Experiment III, only Polyamide 12 (Table 3, polymer A) was used for melt electrospinning. In Experiment II, in order to test a broader range of polymers, all the polymers shown in Table 3 were used.

In order to obtain a mixed fibre size material, solution electrospinning was added to the process. For solution electrospinning, Polyamide 6/6 was chosen in order to maintain the same polymer group. PA 6/6 (Zytel ST801 nylon resin) and Formic

acid (85%) was purchased from *Sigma-Aldrich* (Darmstadt, Germany). 15% w/v Formic Acid solution of PA 6/6 was prepared and used for solution electrospinning.

2.1.1.1. Characterization of polymers

The degradation temperature for all the polymers was determined by thermogravimetry (Q50, *TA Instruments*, USA) by increasing the temperature at a rate of 10 °C/min, up to 800 °C. The melt flow rate (MFR) was tested according to ISO 1133 Standard by using a melt flow rate meter (C-Flow, *ThermoFisher*, USA) with a weight of 2.16 kg and a polymer melt temperature of 230 °C.

2.1.1.2. Filament preparations

Granular polymers were extruded into filaments following the optimum extrusion temperature below the degradation point. The degradation temperature was determined by thermogravimetric analysis (Q50, *TA Instruments*, USA), while the melt flow rate (MFR) was tested according to ISO 1133 Standard by using a melt flow rate meter (C-Flow, *ThermoFisher*, USA) [5].

2.1.2. Melt electrospinning

Polymer fibre mats were formed by means of a prototype fibre printing apparatus designed and constructed at the Department of Environmental Technology, Kaunas University of Technology, based on the principles of additive printing and melt electrospinning (Fig. 4). The polymer was fed from a coil (Fig. 4 item 2) in a filament form via the filament feeder (Fig. 4 item 4) to a heating system consisting of a heating element and a nozzle (Fig. 4 items 7; 8) mounted on a movable arm (Fig. 4 item 10). Such a setup is unique and allows for the control of the tip-to-collector distance, voltage, and temperature for melting a polymer. A high-voltage source (Fig. 4 item 1) was connected to the changeable nozzle in order to form a positively charged electrode. A spinning collector drum (Fig. 4 item 9) served as a grounded electrode. The high-voltage apparatus, the feeder, the heater, and both the mechanic arm movement and collector rotation motors (Fig. 4 items 5 and 6) were managed by the appropriate controllers (Fig. 4 item 3). To ensure stable environmental conditions controlled by the external air conditioning system, all the parts except for the polymer coil, the high-voltage apparatus, and the control unit, were mounted in a transparent enclosure (Fig. 4 item 11) [5].

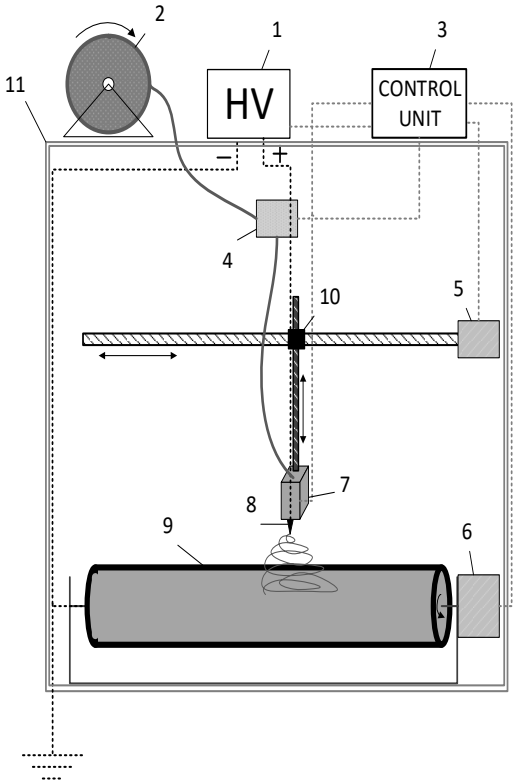

Figure 4. Schematics of fibre printing melt electrospinning apparatus

2.1.3. Combined electrospinning

Polymer fibre mats were formed with a prototype fibre formation (printing) apparatus designed and constructed at the Department of Environmental Technology, Kaunas University of Technology, based on the principles of additive printing and melt electrospinning in combination with solution electrospinning (Figure 5). For the melt electrospinning part, a polymer was fed from a coil (Figure 5 item 2) in the filament form via the filament feeder (Figure 5 item 4) into a heating system consisting of a heating element and a nozzle (Figure 5 items 7; 8) mounted on a movable arm (Figure 5 item 10). Such a setup is unique and allows for controlling the tip-to-collector distance, the voltage, and the temperature required to melt the relevant polymer. For solution electrospinning, the polymer solution was supplied with a syringe pump (Figure 5 item 11) to a stationary holder with a needle attached (Figure 5 items 12; 13). Two high voltage sources (Figure 5 item 1) were mounted. The first one was connected to the changeable melt electrospinning nozzle, whereas the second one was connected to the solution electrospinning needle in order to form a positively charged electrode. A spinning collector drum (Figure 5 item 9) served as a grounded electrode. The high voltage apparatus, the feeder, the heater and both mechanic arm

movement and collector rotation motors for melt electrospinning (Figure 5 items 5 and 6) were managed by the appropriate controllers (Figure 5 item 3). In order to ensure stable environmental conditions controlled by the external air conditioning system, all the parts except for the polymer coil, the high voltage apparatus, the control unit, and the syringe pump, were mounted in a transparent enclosure (Figure 5 item 14).

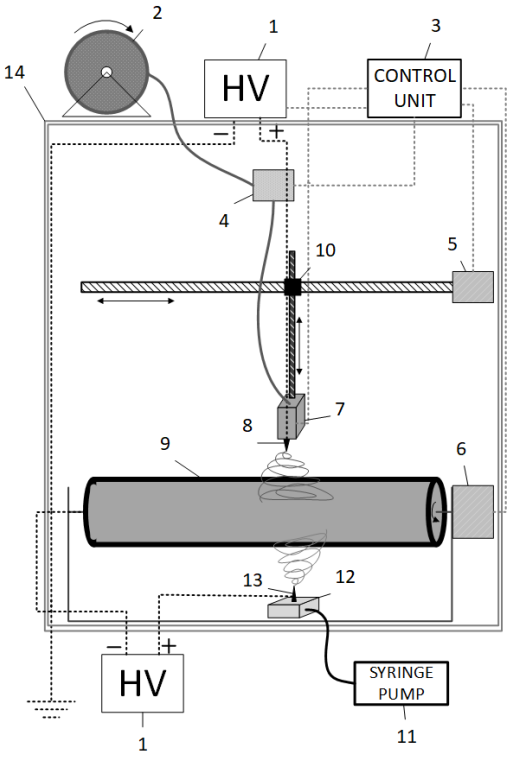

Figure 5. Schematics of combined melt electrospinning and solution electrospinning apparatus

2.1.4. Experiment I

The screening experiment (D-optimal) was performed by using *MODDE 10* (*Umetrics*, Sweden) software. The tip-to-collector distance (TCD) (1 cm; 4.75 cm; 8.5cm), the melting temperature (260 °C; 291 °C; 353°C) and voltage (8 kV; 19 kV; 30 kV) were chosen as the main variables. In total, 75 runs, including quintuplicates, were performed. For all the tests, the polymer feeding speed (0.1 g/min) and the diameter of the nozzle tip (0.3 mm) were constant, while the collector and the needle arm were both kept stationary. The duration of the primary sample collection was 30 s [10].

After optimization, 6 fibrous mats were formed. In order to evaluate the reproducibility, 5 samples were made duplicating the primal experiment conditions.

The last sample was formed by using the distance, voltage and temperature which were generated as optimal by the *MODDE10* built-in function *Optimizer*. For all the mats, the rotation of the collector was on, at the drum surface speed of 10 cm/s, and the duration of spinning was 3–5 min. All the samples for both stages of experimentation were prepared by using aluminum foil as the base for fibre collection [10].

2.1.5. Experiment II

An experimental design was applied to assess the effects of various melt electrospinning operational parameters on the fibre formation. The D-optimal-interaction model, available within the *MODDE 10* software (*Umetrics AB*, Sweden), was set up by means of 14 runs (denoted by N1 to N14) containing 10 original experiments and triplicate middle points for each polymer. 5 different polymers (Table 3) were used during this experiment. The *Pebax* filament appeared to be too soft for efficient feeding and caused polymer accumulation, degradation, and clogging, as a result of which, the experiments with polymer E were repeated with additional runs (denoted by N15E to N25E). A total of 68 polymer mats were formed and subsequently analyzed. The voltage, the nozzle diameter, and the feeding rate were defined as the variable operational parameters with the greatest influence on the morphology of the fibrous mats, while the collector drum rotation velocity (10 cm/s), the nozzle horizontal speed (1 cm/s), the tip-to-collector distance (5 cm), and the polymer melting temperature (approximately 30 °C below the melting point) were maintained constant. The mats were formed on a nonwoven fibrous polypropylene support, with sufficient mechanical stability, and a low pressure drop. All the mats were formed during 1 h of spinning; the resulting surface density varied from 26 to 122 g/m^2. In order to increase the packing density, the mats were processed by hot pressing at a temperature of 90 °C and under a pressure of 0.4 MPa. The fibre formation duration was limited to 60 min in order to avoid variations in the voltage owing to the thickening layer. Subsequently, a higher thickness of the filtering layer (expecting to increase the filtration efficiency) was achieved by stacking layers of material of the same mat [5].

2.1.6. Experiment III

The experimental design was based on the results obtained in prior research [10,177]. Numerous studies showed that higher voltage results in thinner fibres, thus, in our research, we maintained stable 25kV voltage both for the solution and melt electrospinning. The feeding rate and the tip-to-collector distance were defined as parameters exerting a high influence on the morphology of fibrous mats, therefore, several variations of feed rates (0.6 g/h and 1.8 g/h) and tip-to-collector distances (50 mm and 70 mm) were applied. The rotation velocity (10 cm/s), the horizontal speed of the nozzle (1 cm/s), the nozzle diameter (0.4 mm), and the polymer melting temperature (300°C) were kept constant. The mats were formed on a nonwoven fibrous polypropylene support having sufficient mechanical stability and a low

pressure drop. The electrospinning parameters and process combinations are presented in Table 4.

Polyamide 12 (Table 3 A) was used for melt electrospinning, whereas Polyamide 6/6 was used for solution electrospinning, thus sticking to the same polymer family.

Table 4. Electrospinning parameters and process combinations for combined electrospinning

Code				
M	Melt electrospinning			
	I	II	III	
	Voltage – 25 kV Feed rate – 0.6 g/h Tip to Collector Distance – 50 mm Needle diameter – 0.4 mm	Voltage – 25 kV Feed rate – 1.8 g/h Tip to Collector Distance – 50 mm Needle diameter – 0.4 mm	Voltage – 25 kV Feed rate – 0.6 g/h Tip to Collector Distance – 70 mm Needle diameter – 0.4 mm	
S	Solution electrospinning			
	Voltage – 25 kV; Feed rate – 0.2 ml/h; Tip to Collector Distance – 100 mm; Needle diameter – 0.02 mm			
	Process combinations			
MS	Melt electrospinning (0–60 min) + Solution electrospinning (0–60 min)			I II III
M_MS_M	Melt electrospinning (0–60 min) + Solution electrospinning (15–45 min)			I II III
MS_M	Melt electrospinning (0–60 min) + Solution electrospinning (0–30 min)			I II III

As a basis for comparison, the experiments were started with the formation of distinct melt and solution electrospinning mats. The combined electrospinning was performed in three variations: MS – simultaneous melt and solution electrospinning; M_MS_M – permanent melt combined with periodic solution electrospinning in the middle of the process; MS_M – permanent melt combined with periodic solution electrospinning at the beginning of the process. Also, three variations of process parameters were applied to melt electrospinning, while solution electrospinning was performed with the same set of parameters. In order to avoid any variation of voltage due to the thickening layer [19], the duration of fibre formation was limited to 60 min. Three sets of melt electrospinning parameters were combined with three temporal variations of solution electrospinning. Altogether, 13 unique polymer mats were fabricated and subsequently analyzed.

2.2. Mat characterization

The morphology of the mats obtained during Experiments I and II was evaluated by using scanning electron microscopy (SEM) images (*Carl Zeiss EVO MA10*, Germany). At least 10 images were obtained from one sample (1 cm^2) in random locations.

Fibre samples for morphological analysis were prepared by dipping their strips into liquid nitrogen for 30 s and cutting them in half in order to obtain a clear cross section with no alterations to the morphology. The morphology of the samples was evaluated by using Scanning Electron Microscopy (SEM) (*Carl Zeiss EVO MA10*, Germany). For the calculation of numerical fibre ratios (the ratio between the number of submicrometric (<1 μm) and supermicrometric (≥1μm) fibres), from 5 to 10 images (depending on the thickness of the mat) were made. Each image was divided into smaller segments; each segment was marked vertically with three lines. Every fibre crossing each line was counted, and the average values were derived from the three data sets (*ImageJ*, *NIH*, USA). The schematic of the fibre count is shown in Figure 6.

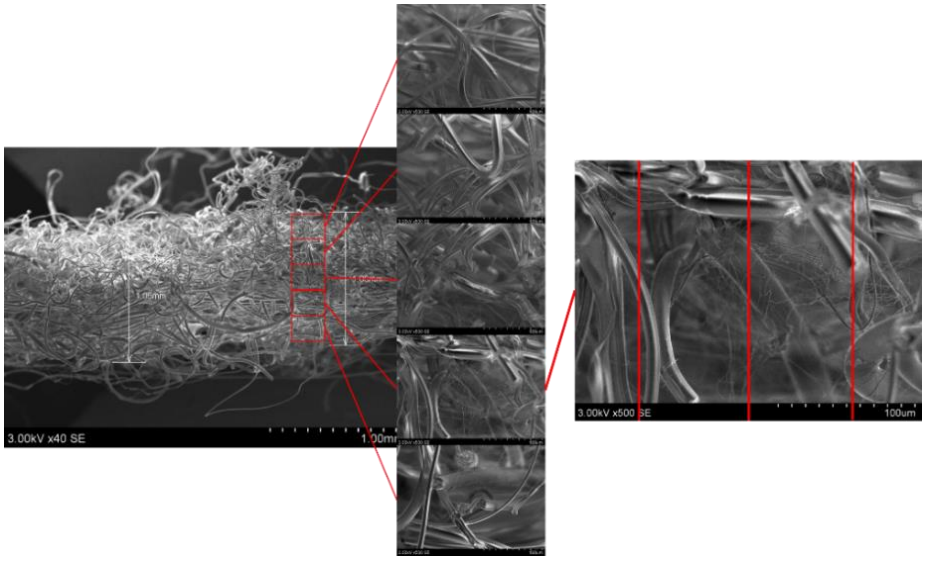

Figure 6. Schematic of fibre count

The morphological composition of the obtained images was observed and analyzed in terms of statistical distributions of the fibre diameters in randomly selected areas of 100 μm^2 (*ImageJ*, *NIH*, USA). The median, the geometric mean, and the interquartile range (IQR) were calculated from the obtained distributions. IQR was chosen as one of the descriptive parameters for the fibre size as, due to the offset data and plenty of outliers, the mean or the median by itself is not capable of fully representing the fibre size distribution. Such a parameter shows the difference between the first and third quartiles ($IQR=Q_3-Q_1$). In our particular case, the bigger IQR means the larger amount of submicrofibres in the polymer mats. The data was

subsequently processed by spreadsheet software (*Excel 2016*; *Microsoft Corp*., USA) [5].

2.3. Testing of filtration efficiency

2.3.1. Experiment II

The obtained fibre mats were subjected to aerosol filtration tests. Considering that electrospinning may impose a substantial electrostatic charge on the mats, they were tested under both 'as-manufactured' and 'charge removed' conditions. The electret charge was eliminated by submerging the mats in isopropanol (≥98%, *Sigma Aldrich*, USA) for 10 min, followed by drying for 48 h until the filter mass reached its original value (Schumacher, Spiegelhoff, Schneiderwind, Finger, & Asbach, 2018). The experimental setup was similar to that described by Matulevicius *et al*. (2016) (Fig. 7). Numerous studies have demonstrated that the shape of the aerosol particle could affect the filtration efficiency due to owing to the particle motions along the fibre (Boskovic *et al*., 2007, p. 6826; Boskovic, Agranovski, Altman, & Braddock, 2008; Miaskiewicz-Peska & Lebkowska, 2012; Science and technology of polymer nanofibres, 2007). It is known that spherical particles result in a higher filtration efficiency compared to cubic particles (Boskovic *et al*., 2008). Therefore, NaCl was selected to test the filtration efficiency as its aerosol forms cubic particles with rounded edges. With its intermediate shape, NaCl is well suited to average the filtration efficiency [5].

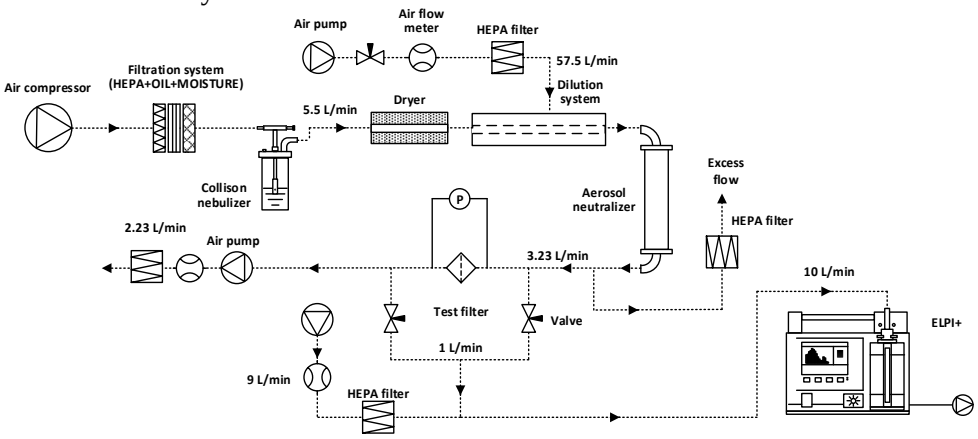

Figure 7. Experimental setup for filtration efficiency and pressure drop measurements

NaCl aerosol was generated by being dissolved in deionised water (0.1% w/v) and fed through a Collison nebuliser (*Model CN 24 J*, *BGI Inc*., USA), and then being dried with a diffusion dryer packed with silica gel, and diluted with dry air, followed by charge equalization by using a bi-polar neutralizer (*3054 A*, *TSI Inc*., Germany). Each sample mat was investigated by taking three random 37 mm diameter circle specimens with a further filtration efficiency and pressure drop test against the polydisperse aerosol particles to follow. The upstream and downstream concentrations of the particulate matter were measured by using an Electrical Low-

Pressure Impactor (*ELPI+*, *Dekati Ltd*., Finland). The pressure drop before and after the sample media was indicated by a pressure sensor (*Model P300-5-in-D, Pace Scientific Inc*., USA) at a face velocity of 5.3 cm/s [19,5].

2.3.2. Experiment III

The obtained fibre mats were subjected to aerosol filtration tests. Considering that electrospinning may impose a substantial electrostatic charge on mats, they were tested in both 'as-manufactured' and 'charge removed' conditions. Electret charge was eliminated by submerging the mats into isopropanol (≥98%, *Sigma Aldrich*, USA) for 10 minutes and then drying for 48 hours until the mass of the filter reached its original value [5,178].

Filtration efficiency and pressure drop tests were carried out at the *Institut für Energie und Umwelttechnik* (IUTA, Duisburg, Germany). In order to test the removal efficiency of the fibre mats for a wide range of particle sizes, two setups (S1 and S2) were used (Figure 3). NaCl particles were generated in setup S1 (Figure 3, S1) from 5% v/w aqueous solution. The generated aerosol was dried and neutralized. The number particle size distribution was measured by using both an optical particle sizer (OPS) -Fidas® Frog (0.3-10 μm, *Palas Gmb*, Karlsruhe, Germany) and a SMPS – a Scanning Mobility Particle Sizer (U-SMPS) 3050 XB, consisting of a DEMC XB control unit, a Differential Electrical Mobility Classifier (DEMC) 3000 (0.01–1.4 um) coupled with a Condensation Particle Counter (UF-CPC) 50, all from *Palas Gmb*, Karlsruhe, Germany. The two instruments and a pump sampled in parallel through a 4-way TSI 3708 flow splitter behind the filter holder containing the fibre mat were used for the tests.

OPS measures simultaneously the environmentally relevant mass fractions PM_1, $PM_{2.5}$, PM_4, PM_{10}, TSP as well as the particle number and the particle size distribution within the particle size range of 0.18–100 μm. By providing fine dust values with high time resolution, the operator receives comprehensive information for the evaluation and assessment of the fine dust pollution for the investigated application. It uses the recognized measurement technology of optical light scattering of single particles and is equipped with a LED light source with high intensity (dp min = 180 nm) [179,180].

The SMPS spectrometer is a nanoparticle sizer capable of measuring the size distribution of airborne submicron particles with accuracy and precision. It combines electrical mobility sizing with single-particle counting in order to deliver nanoparticle concentrations in discrete size channels. The size resolution capability of the SMPS is as high as 128 channels per decade, resulting in up to 192 channels in total [179,181].

In order to test larger aerosol particles, a second setup (Figure 3 S2) was used. Due to the specifications of the aerosol generator and filter testing system, KCl was used for particle generation. Particles were generated in S2 test setup by using a large-particle aerosol generator 8108 (*TSI*, *Shoreview*, USA) from 12.5% KCl aqueous solution. This aerosol generator meets the requirements of the established ISO/TS 11155-1 and ASHRAE 52.2 test codes, as well as the proposed ISO 16890 Part 2 code. The test aerosol was fed into a test rig according to ISO 16890. Only a small part of the generated aerosol was used to test the retention efficiency of the fibre mats.

The particle number size distribution in raw and clean gas was measured only with the Fidas® Frog OPS (Figure 3 S2). The measurement was performed by switching raw/clean gas three times for each sample. All the measurements were performed at a face velocity of 5.3 cm/s.

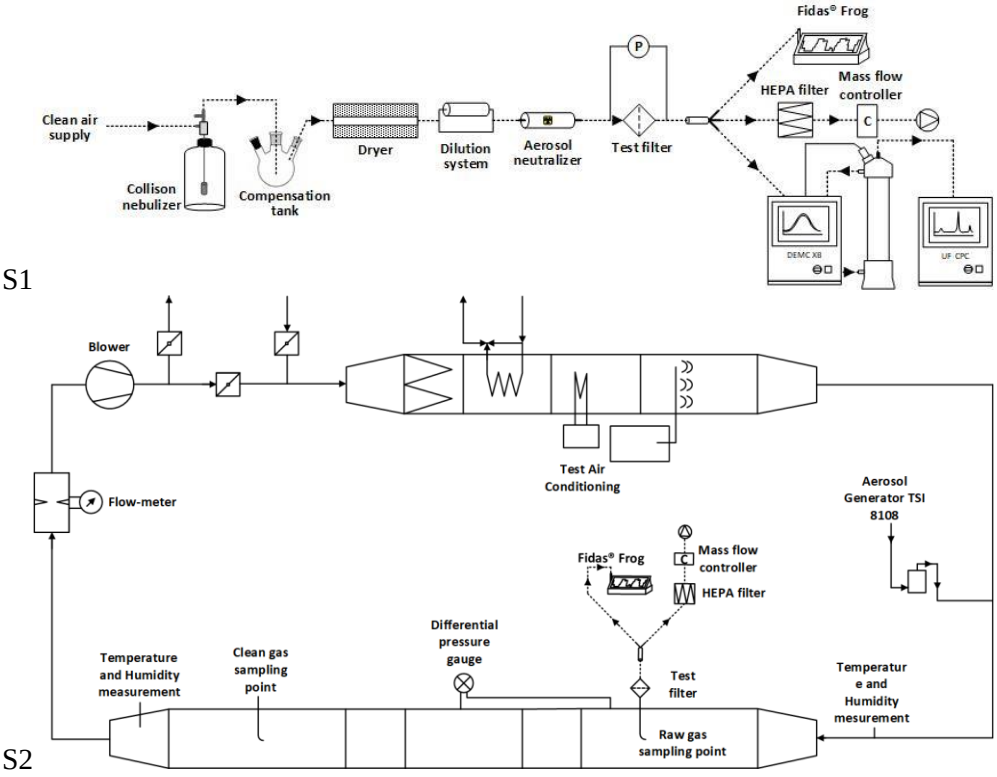

Figure 8. Experimental setups for filtration efficiency and pressure drop measurements (S1 – small NaCl particles; S2 – large KCl particles)

2.4. Characterization of filter media

The filtration efficiency of ePM1 was calculated according to ISO 1689-1:2016 Standard. Other parameters, such as the packing density, the porosity, and the quality factor were calculated by using Equations 9–11.

Due to the specificity of the performed research, the author introduced a special unit of measurement – the Numerical Fibre Ratio (NFR) which shows the ratio between the number of submicron (<1 μm) and micron (≥1μm) fibres. The ratio should serve as an indicator of the fibre structure in relation to the filtration performance parameters.

2.5. Quality assurance

The experiments were conducted with the aim of minimizing both random and systematic errors. The random error was minimized by introducing the randomization of the run order within the entire experimental design. This primarily addresses the

repeatability issue that occurs owing to the fluctuating environmental conditions. The ambient temperature and humidity remained stable at 21 ± 1 °C and 65 ± 5%, respectively. During the experiments, all the mat formations were repeated three times. Filtration efficiency measurements were performed by switching raw/clean gas three times for each sample, while ultimately providing the average value. Moreover, the consistency of the experiments was ensured by introducing samples of known efficiency filters, and one empty sample was analyzed for every 10 samples [5].

The systematic error was minimized by ensuring instrument calibration and verification. The Electrical Low-Pressure Impactor (*ELPI+, Dekati Ltd*., Finland), the pressure sensor (*Model P300-5-in-D, Pace Scientific Inc*., USA), and the flowmeters were calibrated by the manufacturers, while the latter was additionally checked by the metrological centre [5].

The results of the analyses for experiments I and II were statistically processed by using *MODDE 10* (*Umetrics AB*, Sweden), *Microsoft Excel*®, and *SPSS* (*IBM Corp*.) software. Descriptive statistics was used for representing the parameter effects on the fibre diameter [5].

3. RESULTS AND DISCUSSION

3.1. Primary Melt Electrospinning Parameter Testing (Experiment I)[1]

The main process parameters of melt electrospinning are the polymer feed rate, the tip-to-collector distance, the collector speed, the melting temperature, and the voltage. There are a number of studies considering the effects of different process parameters on the fibre diameter and the shape fidelity of electrospun structures [157–159]; however, a few researches explored their counterinfluence and interactions [120]. Because of that, determining the influence of the process parameters on the shape and the diameter of the deposited fibres is crucial in predicting the relevant set of process parameters in order to achieve the desired fibre diameter.

3.1.1. Fibre formation by customized electrospinning setup

The performance of fibre formation by customized electrospinning setup was investigated by microscopic analyzing of the produced fibre membranes (Figure 9). Five distinct types of fibre membranes representing different combinations of the process parameters indicated the following trends.

[1] The data described in Chapter 3.1. was published in the article "Formation of PA12 fibres via melt electrospinning process: parameter analysis and optimization" 2019, Buivydiene *et al.* [10]

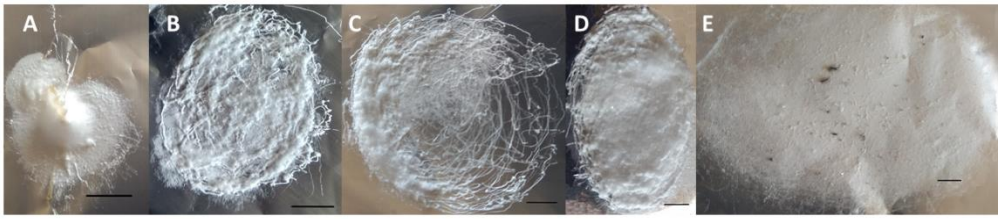

Figure 9. Microscopic pictures of the produced fibre membranes (scale bar – 5mm):
A (N3): Tip-to-collector distance – 1.0 cm, melt temperature – 349 °C, voltage 8kV;
B (N17): Tip-to-collector distance – 4.75 cm, melt temperature – 294 °C, voltage 19kV;
C (N14): Tip-to-collector distance – 4.75 cm, melt temperature – 292 °C, voltage 30kV;
D (N10): Tip-to-collector distance – 8.5 cm, melt temperature – 298 °C, voltage 19kV;
E (N8): Tip-to-collector distance – 8.5 cm, melt temperature – 354 °C, voltage 30kV.

The tip-to-collector distance as small as 1 cm results in the fibre deposition diameter of 0.5–1 cm, whereas a higher distance results in a larger diameter of the deposit and variations between its shape (when TtCD is 4.75 cm, the diameter of fibre accumulation equals ≈ 2–4 cm; TtCD = 8.5 cm Ø ≈ 3–8 cm). It was observed that when the tip-to-collector distance is small, fibres tend to form a bamboo hat structure (Fig. 9A). According to Huaizhong Xu *et al*. (2017), changes in the topography of the fibrous layer of a membrane could be due to the jet break-up. Due to Rayleigh instability, the polymer melts break up into droplets. The curve peak in the middle of the polymer layer becomes higher as the breakup frequency increases since the broken jet with a heavier weight and a lower bending stiffness easily accumulates at the centre of the target [20].

The difference in the deposition diameter within the same TtCD is influenced by the temperature of melt and the applied voltage [20]. With an increase of the applied voltage, the fibre membrane on the target becomes larger (Figure 2 B and C). This could be attributed to a more pronounced whipping motion. Shu-Xin Yu *et al*. (2018) noted that the PLA melt electrospun fibre yield increased while increasing the applied voltage [157]. As the viscoelastic force of the molten polymer decreases by increasing the processing temperature, it results in a higher flowrate of the molten polymer. Due to such a combination of the variables, a widely spread thin layer of the fibre was formed.

An increase of the melt temperature resulted in a considerably larger deposition area of the fibre membrane (Figure 9 D and E). Huaizhong Xu *et al*. (2017) argues that a high melt temperature is favorable for a larger size of the fibre membrane due to the high flexibility of the thin jet. With an increase of the melt temperature, the jet gets thinner, and the maximum axial velocity of the jet increases [20]. The same trends were observed in our work.

3.1.2. Distribution of fibre diameter

The experimental process parameters and the obtained fibre diameter values as well as the type of the fibre size distribution data is presented in Table 5. Due to the different tip-to-collector distances (TtCD), temperatures and voltages, the obtained

melt electrospun mats revealed a broad range of fibre diameters. The average fibre diameter ranged from 2.40 ± 0.3 to 14.97 ± 2.43 μm, respectively, whereas the median of the fibre diameters varied from 2.48 to 15.10 μm.

Table 5. Experimental process parameters and obtained fibre diameter values

Sample ID	TtCD, cm	Temperature, °C	Voltage, kV	Average Diameter ±SD, μm	Diameter Median, μm	Fibre size distribution type
N1	1	261	8	14.97 ± 2.43	15.10	Normal
N2*	8.5	230	8	–	–	–
N3	1	349	8	2.73 ± 0.72	2.23	Lognormal
N4*	8.5	353	8	–	–	–
N5*	1	230	30	–	–	–
N6	8.5	267	30	4.48 ± 0.17	4.45	Normal
N7*	1	353	30	–	–	–
N8	8.5	354	30	5.44 ± 0.93	5.07	Lognormal
N9*	1	291.5	19	–	–	–
N10	8.5	298	19	4.50 ± 0.66	4.20	Lognormal
N11	4.75	263	19	2.94 ± 0.33	2.49	Lognormal
N12	4.75	353	19	3.20 ± 0.81	2.64	Lognormal
N13	4.75	291.5	8	9.72 ± 0.49	9.53	Normal
N14	4.75	292	30	2.40 ± 0.35	2.48	Normal
N15	4.75	291	19	4.70 ± 0.62	4.54	Normal
N16	4.75	290	19	2.60 ± 0.77	2.19	Lognormal
N17	4.75	294	19	4.79 ± 0.82	4.45	Lognormal

* Non-consistent formation of fibres

The SEM analysis of fibre mats revealed two distinct patterns of the fibre diameter distribution: normal (Fig. 10, A and B) and lognormal (Fig. 10, C and D). It was observed that more than a half of the samples exhibited a well-pronounced lognormal fibre size distribution. All the lognormal samples had a higher peak in the smaller side of the fibre diameter with a lower count of large diameter fibres.

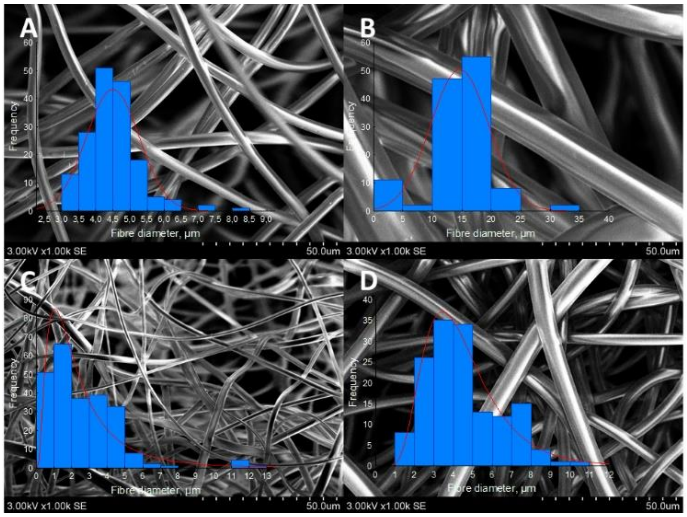

Figure 10. Stereomicroscopy images and fibre diameter histograms (magnification ×1000): A – N6; B – N1; C – N16; D – N10

Even though A and B samples (Fig. 10) had similar fibre diameter distributions, the median of the fibre diameter differed significantly (by 3.4 times). Our experimental results correspond to the findings of other authors who state that variations between the fibre size distributions are commonly observed for both solution (Park *et al*., 2018; Amin, Merati, Bahrami, & Bagherzadeh, 2016; Beigmoradi, Samimi, & Mohebbi-Kalhori, 2018) and melt electrospun fibres (Nazari & Garmabi, 2018; Li *et al*., 2015). This could be attributed to the high voltage, the low polymer viscosity, or to the specific qualities of the polymer. As it could be seen from the experimental results (Table 5) there is no single dominant parameter but rather a combination of parameters which results in specific distributions of the fibre diameter.

3.1.3. Impact of process parameters on fibre diameter

One of the objectives of the screening experiment was to determine the significance of different melt electrospinning process parameters on the fibre diameter. The general observed trend was that an increase of the investigated process parameters resulted in a decrease of the fibre diameter.

The tip-to-collector distance and the melt temperature had a moderate effect on the fibre diameter, while voltage was the most pronounced parameter. Similar findings were reported in numerous studies both for melt *(Yu et al*., 2018; Shen, Liu, Deng, Yao, & Xia, 2016; Ko, Ahsani, Yao, & Mohtaram, 2016) and solution (Zeng *et al*., 2018; Abolhasani *et al*., 2018; Senthil & Anandhan, 2013) electrospinning. It was noted that voltage exerted a greater influence on the fibre diameter between 8 to 10 kV, and, with a further increase, the decrease of the fibre diameter was subtler. Several authors reported that, in some instances, high values of voltage could result in a slight increase of the fibre diameter (Yu *et al*., 2018; Shen *et al*., 2016). Shen *et al*. (2016) argued that a further decrease of the fibre diameter with a higher voltage

could be attributed to the electric field force being too strong, therefore, the dropping force of the jet becomes greater than the tensile force, and the jet stretching is thus unstable [104].

An increase of the melting temperature caused a decrease of the fibre diameter, however, when the melting temperature reached ≈ 300 °C and went higher, it had no significant effect on the fibre diameter decrease. This is beneficial as a lower temperature of the process requires less energy for achieving high quality fibres. In the research by Shu-Xin Yu *et al*. (2018), it was reported that, with the temperature increasing from 200 °C to 240 °C, the average diameter of melt electrospun polylactic acid fibres decreased from 58.46 to 2.96 μm. Also, beaded fibres and microspheres were collected when the spinning temperature was further increased to 260 °C [157]. In our case, the temperature of melt did not exceed the degradation point, thus, beaded fibres were not observed.

The dependencies among each process parameter and the median of the fibre diameter are presented in Figure 11. Based on the presented dependencies, we developed a combined response-surface plot of the process parameters for the production of fibres with the desired fibre diameters (Fig. 12). Similarly, the optimization of the electrowriting process parameters was performed by Dayan *et al*. (2018).

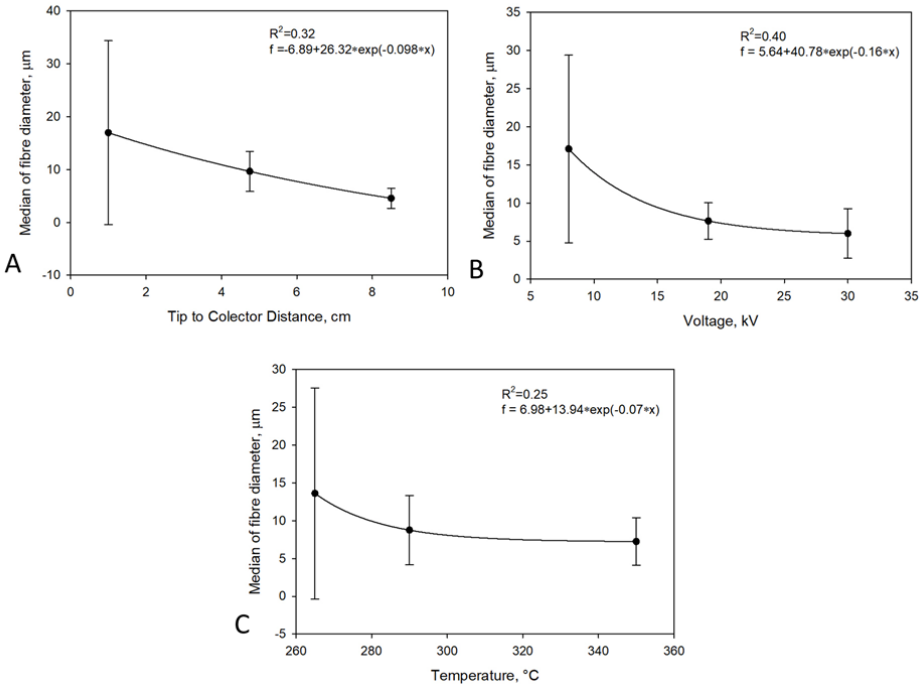

Figure 11. Different parameter effect on fibre diameter (A – Tip-to-collector distance; B – Voltage; C – Temperature

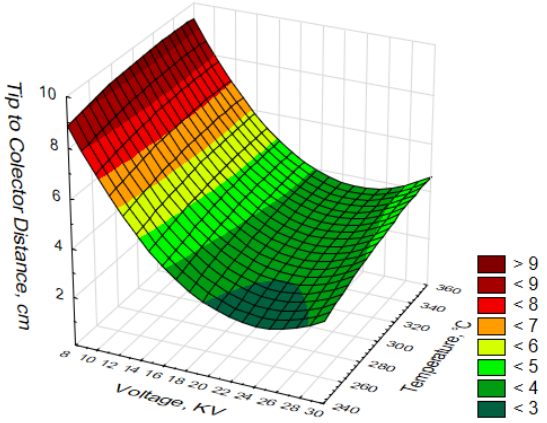

Figure 12. Response-surface plot of process parameters for production of fibres with the desired fibre diameters (different fibre diameters, µm, are represented by different colors)

When all the three electrospinning parameters were combined into a response surface plot (Fig. 12), both voltage and TtCD affected the fibre diameter more than the temperature of melt. TtCD showed the most significant effect on the fibre diameter in combination with the analyzed parameters. The diameter quickly decreased with the shorter distance up to the point of 2 cm, and then slightly increased. The increase of the fibre diameter that is seen with the minimum values of TtCD could be attributed to the limitation of voltage that could be safely applied without forming the discharge.

3.1.4. Optimization of melt electrospinning parameters

Based on the results of the combined effect of the process parameters on the fibre diameter, we reproduced the screening experiment. In order to adjust the input values of the process parameters, *MODDE 10* (*Umetrics*, Sweden) software with the built-in function *Optimizer* was applied. The input parameters for the five screening experiments were modified accordingly, and one experiment was assigned the new input values. The optimized input parameters as well as the obtained fibre diameter and the median fibre diameter values are presented in Table 6.

Table 6. Input process parameters and obtained fibre diameter values of the reproduced screening experiment

No	Code	TtCD, cm	Temp. °C	Voltage, kV	Average fibre diameter ± SD, µm	Median fibre diameter, µm
1	N15_II	4.75	263	19	4.35±0.48	4.48
2	N11_II	4.75	290	19	3.07±0.52	3.02
3	N14_II	4.75	290	26	2.59±0.25	1.94
4	N12_II	4.75	348	19	2.60±0.57	2.46
5	N8_II	8.5	347	30	4.50±1.13	5.14
6	Optim.	3	348	19	1.53±0.22	1.27

The SEM analysis of the reproduced samples revealed a high variation of the fibre diameters (Fig. 13). The average fibre diameter ranged from 1.53 ± 0.22 to 4.50 ± 1.13 μm, respectively, whereas the median of the fibre diameter varied from 1.27 to 4.48 μm. The slight differences of the fibre diameter between the first and the second experiments could be attributed both to the standard deviation and to the collector drum rotation. As the collector rotates, it reveals a new surface with no fibre deposition; thus, the process is not affected by the insulating qualities of polymeric fibres.

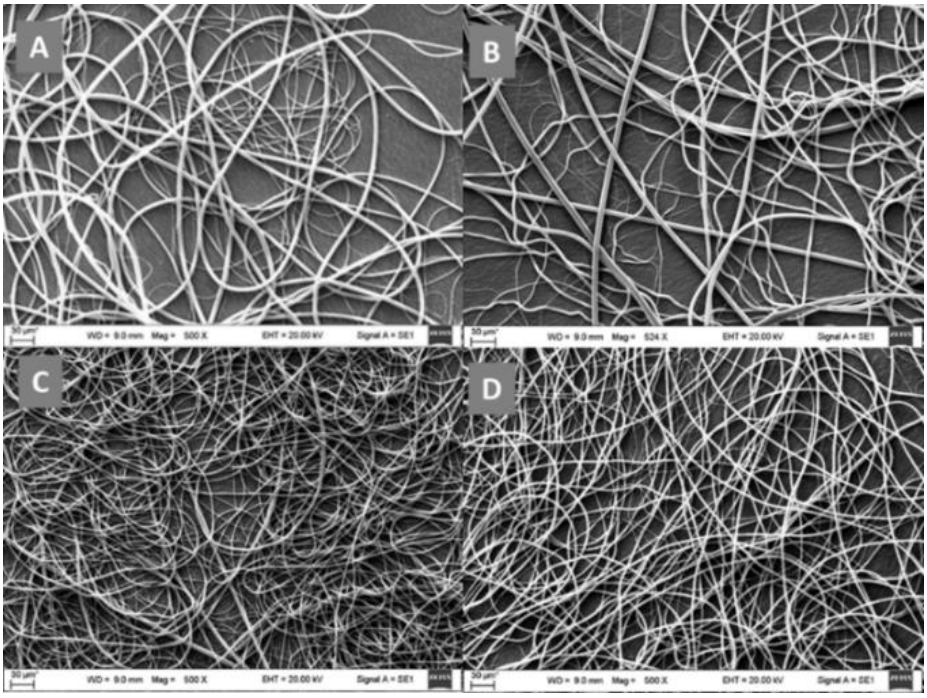

Figure 13. SEM images of repeated samples with a rotating drum (A – N8_II; B – N11_II; C – N12_II; D – N14_II)

As it is seen in the SEM images of Figure 13 (A, B) and Figure 14, some cases showed extreme variations in the fibre size diameter (from 0.81 μm to 15.98 μm in case of N11_II). This variation in the fibre size could be attributed to the jet instabilities caused by a combination of high voltage and low viscosity due to the higher temperature of melt.

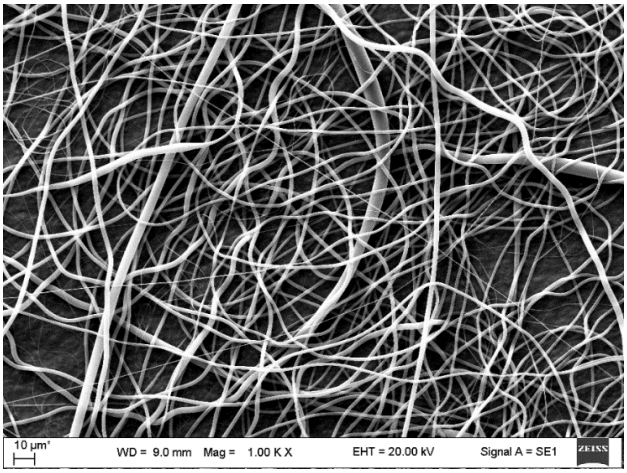

Figure 14. SEM image of polymer mat prepared with optimized conditions

The lowest fibre diameters were identified for sample 'Optim.' (Fig. 14) when a high temperature (348 °C), medium voltage (19kV), and a relatively small Tip-to-collector distance (3cm) were selected. The above outlined combination of the process parameters ensured low viscosity of the polymer and allowed sufficient whipping motion. Because of that, a decrease of the average fibre diameter by 1.06 µm was observed between the 'Optim.' and N14_II samples (Table 6) which had the smallest average fibre diameter out of all the reproduced membranes.

While this analysis shows that the simple screening process and the linear regression model could help to achieve the optimal conditions for the melt electrospinning process, there is still more work ahead regarding the other process parameters such as the nozzle size, the ambient temperature, or the ambient air humidity. These parameters shall be analyzed more thoroughly in the following chapter.

3.2. Characterization of air filter material printed by melt electrospinning (Experiment II)[2]

3.2.1. Morphology of filter mats

The obtained melt electrospun mats revealed a broad range of fibre morphologies which were further grouped into several categories, as summarized in the supplementary material (Appendix 2). The most common morphology exhibited a high dispersion of fibre diameters and was thus referred to as 'Dispersed' (Figure 15-A). Such a structure has been reported to occur when the whipping motion of fibres travelling between electrodes is strong [133,189–191]. Dispersed fibrous structures were

[2] The data described in Chapter 3.2. was published in article "Formation and characterisation of air filter material printed by melt electrospinning" 2019, Buivydiene *et al.* [5]

observed in all the analyzed polymer mats, however, this pattern was dominant among the polyamide-based mats.

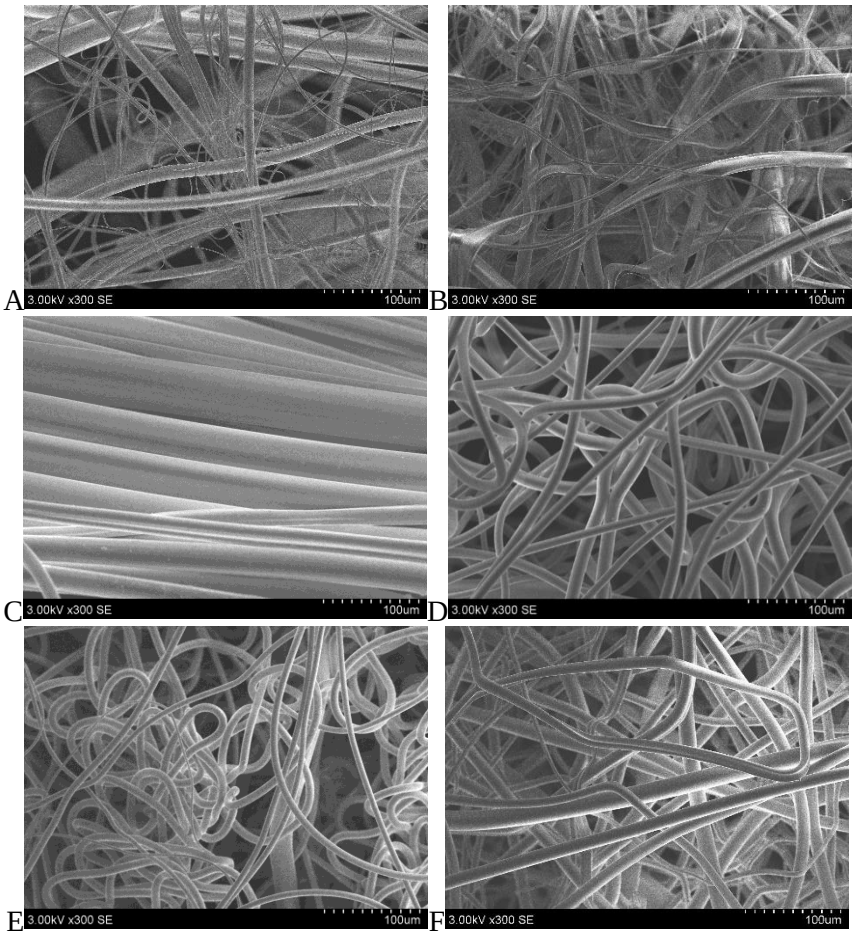

Figure 15. SEM images of typical morphologies (A – disperse (N9D); B – ribbon (N7B); C – parallel (N25E); D – normal (N4A); E – suppressed whipping (N8A); F – glued (N3C)

Another distinct morphology included flat-structured fibres and was thus referred to as 'Ribbons' (*Figure 15*-B). Ribbon structures have been reported mainly during solution electrospinning and are associated with the formation of a mechanically strong 'skin' being formed on the jet, thereby preventing the diffusion of the remaining solvent. During the continuing solvent evaporation, the skin transforms into a hollow tube and collapses into a flat ribbon [192]. Melt electrospinning does not use solvents, thus, such evaporation should not determine the mechanism for the ribbon formation. It is more likely that a droplet with a larger surface area will form on the nozzle due to the combination of the medium or large nozzle tip diameters (0.4 to 0.5 mm) and the high feed rate (20 g/min). As it is exposed to a lower ambient

temperature, the droplet cools down and its outer layer solidifies thus forming a shell on the outer layer of the polymer, while the jet core is spun according to a different regime. The 'ribbon' morphology was mostly observed as secondary, rather than dominating.

The morphology involving parallel-formed fibres (referred to as 'Parallel', *Figure 15*-C) generally occurred under low voltage conditions, with a high polymer feed rate, or with a combination of both. In the cases of overly high polymer viscosity, the electric field is not capable of initiating sufficient formation of fibre jets or whipping, thereby resulting in a process of simple drawing of the melt as opposed to electrospinning. Thus, a mat of uniform parallel aligned fibres with relatively large diameters was formed as a result of the collector drum rotation and arm movement (Lyons & Li, 2014; Xu *et al*., 2017). The same trend was observed in our case, and a large nozzle diameter was common for all the cases in which such a structure was observed. Polymers C, D, and E exhibited tendencies of 'parallel' fibre alignment in 3 to 5 mats, whereas, for E, this structure dominated (5 out of 12 cases). Again, the dominance of 'parallel' structures to a major extent was influenced by the melt electrospinning parameters.

The three morphologies described above represent the majority of the formed structures, while several less frequent ones occurred at the same time. A normal fibre diameter distribution (*Figure 15*-D) was observed in only eight cases. This was most common for C, in which, four mats with this morphology were noted. Interestingly, this polymer had the widest range of morphologies, where all six distinctive morphologies were dominant in one or more cases. As no clear pattern of formation conditions influencing such a fibre distribution could be identified, it appears that the polymer itself and its molecular structure could have been the main factor. Such a distribution has been reported for solution electrospinning *(*Deitzel *et al*., 2001; Lian & Meng, 2017; Casasola, Thomas, Trybala, & Georgiadou, 2014; Liu & Tang, 2007), while lognormal fibre diameter distributions are more common in melt electrospinning *(*Chen *et al.*, 2016; Guo, Zhou, & Lv, 2013; Karahaliloglu *et al*., 2014; Lyons *et al*., 2004; Wang *et al*., 2014).

Both 'supressed whipping' and 'glued' structures (*Figure 15*-E and F) were observed in only a few mats and were dominant in only a few samples. 'Suppressed whipping' is similar to melt electrowriting, in which, no whipping occurs, and the fibres coil owing to buckling. The coiling wavelength decreases with an increasing collector speed. When the collector speed matches the melt electrospinning jet speed (the critical translation speed), the fibre coiling wavelength becomes infinite, which results in a straight fibre in the direction of the collector movement [126,135,144]. As the collector speed was relatively low during the fibre mat formation, only buckling occurred, thereby forming parallel rows of coiled fibre. The 'glued' structure occurred when the polymer had not cooled down sufficiently during the formation. The molten polymer reached the collector and fused with the other fibres [21,104,138].

3.2.2. Fibre diameter distribution

The fibre diameter is generally considered as the main parameter of melt electrospun mats. A fibre diameter distribution plot was derived in order to reflect the full range of the fibre diameter dispersion (Fig. 16). Clear distribution patterns that are typical for different polymers emerged. Despite the conditions of the fibre media formation, polymer A had the lowest diameters ranging from the submicron scale to 15 μm, excluding several exceptional cases (Table A2). Both polymers C and D had a diameter mode in the same range as A, but not equally well pronounced. Starting from 15 μm, the number of polymer D fibres gradually decreased with an increasing diameter, while polymer C had another mode at 17 to 27 μm. No clear fibre number distribution patterns were distinguished for polymers B and E.

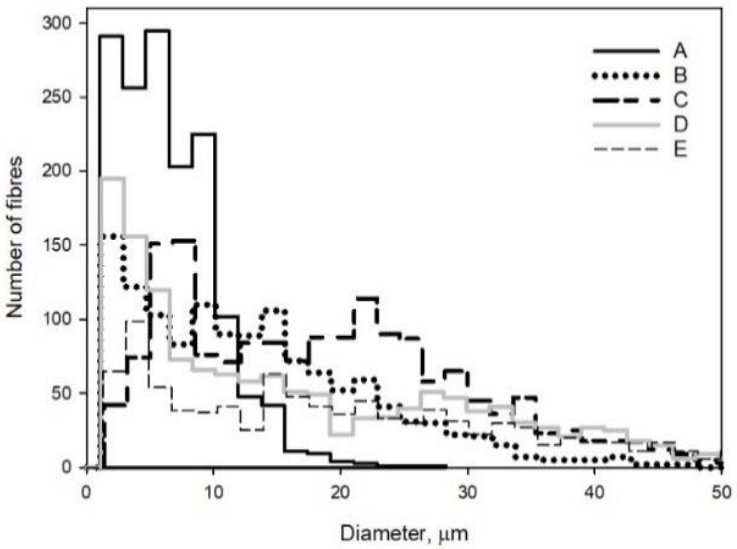

Figure 16. Fibre diameter distributions of melt electrospun mats obtained from various polymers (A – Vestamid™ L 1600; B – Vestamid™ L 1901; C – Arnitel® 3106; D – Rilsamid® AMN 0 TLD; E – Pebax® 35R53 SP 01)

Polymer A had the highest MFR (132 g/min), which means that the whipping motion was well pronounced during the mat formation. This tended to result in the stretching of the material as it transited towards the collector, thus significantly thinning the jet diameter, while the ambient air simultaneously cooled off the jet, and solidification occurred along the route [198]. Moreover, polymer A had the lowest fibre size distribution. The lower MFRs of the other polymers resulted in higher average diameters and greater distributions of the fibre diameters. As MFR is an indirect measure of molecular weight (a high MFR corresponds to a low molecular weight [199]), it is suggested that polymers with low spinnability could potentially have a higher molar mass, which has been proven to exert a significant effect on the sizes of melt electrospun fibres [133,141,158].

3.2.3. Effects of process parameters on fibre diameter

3.2.3.1. Voltage

In general, the voltage applied to the fibre formation had an inverse effect on the fibre diameter: a higher voltage resulted in a smaller fibre diameter. Similar results have been extensively reported for both solution electrospinning [190,200] and melt electrospinning (Bässmann, 2000; Doustgani & Ahmadi, 2016; Lyons & Li, 2014). In our case, the same effect was observed for four out of five tested polymers. Only polymer E exhibited an insignificant direct relationship between the voltage and the fibre diameter.

The higher voltage also resulted in lower dispersed fibre diameters in three out of the five polymers. Moreover, A and E showed a higher dispersion with the increase in voltage. It was also observed that a change in the voltage between 15 and 25 kV ensured a narrow fibre diameter distribution range.

3.2.3.2. Feed rate

A higher feed rate generally resulted in a larger fibre diameter. It has been widely noted that the diameter of the obtained fibre is directly related to the feed rate in both solution electrospinning [190,192] and melt electrospinning (Macossay, Marruffo, & Rincon, 2007). Doustgani *et al*. [158] reported that the mean fibre diameter increased with a higher flow rate, owing to the increase in the amount of the material flowing through the nozzle, which, in turn, resulted in a larger fibre diameter. This effect was observed for all the samples except polymer B, where the feed rate had no significant effect on the fibre diameter, with the voltage being the single major effect. Furthermore, the higher feed rate increased the dispersion of the fibre diameters for three polymers.

A major feed rate influence on the average diameter and diameter dispersity was observed for polymer E. The MFR for this polymer was one of the lowest, while the tensile modulus was 25 times lower than that of the other investigated polymers (*Table A1*). This made it difficult for the polymer to be squeezed through the smaller diameter nozzle without clogging the system. A stable formation process was achieved only by reducing the initial feed rate.

3.2.3.3. Nozzle diameter

The general trend for all the analyzed polymers was that the nozzle size had no effect on the fibre diameter median or the geometric mean; however, it did have a direct effect on the fibre diameter dispersion. The most significant influence of the nozzle size on the fibre diameter dispersion was observed for polymer C. No correlation between the diameter of the needle used and the average fibre diameter was observed with poly(methyl methacrylate) fibres (Macossay, Marruffo, & Rincon, 2007), but the decrease in the needle diameter caused an increase in the polydispersity of the fibre diameters.

3.2.3.4. Modeling of process parameters versus fibre diameter

Based on the results obtained via the planned experimental design, the response surface plots were derived for the resultant fibre diameters. The effects of the voltage and polymer filament feed rate on the fibre diameter for different nozzle diameters are presented in Figure 17. The sequence of the IQR plots illustrates that the influence of the feed rate (as opposed to the voltage) on the fibre diameter decreased as the nozzle size increased. It is also evident that, with a similar voltage and feed rate, the nozzle diameter had a direct influence on the dispersion of the fibre diameters.

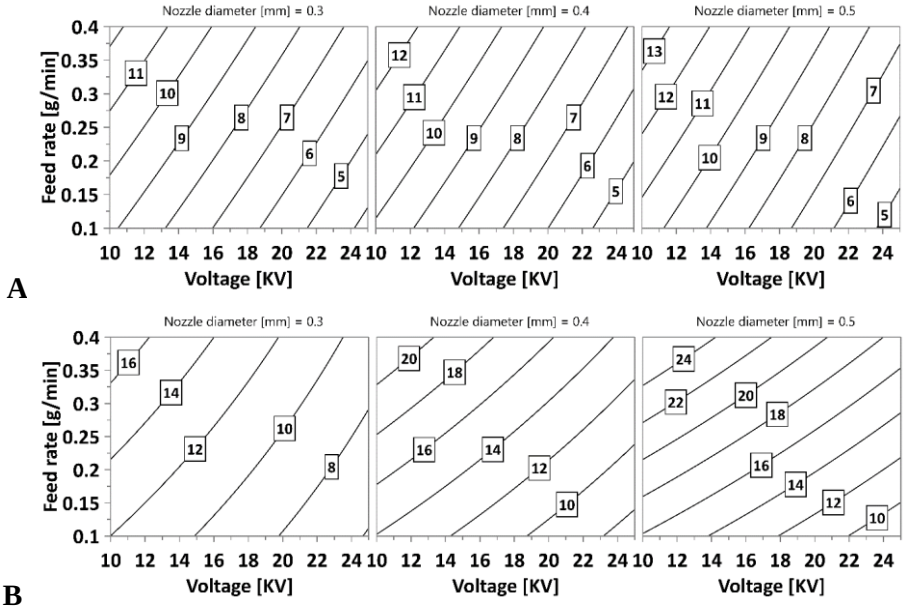

Figure 17. Effects of melt electrospinning parameters on the fibre diameter, μm (A – median; B – IQR)

3.2.4. Filtration performance

3.2.4.1. Filtration efficiency

Following the visual inspection and morphological analysis, samples containing flaws (such as aligned fibre strains and insufficient fibrous layers) were eliminated. As a result, 38 samples were selected for the filtration tests, and subsequently, 12 samples passed the threshold of $e\mathrm{PM}_{1,\min} \geq 50\%$ (Table 7). All of these mats were fabricated from polymer A.

Table 7. Summary of filtration performance data of polymer A mats passing ePM1, min ≥ 50%

Code	Base mass, g/m^2	*e*PM$_1$, %	*e*PM$_{1\ min}$, %	Pressure drop, Pa	Packing density	Quality Factor, Pa^{-1}	Porosity, %	Median Fibre diameter, µm	Interquartile Range of Fibre diameter, µm
N2A	97.66	55	52	29.7 ± 4.0	0.1288	0.027	98.5	1.7	3.6
N3A	86.03	61	56	45.5 ± 5.7	0.1753	0.021	97.9	4.2	3.6
N4A	101.95	58	50	23.5 ± 3.3	0.2120	0.037	97.4	8.2	2.8
N5A	324.97	80	79	121.3 ± 9.2	0.2825	0.013	96.6	6.4	6.8
N6A	376.81	63	62	43.4 ± 5.4	0.1519	0.023	98.2	4.1	1.8
N7A	89.11	74	70	79.4 ± 6.3	0.2595	0.017	96.9	5.1	5.6
N9A	321.67	56	53	23.7± 3.5	0.1578	0.035	98.1	3.8	2.8
N10A	106.68	61	56	40.2 ± 5.0	0.2426	0.023	97.1	5.7	3.3
N11A	349.64	58	57	24.8 ± 2.9	0.1778	0.035	97.9	5.3	6.0
N12A	255.80	69	68	44.4 ± 4.9	0.2040	0.026	97.5	3.8	7.3
N13A	268.50	63	60	29.7 ± 4.2	0.2073	0.033	97.5	2.2	5.2
N14A	294.49	77	75	73.6 ± 6.8	0.2217	0.020	97.3	4.8	6.8

The filtration efficiency curves for mats N4A and N5A are presented in Figure 18 as the representative specimens regarding the filtration performance. The electrostatic charge neutralization did not have a significant effect on the filtration efficiency, although electrostatic capture is generally associated with synthetic fibre filters [202]. This implies that the prevailing mechanism in the capture of aerosol particles may be associated with the diffusion and interception resulting from the unique fibre morphology.

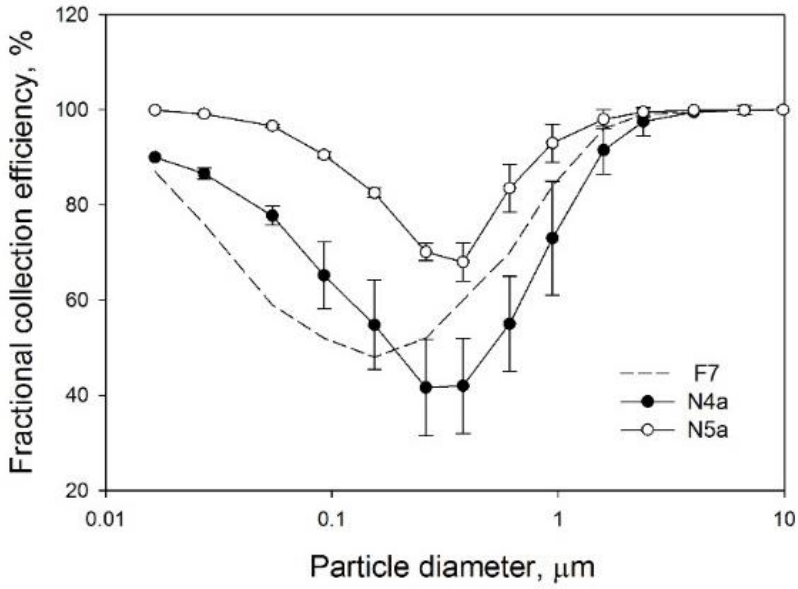

Figure 18. Filtration efficiencies for N4A and N5A filter media compared to F7 filter (the positive error bar indicates the initial efficiency, the negative error bar indicates the minimum efficiency after charge neutralization)

The *e*PM_1 of the 12 mats ranged from 55% to 80%, which, according to EN 779 Standard, is equivalent to F7 to F9 filter classes. The best performance was achieved by mat N5A (*e*PM_1 = 80%). One of the hypotheses raised within this study implies that not only does the average fibre diameter affect the filtration efficiency, but the combined effect of the median fibre diameter together with the dispersion extent is important for achieving higher filtration efficiencies and QFs. The direct effect of the median of the fibre diameters on the filtration efficiency for *e*PM_1 (Figure 19-A) was not pronounced (R^2 = 0.21), while the IQR of the fibre diameters (as a measure of dispersion) had a moderate effect (R^2 = 0.49). The filtration efficiency enhancement can be explained by the more dispersed distribution of the fibre diameters.

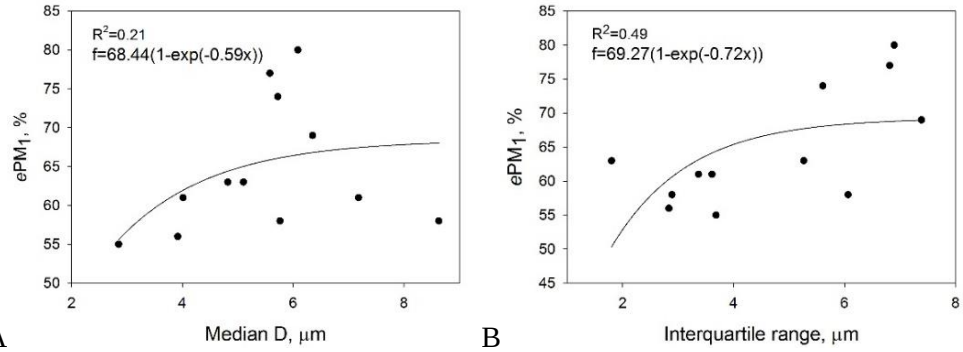

Figure 19. ePM1 dependency on the fibre diameter (A – median; B – IQR)

Similar to our findings, Kadam *et al.* [203] reported that the fibre diameter distribution could influence the filtration performance. Dispersed fibres cause a lower pressure drop and normalize the mat thickness compared to a wider distribution of the same fibre diameter (Zhang, Shim, & Kim, 2009). The bimodal distribution of polyacrylonitrile nanofibres created a scaffold-like structure that decreased the packing density and facilitated the airflow across the membranes. This could potentially be useful for high-performance filter media.

The base mass also had a medium effect on the filtration efficiency ($R^2 = 0.34$, Figure 20-A) and a comparatively high filtration efficiency for low base mass values. Compared to the commercial F9 class filter material, the melt electrospun filter mats achieved a comparable filtration efficiency with more than twice as low base mass values. The packing density indicated an even greater impact on the filtration efficiency ($R^2 = 0.58$, Figure 20-B). As the packing density increases, the interstitial space decreases, and, thus, impaction and interception for larger aerosols prevails. A higher packing density also indicates an additional filtering material and a larger surface area for aerosol deposition. Therefore, the aerosol penetration decreases with an increasing packing density for all the particle sizes [205]. An increase in the base weight would cause a decrease in the pore size and a shift in the pore size distribution towards lower values, which leads to a synchronous increase in the filtration efficiency and the pressure drop (Wang & Pan, 2015; Zhang, Liu, Zuo, *et al*., 2017).

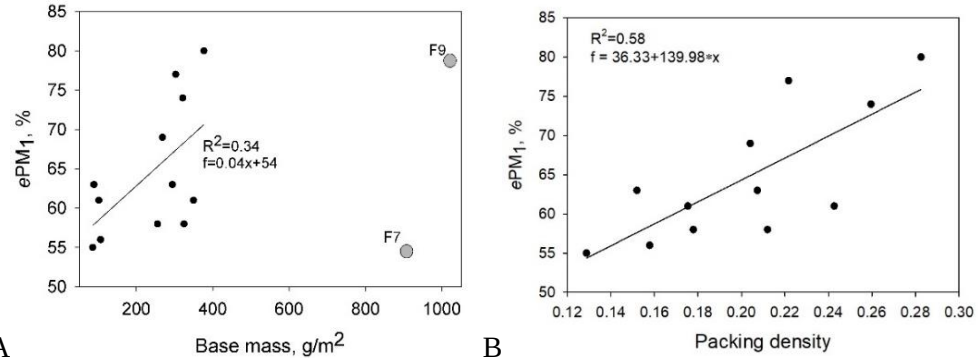

Figure 20. Effects of base mass (A) and packing density (B) on ePM1

Highly porous filter media can allow particles to pass through easily and not perform the filtration function satisfactorily [202]. Furthermore, the airflow may have additional path choices for passing through the medium; thus, according to the minimal resistance principle, the length and tortuosity of the air penetration path can be reduced significantly, which results in a lower air resistance (Zhang, Liu, Yin, *et al*., 2017).

3.2.4.2. Pressure drop

The pressure drop across the 12 mats ranged from 23.5 to 112.3 Pa, with a mean of 50.0 Pa. In contrast to the solvent electrospun filtration media, melt electrospun mats exhibit a lower filtration efficiency combined with a significantly lower pressure drop. The filtration efficiency of the solvent electrospun membranes was demonstrated to vary in the range of 77.7% to 99.616%, which is associated with a pressure between 282 and 1243 Pa [19,93].

A wider fibre size distribution moderately affected the filtration efficiency, while the pressure drop was not affected as much (Figure 21-A). This could be explained by the fact that the increase in the fibre size dispersion results in an increasing amount of fine fibres, thus obstructing air permeation. With the lognormal distribution and a higher count of smaller fibres being achieved, a lower total permeation level is observed [207]. As the fibre size distribution is shifted to the smaller side, the presence of several larger fibres results in a lower pressure drop, while still maintaining high filtration efficiency and higher mechanical stability.

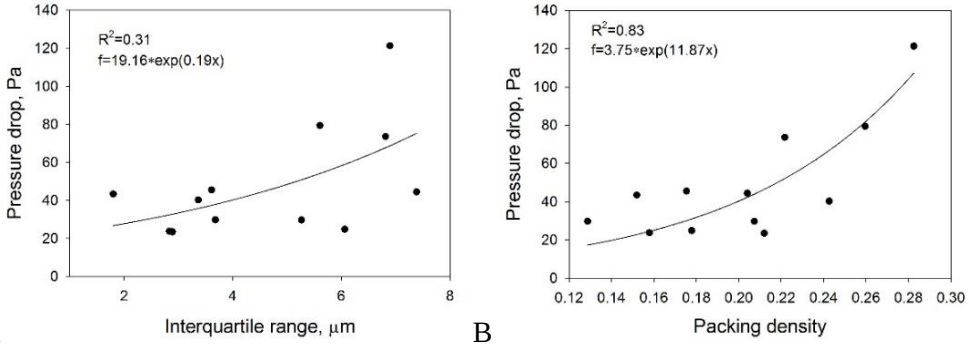

A B

Figure 21. Effects of IQR of fibre diameter (A) and packing density (B) on pressure drop

The regression between the packing density and the pressure drop (see Figure 21-B) indicated an exponential relationship, in which, the change in the packing density at a higher range could double the pressure drop, as expected (Hung & Leung, 2011; Leung, Hung, & Yuen, 2010; Wang & Pan, 2015). Accordingly, the pressure drop and the filtration efficiency for *e*PM_1 were also closely associated exponentially (R^2 = 0.94, Figure 22). This indicates that, similarly to the other filtration products, the filtration efficiency and pressure drop should be balanced.

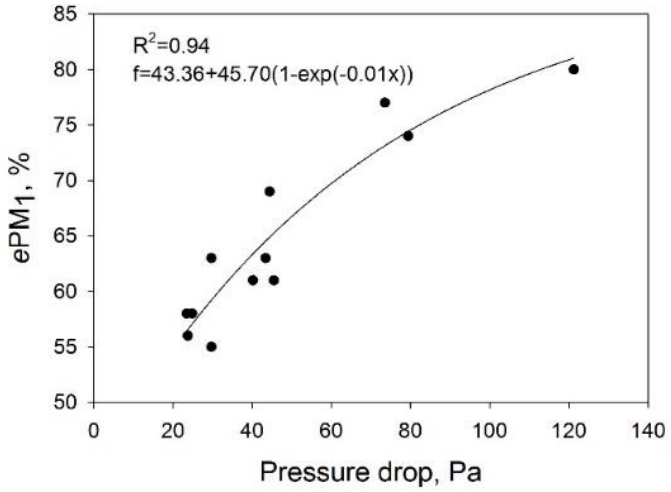

Figure 22. Relationship between filtration efficiency (ePM1) and pressure drop

3.2.4.3. Quality factor

The objective of the filter media design is to balance the filtration efficiency and the pressure drop by assessing the filter QF. As a result, the filter media QFs were

calculated for the analyzed fibrous mats (Table 2-A). The filter media (N5A) with the highest efficiency (ePM_1 = 80%) and the highest pressure drop (121.3 Pa) exhibited the lowest quality factor (QF = 0.013). The highest quality factor (QF = 0.037) was obtained for N4A filter media thus indicating moderate filtration efficiency (ePM_1 = 58 %) and the lowest pressure drop (23.5 Pa). In general, the QF was adversely associated with the fibre diameter.

The pressure drop has been demonstrated to decrease more rapidly than the decrease in the filtration efficiency with an increasing fibre diameter. This phenomenon reveals the complexity of the dependence of the QF on the structural parameters as the pressure drop decrease can be outweighed by the decrease in the filtration efficiency [208].

Moreover, the QF range obtained with the melt electrospun fibre mats was within a higher range of filtration materials of the same efficiency (0.017 to 0.036 vs. 0.018 of the tested commercial F7 filter material). This confirms our hypothesis that a broad fibre size distribution is favorable in achieving relatively high filtration efficiency with a relatively low pressure drop.

3.3. Multi-layered air filter formation: melt/solution electrospinning for micro/nano fibrous material (Experiment III)

3.3.1. Mat morphology and characterization

Four distinct variations of mat morphologies were obtained during the fabrication process by combined melt and solution electrospinning (Figure 23). Microstructures were obtained via melt electrospinning (Figure23-A), while submicrometer structures were fabricated via the solution electrospinning method (Figure 23-D). By combining both methods and variating the timing of solution electrospinning, different intermediate structures were generated (Figure 23 B–C). By combining the regular melt with solution electrospinning for 30 minutes, in the middle of the melt electrospinning process (Figure 23-B), a mat with a relatively large amount of supermicrometer fibres and large pore size was formed. In the case of simultaneous melt and solution electrospinning (for the whole process duration), a mesh of densely packed nanofibres was formed on the randomly placed micro fibres (Figure 23-C).

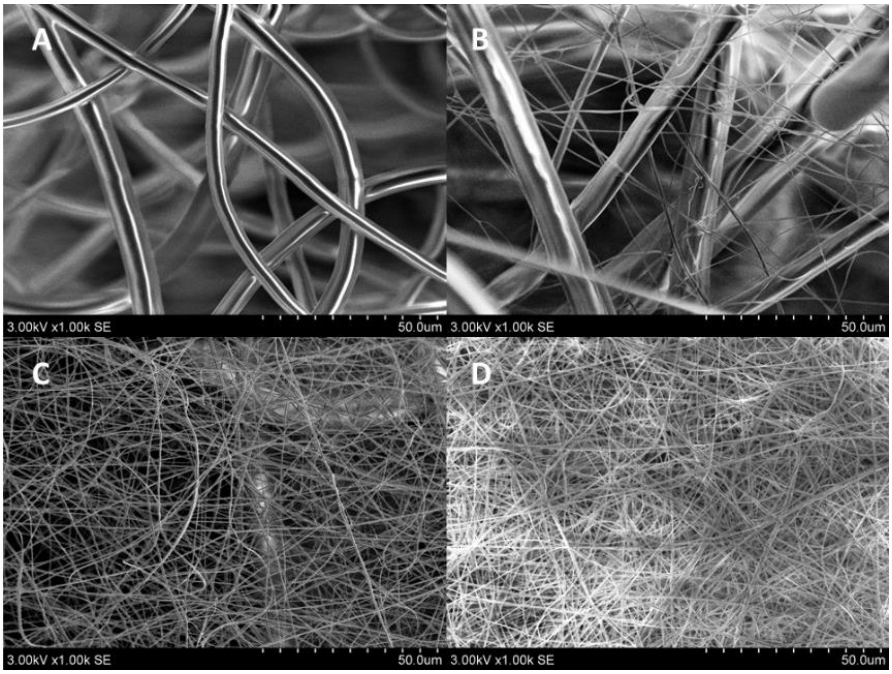

Figure 23. SEM images of fibre surfaces with different process combinations at magnification x1000 (A – M; B – M_MS_M; C – MS; D – S)

The characteristic parameters of the resulted fibre mats are presented in Table 8. The analysis showed high porosity (the ratio of the open space in a filter matrix to the amount of the volume taken by the filter media itself) of melt electrospun mats. The porosity of the mats formed by using combined melt and solution electrospinning (average – 94.9%) did not significantly differ from the porosity of the melt electrospun mats (average – 92.8%); however, a significant porosity difference was observed in comparison to the solution electrospun mats (47.67%).

Surprisingly, even though a highly porous material was obtained, additional solution electrospinning did not increase the thickness of the mat; in most cases, the thickness was reduced. Generally, both thickness and radius of the fibre deposition tends to increase with a longer formation period [209]. The reduction of thickness in our study might be due to the fact that sub-micrometre fibres had intertwined super-micrometre fibres thus resulting in a tighter material but still maintaining a high porosity level.

Table 8. Parameters of formed fibre mats

Code	Numerical Fibre Ratio*	Weight, g/m^2	Weight, g/m^2 (without base)	Pressure drop, Pa	Porosity, %	Thickness, mm
S	Submicrometer fibres only	57.94	10.67	140.80	47.67	0.02
M(I)	0.31	85.78	38.52	4.33	97.64	1.60
MS(I)	2.31	75.51	28.24	15.92	97.67	1.19
MS_M(I)	2.03	86.10	38.84	23.67	96.44	1.07
M_MS_M(I)	2.29	75.13	27.86	16.00	97.02	0.92
M(II)	Supermicrometer fibres only	121.87	74.61	6.17	93.80	1.18
MS(II)	15.62	119.34	72.08	20.33	91.76	0.86
MS_M(II)	1.19	132.40	85.14	15.50	92.27	1.08
M_MS_M(II)	0.90	125.94	78.68	7.33	92.72	1.06
M(III)	0.21	77.44	30.18	7.00	87.02	0.23
MS(III)	7.38	82.37	35.10	50.17	95.99	0.86
MS_M(III)	1.11	84.54	37.28	14.17	95.91	0.89
M_MS_M(III)	0.40	80.18	32.92	8.08	95.07	0.66

* Ratio between the number of submicrometer (<1 μm) and supermicrometer (≥1μm) fibres

The analysis of cross sections of fibre mats produced via melt and combined melt/solution electrospinning revealed differences in structures (see Figure 24). While the voltage (25 kV) and nozzle diameter (0.4 mm) were kept constant, for the feed rate (0.6 g/h and 1.8 g/h) and the tip-to-collector distance (50 mm and 70 mm), three variations were chosen. Variation I (the feed rate – 0.6 g/h, the tip-to-collector distance – 50 mm) resulted in rather uniform fibres, thick mats, and porous structures.

Variation II (the feed rate – 1.8 g/h, the tip-to-collector distance – 50 mm) resulted in material overflow and ribbon structure formation. Such a structure occurs when the surplus polymer melt is not stretched from the tip of the nozzle fast enough. This causes solidification of the outer polymer layer which tends to break apart. As the solidified outer layer bursts, it forms the ribbon structure. At the same time, the melted inner core is spun into fibres. The same mechanism was observed during Experiment II and described in Subchapter 3.2.1. “Morphology of filter mats”.

Variation III (the feed rate – 0.6 g/h, the tip-to-collector distance – 70 mm) formed densely packed fibre mats; the thickness decreased almost twice in comparison with these of Variation I. This was achieved due to the longer tip-to-

collector distance which allowed for a longer stretching time of the polymer melt and a lowered average fibre diameter [108,127,128].

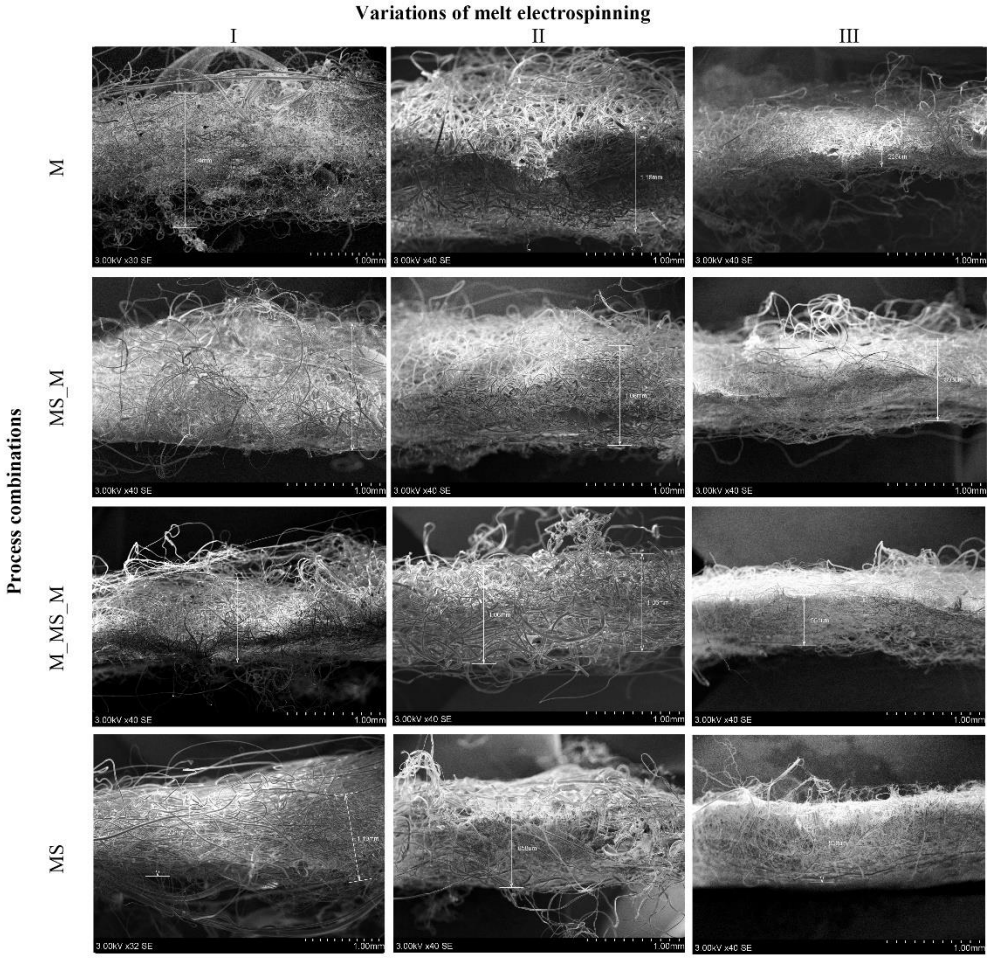

Figure 24. Cross sections of fibre mats (without a supporting layer): (I) feed rate – 0.6 g/h, tip-to-collector distance – 50 mm; (II) feed rate – 1.8 g/h, tip-to-collector distance – 50 mm; (III) feed rate – 0.6 g/h, tip-to-collector distance – 70 mm.

3.3.2. Filtration efficiency and quality factor

For smaller aerosol particles (NaCl) ranging in size from 0.02 μm to 5 μm, the particle fractional deposition efficiency of the fibre mats was determined in setup S1, while for the larger (KCl) particles, it was determined in setup S2. The obtained fractional deposition efficiencies of fibre mats fabricated via different formation conditions are presented in Fig. 25.

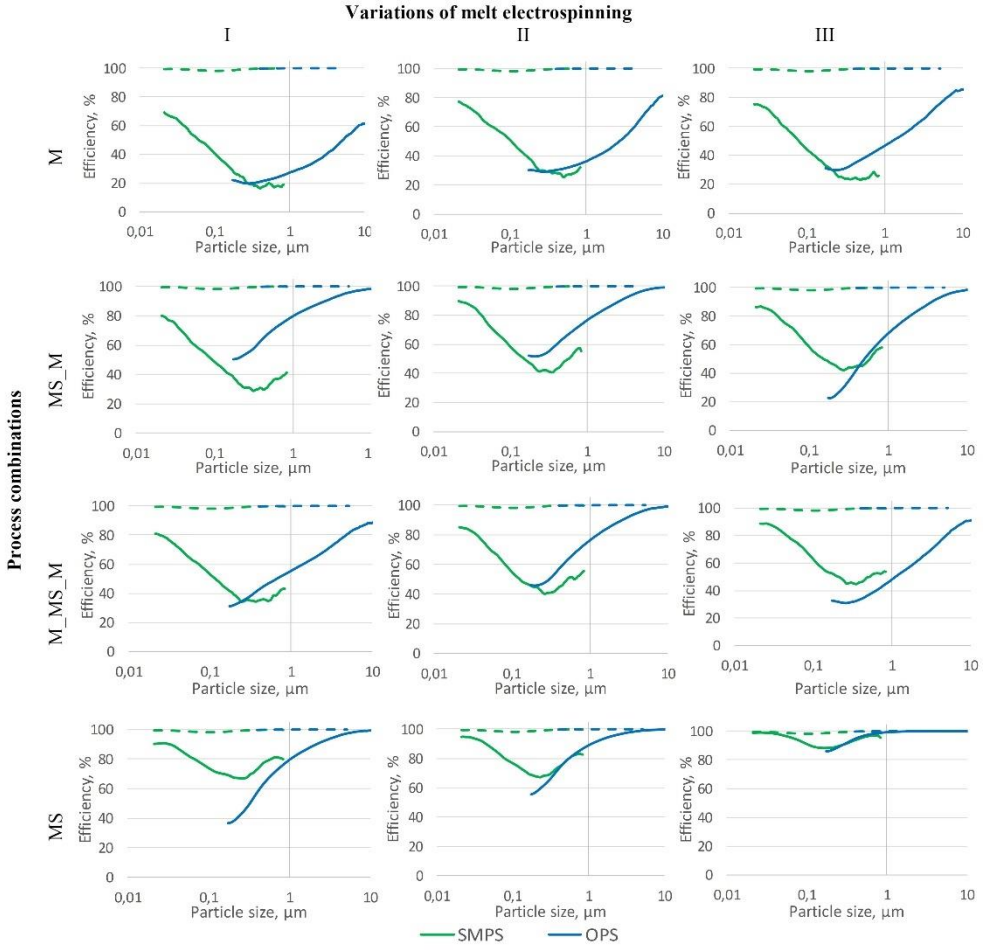

Figure 25. Particle trapping efficiencies of fibre mats fabricated by various formation methods (the dotted line represents solution electrospinning filtration efficiency)

As it was discussed in Chapter 1.2 “Theory of air filtration,” an increase in the particle size will cause increased filtration by the interception and inertial impaction mechanisms, whereas a decrease in the particle size will enhance collection by Brownian diffusion. As a consequence, there is an intermediate particle size region where two or more mechanisms are simultaneously operating, yet none of them is dominating. This is the region where the particle penetration through the filter is at the maximum, and it is called the most penetrating particle size (MPPS). Although the minimum filter efficiency and the particle size at which the minimum efficiency occurs will vary depending on the type of the filter and the flow velocity, the existence of such minimum filter efficiencies has been well established for different types of filters. For most fibrous filters operating at relatively low filtration velocities, the

minimum filter efficiency is generally known to occur in the vicinity of 0.3 μm [210]. Such an effect is clearly seen in Fig. 25.

Regardless of the melt electrospinning parameters, the mats formed by pure melt electrospinning (M) showed low filtration efficiencies (Figure 25, M). This is not surprising since a high number of supermicrometer fibres are denoted by limited capability to capture aerosol particles, especially when approaching the most penetrating particle size. In order to achieve higher filtration efficiencies ((ePM$_1$) up to 80%), melt electrospun mats require additional treatment, such as hot pressing or layer stacking, as it was demonstrated in Experiment II (Subchapter 3.2.4.1 "Filtration efficiency").

In both cases when constant melt electrospinning was combined with partial solution electrospinning (MS_M and M_MS_M), filtration efficiencies increased. Introducing submicrometer fibres at the beginning of the mat formation process (MS_M) was more advantageous compared to the case when submicrometer fibres were introduced in the middle of the formation process (M_MS_M). The difference in the filtration efficiency might be due to the fact that – when melt electrospinning is used prior to solution electrospinning – it creates a thicker and fluffier background which resists the deposition of solution electrospun fibres.

Higher filtration efficiencies (excluding solution electrospinning) were reached when both melt and electrospinning methods (MS) were being applied simultaneously (see Table 9). The filtration efficiency for different PM fractions increased from two to three times compared to the above described variations of the combined melt and solution electrospinning. It was also observed that the melt electrospinning process parameters influenced the mat morphology and filtration efficiency accordingly. As supposed, a higher feed rate and a longer tip-to-collector distance increased the filtration efficiencies.

Table 9. Filtration efficiencies of different PM fractions for the produced fibre mats based on different methods

Code	**NaCl**				**KCl**			**Discharged + KCl**		
	SMPS	OPS			OPS			SMPS	OPS	
	ePM$_1$	ePM$_1$	ePM$_{2,5}$	ePM$_5$*	ePM$_1$	ePM$_{2,5}$	ePM$_{10}$	ePM$_1$	ePM$_1$	ePM$_{2.5}$
S	99.5	99.7	99.9	99.9	96.3	96.6	97.8	91.2	91.4	92.7
M(I)	26.3	5.4	5.8	7.4	21.5	25.5	39.4	13.6	12.9	13.5
MS(I)	72.7	57.2	68.2	77.7	55.3	65.2	83.4	57.3	44.7	54.6
MS_M(I)	38.4	30.5	41.0	53.3	62.1	68.6	84.1	32.3	29.0	37.0
M_MS_M(I)	47.9	34.8	43.4	51.5	57.2	65.7	83.6	33.5	37.2	46.3
M(II)	35.6	18.3	19.7	21.1	30.6	35.3	51.8	34.4	15.3	19.1
MS(II)	74.0	75.5	82.2	88.6	71.3	76.8	90.2	58.8	69.6	75.5

Code	NaCl				KCl			Discharged + KCl		
	SMPS	OPS			OPS			SMPS	OPS	
	ePM$_1$	ePM$_1$	ePM$_{2,5}$	ePM$_5$*	ePM$_1$	ePM$_{2,5}$	ePM$_{10}$	ePM$_1$	ePM$_1$	ePM$_{2.5}$
MS_M(II)	49.4	36.7	45.1	53.2	59.8	67.4	82.7	41.4	26.3	36.8
M_MS_M(II)	41.3	23.2	26.5	33.4	41.2	48.1	65.7	28.2	12.4	16.3
M(III)	30.6	9.8	12.3	15.2	35.4	41.3	60.1	28.5	24.7	29.6
MS(III)	92.4	96.0	96.9	99.3	92.5	94.5	98.3	73.2	84.1	88.0
MS_M(III)	50.2	23.9	32.3	41.8	41.4	52.3	76.3	38.1	12.4	17.5
M_MS_M(III)	52.6	21.2	25.6	31.6	34.7	42.9	63.2	25.8	28.6	34.7

*In case of NaCl, larger particles than PM_5 were not measured, therefore, the efficiency was calculated for ePM$_5$

The differences between the filtration efficiency were determined with the OPS and SMPS. These differences might be explained by the fact that the two devices are based on different measurement principles, light scattering, and electrical mobility, respectively. The differences were also observed between the filtration efficiencies measured with the OPS when using different types of test aerosols. Likely, this occurred because of the shape of the aerosol particles [211,212]. In S1 setup, the aerosol was generated from NaCl which forms cubic particles with rounded edges, while, in S2, the measurements were performed with KCl particles with a more spherical shape. In general, our observations confirm the findings that spherical particles indicate a higher filtration efficiency compared to cubic particles [213]. Some differences in filtration efficiencies could also be attributed to the particle charges duo to the differences in the setups. KCl aerosol might have some charge, and, as the filters are also charged, the KCl particles could be removed with a higher efficiency. For the NaCl aerosol, we used a Kr neutralizer, which means that the particles are also slightly negatively charged (bipolar distribution according to Fuchs). In the case of the KCl aerosol generator, the drying air is ionized by a corona charger, both positive and negative.

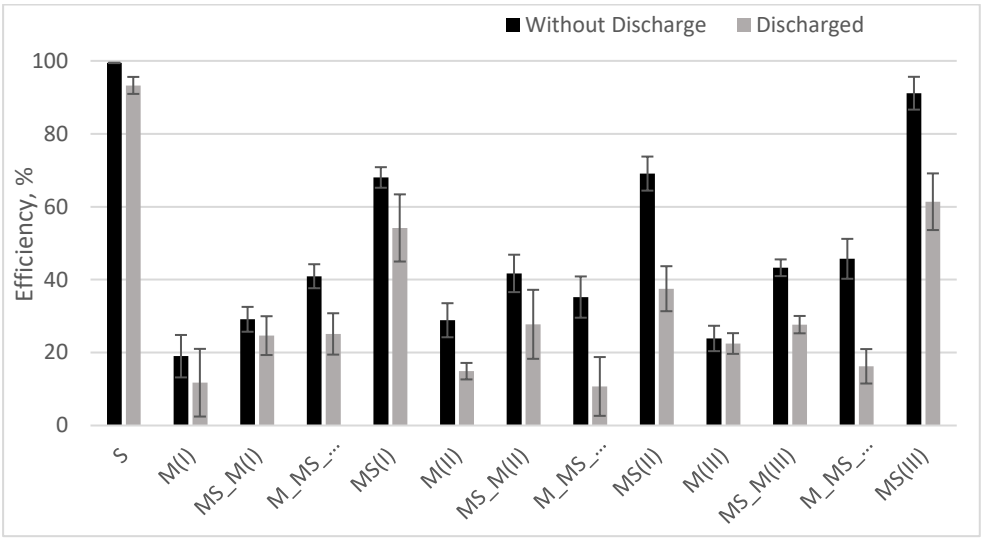

Figure 26. Filtration efficiencies of ‘without discharge’ and ‘discharged’ fibrous mats at the Most Penetrating Particle Size

As regulated by ISO 16890:2016 Standard, the minimum fractional test efficiency was measured for charged filters. In order to estimate the impact of electrostatic forces on the filtration efficiency, a series of tests for the discharged fibrous mats were performed. The comparison of ‘without discharge’ and ‘discharged’ filtration efficiencies for the Most Penetrating Particle Size (MPPS) of 0.3 μm indicated the general trend that ‘discharged’ fibrous media showed lower efficiencies compared to ‘without discharge’ samples (Fig. 26). For the solution electrospun mats, the filtration efficiency difference was 6.2%. This corresponds to the findings of the other authors and supports the assertion that, due to the charge on the material, 9, 33, 34 mats demonstrate higher filtration efficiencies while the filtration efficiency difference for melt and combined melt-solution electrospun mats ranged from 5.8% to 69.6% and did not show any regular relation. The morphological analysis of the samples revealed that the initial nano-submicron structures of the mats were destroyed during the discharge process, which was based on the submersion into isopropyl alcohol. As a result, we shall study this aspect more profoundly in future experiments.

Table 10. Pressure drop, average filtration efficiencies and quality factors for tested mats

	Pressure drop, Pa	***e*PM$_1$, %**	***e*PM$_{2,5}$, %**	***e*PM$_{10}$, %**	**QF (*e*PM$_1$), Pa^{-1}**	**QF (*e*PM$_{2,5}$), Pa^{-1}**	**QF (*e*PM$_{10}$), Pa^{-1}**	**QF Pa^{-1}**
S	140.8	98.7	98.5	99.0	0.031	0.030	0.033	0.031
M(I)	4.3	17.7	15.5	23.0	0.045	0.039	0.060	0.048
MS(I)	**15.9**	**61.7**	**66.5**	**80.5**	**0.060**	**0.069**	**0.103**	**0.077**
MS_M(I)	23.7	43.3	55.0	68.5	0.024	0.034	0.049	0.036
M_MS_M(I)	16.0	46.3	54.5	68.0	0.039	0.049	0.071	0.053
M(II)	6.2	28.3	27.5	36.5	0.054	0.052	0.074	0.060
MS(II)	**20.3**	**73.7**	**79.5**	**89.5**	**0.066**	**0.078**	**0.111**	**0.085**
MS_M(II)	15.5	48.7	56.0	68.0	0.043	0.053	0.074	0.056
M_MS_M(II)	7.3	35.0	37.5	49.5	0.059	0.064	0.093	0.072
M(III)	7.0	25.3	26.5	37.5	0.042	0.044	0.067	0.051
MS(III)	**50.2**	**93.7**	**96.0**	**98.5**	**0.055**	**0.064**	**0.084**	**0.068**
MS_M(III)	14.2	38.3	42.0	59.0	0.034	0.038	0.063	0.045
M_MS_M(III)	8.1	36.3	34.5	47.5	0.056	0.052	0.080	0.063

When analyzing different mat characteristics and filtration parameters, a clear relationship between the air pressure drop and mat porosity was observed. As it is seen in Figure 27, the pressure drop tends to decrease with an increase of the porosity. This is not surprising as, through a more porous structure, the air stream would face less resistance to pass through the fibrous mats. Similar results were found throughout the literature as porosity is always shown to have the same effect on the air pressure drop [62,71,91].

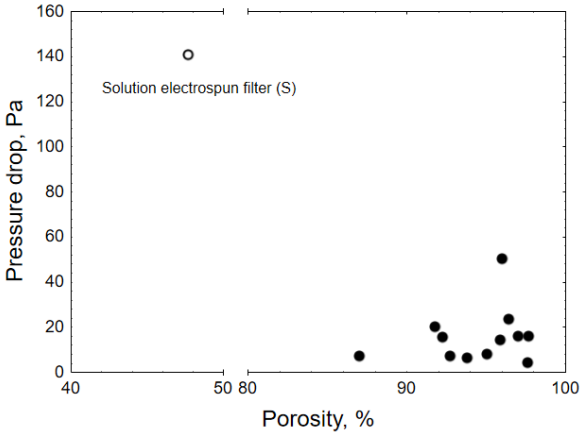

Figure 27. Relationship between porosity and pressure drop of the tested mats

The summarized values of the pressure drop and the average filtration efficiency indicated that the higher quality factors were reached for simultaneously melt and solution electrospun (MS) mats (Table 10). For MS mats, the quality factor ranged from 0.068 to 0.085 Pa^{-1}. The high quality factors were reached due to the low values of the pressure drop (15.92–50.17 Pa), though the filtration efficiencies in different particle mass fractions (ePM$_1$, ePM$_{2.5}$, ePM$_{10}$) were rather moderate (61.7–98.5 %). The correlation between the filtration efficiency (ePM$_1$) and the pressure drop of the mats is presented in Figure 28.

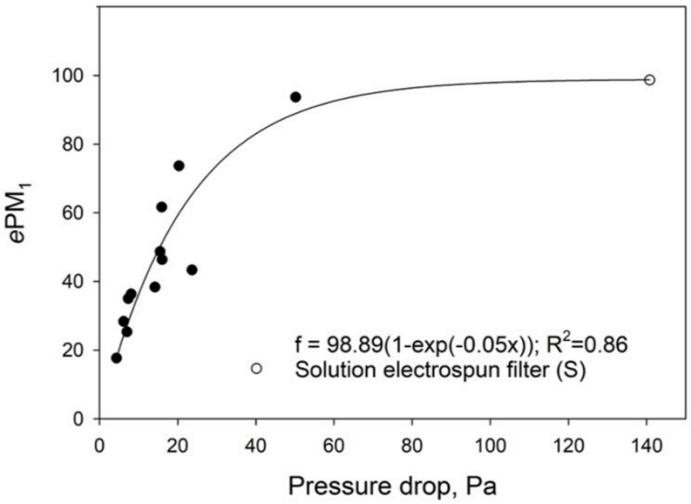

Figure 28. Relationship between filtration efficiency (ePM$_1$) and pressure drop of mats

The solution electrospun (S) mat showed a better filtration efficiency for all the mass fractions, however, the pressure drop on average was two times lower for all the MS mats, thus, the S mat indicated a quality factor which was more than two times lower (0.031 Pa^{-1}). In contrast to our research, other studies [88,91,214] indicated extremely high filtration efficiencies, however, the quality factors on average were more than two times lower for multilevel structured nanofibrous membranes.

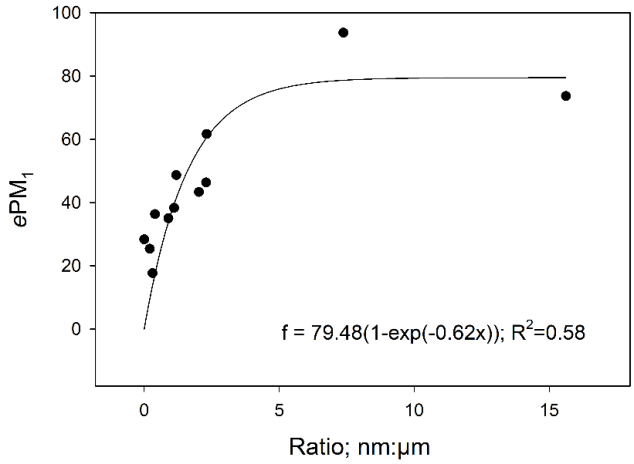

Figure 29. Fibre ratio (sub- vs. super- micrometre as nm:µm) effect on filtration efficiency

One of our hypotheses was that blending nano-submicrometer and supermicrometer fibres into coarse fibrous filter media is a promising way to improve the filtration performance. It was found that a higher ratio between nano-submicrometer fibres (<1 µm) and supermicrometer (≥1µm) fibres in the mat structure leads to a higher filtration quality factor. Comparative analysis of the quality factors (Table 10) and Numerical Fibre Ratios (NFR) (Table 8) showed good correlation R^2=0.58 (Figure 29). The higher NFR values were obtained for all the three MS mats.

4. Conclusions

1. The screening experiments proved that melt electrospinning process parameters, e.g., the voltage, the feed rate, and the nozzle diameter are the main variables affecting the fibre diameter and the fibre diameter dispersion.
   The combined effect of the fibre diameter as well as the fibre diameter dispersion is an important factor in achieving higher filtration efficiencies.
   Not a single process parameter but rather a combination of process parameters results in a specific fibre diameter. Accordingly, this allows developing the combined response-surface plot of the process parameters for the production of fibrous mats with the desired fibre diameters.
2. 12 out of 68 melt electrospinning produced fibre mats passed the standardized *e*PM_1 test (ISO 16890). Polyamide 12 (Vestamid™ L1600), due to its low fibre diameter dispersion median values, showed the most favorable filtration efficiencies ranging from 55% to 80%.

3. A prototype fibre printing apparatus based on combined melt and solution electrospinning principles was designed. A novel method for the production of mixed nano-submicrometer and supermicrometer fibre diameter structures was developed.
4. Melt electrospun mats displayed the highest porosity (94.78%), whereas the porosity of the mats formed by using combined melt and solution electrospinning was 92.82%, while the porosity of solution electrospun mats was significantly lower (47.67%).
   Regardless of the melt electrospinning parameters, mats formed by pure melt electrospinning showed the lowest filtration efficiencies, while higher filtration efficiencies were reached when both melt and solution electrospinning methods were applied, the electrospun mats showed the highest filtration efficiencies (98.7–99.0%) across all the particle size categories.
5. The solution electrospun mats indicated 0.031 Pa^{-1} average filtration quality factor, while the quality factor of the melt/solution electrospun mats ranged from 0.068 to 0.085 Pa^{-1}. The high filtration quality factors of the melt/solution electrospun mats were reached due to the low values of the pressure drop (15.92 – 50.17 Pa).
   The blending of nano and sub-micron fibres into coarse fibrous media increases the filtration quality factor. A higher amount of nano and sub-micron fibres within such composite materials resulted in a higher filtration quality factor.

5. References

1. Cui X, Li F, Xiang J, et al. Cardiopulmonary effects of overnight indoor air filtration in healthy non-smoking adults: A double-blind randomized crossover study. *Environ Int*. 2018;114(December 2017):27-36. doi:10.1016/j.envint.2018.02.010
2. Matson U. Indoor and outdoor concentrations of ultrafine particles in some Scandinavian rural and urban areas. *Sci Total Environ*. 2005;343(1-3):169-176. doi:10.1016/j.scitotenv.2004.10.002
3. Bräuner EV, Forchhammer L, Møller P, et al. Indoor particles affect vascular function in the aged: An air filtration-based intervention study. *Am J Respir Crit Care Med*. 2008;177(4):419-425. doi:10.1164/rccm.200704-632OC
4. Anderson JO, Thundiyil JG, Stolbach A. Clearing the Air: A Review of the Effects of Particulate Matter Air Pollution on Human Health. *J Med Toxicol*. 2012;8(2):166-175. doi:10.1007/s13181-011-0203-1
5. Buivydiene D, Krugly E, Ciuzas D, Tichonovas M, Kliucininkas L, Martuzevicius D. Formation and characterisation of air filter material printed by melt electrospinning. *J Aerosol Sci*. 2019;131(March):48-63. doi:10.1016/j.jaerosci.2019.03.003
6. HEI Review Panel. Understanding the Health Effects of Ambient Ultrafine Particles. *Heal Eff Inst*. 2013;(January):122. http://pubs.healtheffects.org/view.php?id=394.
7. Tobías A, Rivas I, Reche C, et al. Short-term effects of ultrafine particles on daily mortality by primary vehicle exhaust versus secondary origin in three Spanish cities. *Environ Int*. 2018;111(October 2017):144-151. doi:10.1016/j.envint.2017.11.015
8. Martin J, Demokritou P, Woskie S, Bello D. Indoor Air Quality in Photocopy Centers, Nanoparticle Exposures at Photocopy Workstations, and the Need for Exposure Controls. *Ann Work Expo Heal*. 2017;61(1):110-122. doi:10.1093/annweh/wxw016
9. Oliveira MLS, Navarro OG, Crissien TJ, et al. Coal emissions adverse human health effects associated with ultrafine/nano-particles role and resultant engineering controls. *Environ Res*. 2017;158(May):450-455. doi:10.1016/j.envres.2017.07.002
10. Buivydiene D, Dabasinskaite L, Krugly E, Kliucininkas L. Formation of PA12 fibres via melt electrospinning process: Parameter analysis and optimisation. *J Polym Eng*. 2019. doi:10.1515/polyeng-2019-0190
11. Jatana S, Palmer BC, Phelan SJ, Delouise LA. Immunomodulatory Effects of Nanoparticles on Skin Allergy. *Sci Rep*. 2017;7(1). doi:10.1038/s41598-017-03729-2
12. Baroli B, Ennas MG, Loffredo F, Isola M, Pinna R, López-Quintela MA. Penetration of metallic nanoparticles in human full-thickness skin. *J Invest*

Dermatol. 2007;127(7):1701-1712. doi:10.1038/sj.jid.5700733
13. Cross SE, Innes B, Roberts MS, Tsuzuki T, Robertson TA, Mccormick P. Human Skin Penetration of Sunscreen Nanoparticles: In-vitro Assessment of a Novel Micronized Zinc Oxide Formulation. 2007. doi:10.1159/000098701
14. Singer BC, Delp WW, Black DR, Walker IS. Measured performance of filtration and ventilation systems for fine and ultrafine particles and ozone in an unoccupied modern California house. *Indoor Air*. 2017;27(4):780-790. doi:10.1111/ina.12359
15. Pui DYH, Qi C, Stanley N, Oberdörster G, Maynard A. Recirculating air filtration significantly reduces exposure to airborne nanoparticles. *Environ Health Perspect*. 2008;116(7):863-866. doi:10.1289/ehp.11169
16. Ramadan R. Identifying and Evaluating Air Filtration Methods for Personal Protection from Airborne Particulate Matter. 2011;(May):1-34.
17. Zhu M, Hua D, Pan H, et al. Journal of Colloid and Interface Science Green electrospun and crosslinked poly (vinyl alcohol)/ poly (acrylic acid) composite membranes for antibacterial effective air filtration. *J Colloid Interface Sci*. 2018;511:411-423. doi:10.1016/j.jcis.2017.09.101
18. Zhang S, Liu H, Zuo F, Yin X, Yu J, Ding B. A Controlled Design of Ripple-Like Polyamide-6 Nanofiber/Nets Membrane for High-Efficiency Air Filter. *Small*. 2017;13(10):1-10. doi:10.1002/smll.201603151
19. Matulevicius J, Kliucininkas L, Prasauskas T, Buivydiene D, Martuzevicius D. The comparative study of aerosol filtration by electrospun polyamide, polyvinyl acetate, polyacrylonitrile and cellulose acetate nanofiber media. *J Aerosol Sci*. 2016;92:27-37. doi:10.1016/j.jaerosci.2015.10.006
20. Xu H, Yamamoto M, Yamane H. Melt electrospinning: Electrodynamics and spinnability. *Polymer (Guildf)*. 2017;132:206-215. doi:10.1016/j.polymer.2017.11.006
21. Esmaeilirad A, Ko J, Rukosuyev M. The effect of nozzle-exit-channel shape on resultant fiber diameter in melt-electrospinning. *Mater Res*. 2017. doi:10.1088/2053-1591/4/1/015302
22. Choi H, Kumita M, Hayashi S, et al. Filtration Properties of Nanofiber/Microfiber Mixed Filter and Prediction of its Performance. 2017:1052-1062. doi:10.4209/aaqr.2016.06.0256
23. Balgis R, Murata H, Goi Y, Ogi T, Okuyama K, Bao L. Synthesis of Dual-Size Cellulose-Polyvinylpyrrolidone Nanofiber Composites via One-Step Electrospinning Method for High-Performance Air Filter. *Langmuir*. 2017;33(24):6127-6234. doi:10.1021/acs.langmuir.7b01193
24. Lee KS, Hasolli N, Jeon SM, et al. Filter layer structure effect on the most penetrating particle size of multilayered flat sheet filter. *Powder Technol*. 2019;344:270-277. doi:10.1016/j.powtec.2018.12.041
25. Leung WWF, Hung CH, Yuen PT. Effect of face velocity, nanofiber packing density and thickness on filtration performance of filters with nanofibers

coated on a substrate. *Sep Purif Technol*. 2010;71(1):30-37. doi:10.1016/j.seppur.2009.10.017
26. Sidaraviciute R, Buivydiene D, Krugly E, Valatka E, Martuzevicius D. A composite microfibre-supported short-nanofibre photocatalyst for environmental pollutant decomposition. *J Photochem Photobiol A Chem*. 2019;368(September 2018):7-14. doi:10.1016/j.jphotochem.2018.09.017
27. Landrigan PJ, Fuller R, Acosta NJR, et al. The Lancet Commission on pollution and health. *Lancet*. 2018;391(10119):462-512. doi:10.1016/S0140-6736(17)32345-0
28. Peters A, Dockery DW, Muller JE, Mittleman MA. Increased particulate air pollution and the triggering of myocardial infarction. *Circulation*. 2001;103(23):2810-2815. doi:10.1161/01.CIR.103.23.2810
29. Chen Z, Wang JN, Ma GX, Zhang YS. China tackles the health eff ects of air pollution. *Lancet*. 2013;382(9909):1959-1960. doi:10.1016/S0140-6736(13)62064-4
30. WHO | Air pollution. *WHO*. 2019.
31. Amoatey P, Omidvarborna H, Baawain M. Human and Ecological Risk Assessment: An International Journal The modeling and health risk assessment of PM 2.5 from Tema Oil Refinery. 2017. doi:10.1080/10807039.2017.1410427
32. Pratali L, Marinoni A, Cogo A, et al. Indoor air pollution exposure effects on lung and cardiovascular health in the High Himalayas, Nepal: An observational study. *Eur J Intern Med*. 2019;61(October 2018):81-87. doi:10.1016/j.ejim.2018.10.023
33. Aunan K, Hansen MH, Liu Z, Wang S. The Hidden Hazard of Household Air Pollution in Rural China. *Environ Sci Policy*. 2019;93(June 2018):27-33. doi:10.1016/j.envsci.2018.12.004
34. Chi C, Chen W, Guo M, Weng M, Yan G, Shen X. Law and features of TVOC and Formaldehyde pollution in urban indoor air. *Atmos Environ*. 2016;132:85-90. doi:10.1016/j.atmosenv.2016.02.043
35. Bennett J, Davy P, Trompetter B, et al. Sources of indoor air pollution at a New Zealand urban primary school; a case study. *Atmos Pollut Res*. 2019;10(2):435-444. doi:10.1016/j.apr.2018.09.006
36. Majd E, McCormack M, Davis M, et al. Indoor air quality in inner-city schools and its associations with building characteristics and environmental factors. *Environ Res*. 2019;170(August 2018):83-91. doi:10.1016/j.envres.2018.12.012
37. Zhang S, Liu H, Yu J, Luo W, Ding B. Microwave structured polyamide-6 nanofiber/net membrane with embedded poly(m-phenylene isophthalamide) staple fibers for effective ultrafine particle filtration. *J Mater Chem A*. 2016;4(16):6149-6157. doi:10.1039/C6TA00977H
38. Bortolassi ACC, Guerra VG, Aguiar ML. Characterization and evaluate the

efficiency of different filter media in removing nanoparticles. *Sep Purif Technol*. 2017;175:79-86. doi:10.1016/j.seppur.2016.11.010
39. Rautiainen P, Hyttinen M, Ruokolainen J, Saarinen P, Timonen J, Pasanen P. Indoor air-related symptoms and volatile organic compounds in materials and air in the hospital environment. *Int J Environ Health Res*. 2018;29(5):479-488. doi:10.1080/09603123.2018.1550194
40. Baurès E, Blanchard O, Mercier F, et al. Indoor air quality in two French hospitals: Measurement of chemical and microbiological contaminants. *Sci Total Environ*. 2018;642:168-179. doi:10.1016/j.scitotenv.2018.06.047
41. Ruan T, Rim D. Indoor air pollution in office buildings in mega-cities: Effects of filtration efficiency and outdoor air ventilation rates. *Sustain Cities Soc*. 2019;49(May):101609. doi:10.1016/j.scs.2019.101609
42. El-Sharkawy MF, Javed W. Study of indoor air quality level in various restaurants in Saudi Arabia. *Environ Prog Sustain Energy*. 2018;37(5):1713-1721. doi:10.1002/ep.12859
43. Neupane B, Kang S, Li C, Chen P. Trace elements analysis in hair strand of cooks chronically exposed to indoor air pollution in restaurants of Lhasa, Tibet: preliminary results. *SN Appl Sci*. 2019;1(9):1039. doi:10.1007/s42452-019-0890-9
44. Amoatey P, Omidvarborna H, Baawain MS, Al-Mamun A. Indoor air pollution and exposure assessment of the gulf cooperation council countries: A critical review. *Environ Int*. 2018;121(September):491-506. doi:10.1016/j.envint.2018.09.043
45. O'Lenick CR, Wilhelmi O V., Michael R, et al. Urban heat and air pollution: A framework for integrating population vulnerability and indoor exposure in health risk analyses. *Sci Total Environ*. 2019;660:715-723. doi:10.1016/j.scitotenv.2019.01.002
46. Bayat R, Ashrafi K, Shafiepour Motlagh M, et al. Health impact and related cost of ambient air pollution in Tehran. *Environ Res*. 2019;176(June). doi:10.1016/j.envres.2019.108547
47. Wang B, Liu Y, Li Z, Li Z. Association of indoor air pollution from coal combustion with influenza-like illness in housewives. *Environ Pollut*. 2016;216:646-652. doi:10.1016/j.envpol.2016.06.026
48. Jiang W, Lu C, Miao Y, Xiang Y, Chen L, Deng Q. Outdoor particulate air pollution and indoor renovation associated with childhood pneumonia in China. *Atmos Environ*. 2018;174(November 2017):76-81. doi:10.1016/j.atmosenv.2017.11.043
49. Lin N, Mu X, Wang G, et al. Accumulative effects of indoor air pollution exposure on leukocyte telomere length among non-smokers. *Environ Pollut*. 2017;227:1-7. doi:10.1016/j.envpol.2017.04.054
50. Penttinen P, Timonen KL, Tiittanen P, Mirme A, Ruuskanen J, Pekkanen J. Ultrafine particles in urban air and respiratory health among adult asthmatics.

Eur Respir J. 2001;17:428-435. doi:10.1183/09031936.01.17304280
51. Zhao CN, Xu Z, Wu GC, et al. Emerging role of air pollution in autoimmune diseases. *Autoimmun Rev*. 2019;18(6):607-614. doi:10.1016/j.autrev.2018.12.010
52. Barron M, Torero M. Household electrification and indoor air pollution. *J Environ Econ Manage*. 2017;86:81-92. doi:10.1016/j.jeem.2017.07.007
53. Hinds WC. Aerosol Technology: Properties, Behavior, and Measurement of Airborne Particles. In: *Behavior, and Measurement of Airborne Particles (2nd*.); 1999:504.
54. Yang C. Aerosol filtration application using fibrous media - An industrial perspective. *Chinese J Chem Eng*. 2012;20(1):1-9. doi:10.1016/S1004-9541(12)60356-5
55. Barhate RS, Ramakrishna S. Nanofibrous filtering media: Filtration problems and solutions from tiny materials. *J Memb Sci*. 2007;296(1-2):1-8. doi:10.1016/j.memsci.2007.03.038
56. Tang M, Hu J, Liang Y, Pui DYH. Pressure drop, penetration and quality factor of filter paper containing nanofibers. *Text Res J*. 2017;87(4):498-508. doi:10.1177/0040517516631318
57. Lee KW, Liu BYH, Liu KWLYH. Theoretical Study of Aerosol Filtration by Fibrous Filters Theoretical Study of Aerosol Filtration by Fibrous Filters. 2007;6826. doi:10.1080/02786828208958584
58. Liu G, Xiao M, Zhang X, et al. A review of air filtration technologies for sustainable and healthy building ventilation. *Sustain Cities Soc*. 2017;32(December 2016):375-396. doi:10.1016/j.scs.2017.04.011
59. Wang C Sen. Electrostatic forces in fibrous filters - A review. *Powder Technol*. 2001;118(1-2):166-170. doi:10.1016/S0032-5910(01)00307-2
60. Brown RC. *Air Filtration: An Integrated Approach to the Theory and Applications of Fibrous Filters*. Oxford: Pergamon Press; 1993.
61. Abouzar Moshfegh, Mehrzad Shams, Goodarz Ahmadi and RE. A Novel Slip Correction Factor for Spherical Aerosol Particles. *World Acad Sci Eng Technol*. 2009;27(January):709-717. http://citeseerx.ist.psu.edu/viewdoc/download?doi=10.1.1.308.9062&rep=rep1&type=pdf.
62. Hung CH, Leung WWF. Filtration of nano-aerosol using nanofiber filter under low Peclet number and transitional flow regime. *Sep Purif Technol*. 2011;79(1):34-42. doi:10.1016/j.seppur.2011.03.008
63. Su J, Yang G, Cheng C, Huang C, Xu H, Ke Q. Hierarchically structured TiO2/PAN nanofibrous membranes for high-efficiency air filtration and toluene degradation. *J Colloid Interface Sci*. 2017;507:386-396. doi:10.1016/j.jcis.2017.07.104
64. ISO 16890:2016 - Air filters for general ventilation. 2017.
65. Mao N. *Nonwoven Fabric Filters*. Vol i.; 2017. doi:10.1016/B978-0-08-

100573-6.00005-8
66. Wang LY, Yong WF, Yu LE, Chung TS. Design of high efficiency PVDF-PEG hollow fibers for air filtration of ultrafine particles. *J Memb Sci*. 2017;535(April):342-349. doi:10.1016/j.memsci.2017.04.053
67. Chattopadhyay S, Hatton TA, Rutledge GC. Aerosol filtration using electrospun cellulose acetate fibers. *J Mater Sci*. 2015;51(1):204-217. doi:10.1007/s10853-015-9286-4
68. Chen L, Ding S, Liang Z, Zhou L, Zhang H, Zhang C. Filtration efficiency analysis of fibrous filters: Experimental and theoretical study on the sampling of agglomerate particles emitted from a GDI engine. *Aerosol Sci Technol*. 2017;51(9):1082-1092. doi:10.1080/02786826.2017.1331293
69. Leung WWF, Hung CH. Investigation on pressure drop evolution of fibrous filter operating in aerodynamic slip regime under continuous loading of sub-micron aerosols. *Sep Purif Technol*. 2008;63(3):691-700. doi:10.1016/j.seppur.2008.07.015
70. Leung WWF, Chau YT. Experiments on filtering nano-aerosols from vehicular and atmospheric pollutants under dominant diffusion using nanofiber filter. *Sep Purif Technol*. 2019;213(December 2018):186-198. doi:10.1016/j.seppur.2018.12.021
71. Wang Z, Zhao C, Pan Z. Porous bead-on-string poly(lactic acid) fibrous membranes for air filtration. *J Colloid Interface Sci*. 2015;441:121-129. doi:10.1016/j.jcis.2014.11.041
72. Wang N, Zhu Z, Sheng J, Al-Deyab SS, Yu J, Ding B. Superamphiphobic nanofibrous membranes for effective filtration of fine particles. *J Colloid Interface Sci*. 2014;428:41-48. doi:10.1016/j.jcis.2014.04.026
73. Cui F, Han W, Ge J, Wu X, Kim H, Ding B. Electrospinning: A versatile strategy for mimicking natural creatures. *Compos Commun*. 2018;10(September):175-185. doi:10.1016/j.coco.2018.10.001
74. Cheng J, Li H, Cao Z, Wu D, Liu C, Pu H. Nanolayer coextrusion: An efficient and environmentally friendly micro/nanofiber fabrication technique. *Mater Sci Eng C*. 2018;95(January 2018):292-301. doi:10.1016/j.msec.2018.11.011
75. Zhang S, Liu H, Yu J, Luo W, Ding B. Microwave structured polyamide-6 nanofiber/net membrane with embedded poly(m-phenylene isophthalamide) staple fibers for effective ultrafine particle filtration. *J Mater Chem A*. 2016;4(16):6149-6157. doi:10.1039/c6ta00977h
76. Cheng Z, Cao J, Kang L, Luo Y, Li T, Liu W. Novel transparent nano-pattern window screen for effective air filtration by electrospinning. *Mater Lett*. 2018;221:157-160. doi:10.1016/j.matlet.2018.03.110
77. Kang DH, Kang HW. Advanced electrospinning using circle electrodes for freestanding PVDF nanofiber film fabrication. *Appl Surf Sci*. 2018;455(May):251-257. doi:10.1016/j.apsusc.2018.05.211
78. Cao M, Gu F, Rao C, Fu J, Zhao P. Improving the electrospinning process of

fabricating nanofibrous membranes to filter PM2.5. *Sci Total Environ*. 2019;666:1011-1021. doi:10.1016/j.scitotenv.2019.02.207
79. Karatay O, Doğan M. *Design and Implementation of an Electrospinning System*.; 2016. doi:10.1016/B978-0-323-41532-3.00012-9
80. Satilmis B, Budd PM, Uyar T. Systematic hydrolysis of PIM-1 and electrospinning of hydrolyzed PIM-1 ultrafine fibers for an efficient removal of dye from water. *React Funct Polym*. 2017;121(October):67-75. doi:10.1016/j.reactfunctpolym.2017.10.019
81. Thomas D, Pacault S, Charvet A, Bardin-Monnier N, Appert-Collin JC. Composite fibrous filters for nano-aerosol filtration: Pressure drop and efficiency model. *Sep Purif Technol*. 2019;215:557-564. doi:10.1016/j.seppur.2019.01.043
82. Thomas D, Penicot P, Contal P, Leclerc D, Vendel J. Clogging of fibrous filters by solid aerosol particles experimental and modelling study. *Chem Eng Sci*. 2001;56(11):3549-3561. doi:10.1016/S0009-2509(01)00041-0
83. Leung WWF, Hau CWY. Skin layer in cyclic loading-cleaning of a nanofiber filter in filtering nano-aerosols. *Sep Purif Technol*. 2017;188:367-378. doi:10.1016/j.seppur.2017.07.043
84. Elmøe TD, Tricoli A, Grunwaldt JD, Pratsinis SE. Filtration of nanoparticles: Evolution of cake structure and pressure-drop. *J Aerosol Sci*. 2009;40(11):965-981. doi:10.1016/j.jaerosci.2009.09.002
85. Leung WWF, Hau CWY, Choy HF. Microfiber-nanofiber composite filter for high-efficiency and low pressure drop under nano-aerosol loading. *Sep Purif Technol*. 2018;206(May):26-38. doi:10.1016/j.seppur.2018.05.033
86. Signoretta PE, Buffel V, Bracke P. Mental wellbeing, air pollution and the ecological state. *Heal Place*. 2019;57(March):82-91. doi:10.1016/j.healthplace.2019.03.003
87. Zhou T, Jiang Q, Wang L, et al. Facile preparation of nitrogen-enriched hierarchical porous carbon nanofibers by Mg(OAc)2-assisted electrospinning for flexible supercapacitors. *Appl Surf Sci*. 2018;456(February):827-834. doi:10.1016/j.apsusc.2018.06.214
88. Wang Z, Pan Z. Preparation of hierarchical structured nano-sized/porous poly(lactic acid) composite fibrous membranes for air filtration. *Appl Surf Sci*. 2015;356:1168-1179. doi:10.1016/j.apsusc.2015.08.211
89. Zheng J, Zhang H, Zhao Z, Han CC. Construction of hierarchical structures by electrospinning or electrospraying. *Polymer (Guildf)*. 2012;53(2):546-554. doi:10.1016/j.polymer.2011.12.018
90. Sun Q, Leung WWF. Charged PVDF multi-layer filters with enhanced filtration performance for filtering nano-aerosols. *Sep Purif Technol*. 2019;212(November 2018):854-876. doi:10.1016/j.seppur.2018.11.063
91. Wang N, Si Y, Wang N, et al. Multilevel structured polyacrylonitrile/silica nanofibrous membranes for high-performance air filtration. *Sep Purif Technol*.

2014;126:44-51. doi:10.1016/j.seppur.2014.02.017
92. Du J, Liu D, Chen S, Wan D, Pu H. A novel method for fabricating continuous polymer nanofibers. *Polymer (Guildf)*. 2016;102:209-213. doi:10.1016/j.polymer.2016.09.018
93. Amin A, Merati AA, Bahrami SH, Bagherzadeh R. Effects of porosity gradient of multilayered electrospun nanofibre mats on air filtration efficiency. *J Text Inst*. 2016;5000(June):1-9. doi:10.1080/00405000.2016.1264856
94. Jamil SM, Othman MHD, Rahman MA, et al. Properties and performance evaluation of dual-layer ceramic hollow fiber with modified electrolyte for MT-SOFC. *Renew Energy*. 2019;134:1423-1433. doi:10.1016/j.renene.2018.09.071
95. Zhang J, Hou X, Pang Z, et al. Fabrication of hierarchical TiO2nanofibers by microemulsion electrospinning for photocatalysis applications. *Ceram Int*. 2017;43(17):15911-15917. doi:10.1016/j.ceramint.2017.08.166
96. Wan H, Wang N, Yang J, et al. Hierarchically structured polysulfone/titania fibrous membranes with enhanced air filtration performance. *J Colloid Interface Sci*. 2014;417:18-26. doi:10.1016/j.jcis.2013.11.009
97. Li X, Wang N, Fan G, et al. Electreted polyetherimide-silica fibrous membranes for enhanced filtration of fine particles. *J Colloid Interface Sci*. 2015;439:12-20. doi:10.1016/j.jcis.2014.10.014
98. Zhong L, Wang T, Liu L, Du W, Wang S. Ultra-fine SiO2nanofilament-based PMIA: A double network membrane for efficient filtration of PM particles. *Sep Purif Technol*. 2018;202(December 2017):357-364. doi:10.1016/j.seppur.2018.03.053
99. Zhu M, Hua D, Pan H, et al. Green electrospun and crosslinked poly(vinyl alcohol)/poly(acrylic acid) composite membranes for antibacterial effective air filtration. *J Colloid Interface Sci*. 2018;511:411-423. doi:10.1016/j.jcis.2017.09.101
100. Hassan MA, Yeom BY, Wilkie A, Pourdeyhimi B, Khan SA. Fabrication of nanofiber meltblown membranes and their filtration properties. *J Memb Sci*. 2013;427:336-344. doi:10.1016/j.memsci.2012.09.050
101. Erben J, Jencova V, Chvojka J, et al. The combination of meltblown technology and electrospinning - The influence of the ratio of micro and nanofibers on cell viability. *Mater Lett*. 2016;173:153-157. doi:10.1016/j.matlet.2016.02.147
102. Nayak R, Kyratzis IL, Truong YB, Padhye R, Arnold L. Structural and mechanical properties of polypropylene nanofibres fabricated by meltblowing. *J Text Inst*. 2015;106(6):629-640. doi:10.1080/00405000.2014.933512
103. Ghosal K, Agatemor C, Špitálsky Z, Thomas S, Kny E. Electrospinning tissue engineering and wound dressing scaffolds from polymer-titanium dioxide nanocomposites. *Chem Eng J*. 2019;358(September 2018):1262-1278. doi:10.1016/j.cej.2018.10.117

104. Shen Y, Liu Q, Deng B, Yao P, Xia S. Experimental study and prediction of the diameter of melt-electrospinning polypropylene fiber. *Fibers Polym*. 2016;17(8):1227-1237. doi:10.1007/s12221-016-6303-4
105. Zhang K, Li Z, Kang W, et al. Preparation and characterization of tree-like cellulose nanofiber membranes via the electrospinning method. *Carbohydr Polym*. 2018;183(August 2017):62-69. doi:10.1016/j.carbpol.2017.11.032
106. Gee S, Johnson B, Smith AL. Optimizing electrospinning parameters for piezoelectric PVDF nanofiber membranes. *J Memb Sci*. 2018;563(June):804-812. doi:10.1016/j.memsci.2018.06.050
107. Andrady AL. *Science and Technology of Polymer Nanofibers*. John Wiley & Sons, INC; 2008.
108. Reneker DH, Yarin AL. Electrospinning jets and polymer nanofibers. *Polymer (Guildf)*. 2008;49(10):2387-2425. doi:10.1016/j.polymer.2008.02.002
109. You X, Ye C, Guo P. Electric field manipulation for deposition control in near-field electrospinning. *J Manuf Process*. 2017;30:431-438. doi:10.1016/j.jmapro.2017.10.005
110. Burger C, Hsiao BS, Chu B. Nanofibrous Materials and Their Applications. *Annu Rev Mater Res*. 2006;36(1):333-368. doi:10.1146/annurev.matsci.36.011205.123537
111. Nazari T, Garmabi H. The effects of processing parameters on the morphology of PLA/PEG melt electrospun fibers. *Polym Int*. 2018;67(2):178-188. doi:10.1002/pi.5486
112. Bata A. Polymer Melt Viscosity Measuring By an. 2015;2(2):112-117.
113. Nayak R, Padhye R, Kyratzis IL, Truong YB, Arnold L. Effect of viscosity and electrical conductivity on the morphology and fiber diameter in melt electrospinning of polypropylene. *Text Res J*. 2013;83(6):606-617. doi:10.1177/0040517512458347
114. Pimenta AFR, Baptista AC, Carvalho T, et al. Electrospinning of Ion Jelly fibers. *Mater Lett*. 2012;83:161-164. doi:10.1016/j.matlet.2012.04.146
115. Bazbouz MB, Liang H, Tronci G. A UV-cured nanofibrous membrane of vinylbenzylated gelatin-poly(ε-caprolactone) dimethacrylate co-network by scalable free surface electrospinning. *Mater Sci Eng C*. 2018;91(May):541-555. doi:10.1016/j.msec.2018.05.076
116. Leach MK, Feng Z-Q, Tuck SJ, Corey JM. Electrospinning Fundamentals: Optimizing Solution and Apparatus Parameters. *J Vis Exp*. 2011;(47):2-5. doi:10.3791/2494
117. Salas C. *Solution Electrospinning of Nanofibers*. Elsevier Ltd.; 2016. doi:10.1016/B978-0-08-100907-9.00004-0
118. Cuvellier A, Torre-Muruzabal A, Kizildag N, et al. Coaxial electrospinning of epoxy and amine monomers in a pullulan shell for self-healing nanovascular systems. *Polym Test*. 2018;69(February):146-156. doi:10.1016/j.polymertesting.2018.05.023

119. A. Cardona R del, J. J. Materials and Processes for Ion Permeable Separating Membranes by Electro-Spinning. *Adv Nanofibers*. 2013:145-163. doi:10.5772/57094
120. Dayan CB, Afghah F, Okan BS, et al. Modeling 3D melt electrospinning writing by response surface methodology. *Mater Des*. 2018;148:87-95. doi:10.1016/j.matdes.2018.03.053
121. Su C, Lu C, Cao H, et al. Fabrication of a novel nanofibers-covered hollow fiber membrane via continuous electrospinning with non-rotational collectors. *Mater Lett*. 2017;204:8-11. doi:10.1016/j.matlet.2017.05.134
122. Wen P, Zong MH, Linhardt RJ, Feng K, Wu H. Electrospinning: A novel nano-encapsulation approach for bioactive compounds. *Trends Food Sci Technol*. 2017;70(May):56-68. doi:10.1016/j.tifs.2017.10.009
123. Santos RPO, Rodrigues BVM, Ramires EC, Ruvolo-Filho AC, Frollini E. Bio-based materials from the electrospinning of lignocellulosic sisal fibers and recycled PET. *Ind Crops Prod*. 2015;72:69-76. doi:10.1016/j.indcrop.2015.01.024
124. Lee M, Kim HY. Toward nanoscale three-dimensional printing: Nanowalls built of electrospun nanofibers. *Langmuir*. 2014;30(5):1210-1214. doi:10.1021/la404704z
125. Ristovski N, Bock N, Liao S, et al. Improved fabrication of melt electrospun tissue engineering scaffolds using direct writing and advanced electric field control. *Biointerphases*. 2015;10(1):011006. doi:10.1116/1.4914380
126. Brown TD, Edin F, Detta N, Skelton AD, Hutmacher DW, Dalton PD. Melt electrospinning of poly(ε-caprolactone) scaffolds: Phenomenological observations associated with collection and direct writing. *Mater Sci Eng C*. 2015;45:698-708. doi:10.1016/j.msec.2014.07.034
127. Deshawar D, Chokshi P. Analysis of axisymmetric instability in polymer melt electrospinning jet. *J Nonnewton Fluid Mech*. 2018;255(March):1-12. doi:10.1016/j.jnnfm.2018.03.003
128. Deshawar D, Chokshi P. Stability analysis of an electrospinning jet of polymeric fluids. *Polym (United Kingdom)*. 2017;131:34-49. doi:10.1016/j.polymer.2017.10.019
129. Muerza-Cascante ML, Shokoohmand A, Khosrotehrani K, et al. Endosteal-like extracellular matrix expression on melt electrospun written scaffolds. *Acta Biomater*. 2017;52:145-158. doi:10.1016/j.actbio.2016.12.040
130. Tourlomousis F, Chang RC. Dimensional Metrology of Cell-matrix Interactions in 3D Microscale Fibrous Substrates. *Procedia CIRP*. 2017;65:32-37. doi:10.1016/j.procir.2017.04.009
131. Zaiss S, Brown TD, Reichert JC, Berner A. Poly(??-caprolactone) scaffolds fabricated by melt electrospinning for bone tissue engineering. *Materials (Basel)*. 2016;9(4):1-15. doi:10.3390/ma9040232
132. Kim JS, Lee DS. Thermal properties of electrospun polyesters. *Polym J*.

2000;32(7):616-618. doi:10.1295/polymj.32.616
133. Lyons J, Li C, Ko F. Melt-electrospinning part I: Processing parameters and geometric properties. *Polymer (Guildf)*. 2004;45(22):7597-7603. doi:10.1016/j.polymer.2004.08.071
134. Zhou H, Green TB, Joo YL. The thermal effects on electrospinning of polylactic acid melts. *Polymer (Guildf)*. 2006;47(21):7497-7505. doi:10.1016/j.polymer.2006.08.042
135. Dalton PD, Grafahrend D, Klinkhammer K, Klee D, Möller M. Electrospinning of polymer melts: Phenomenological observations. *Polymer (Guildf)*. 2007;48(23):6823-6833. doi:10.1016/j.polymer.2007.09.037
136. Liu Y, Wang X, Li H, Yan H, Yang W. Factors affecting melt electrospinning. *Nano*. 2010:10.1002/spepro.003055. doi:10.1002/spepro.003055
137. Dalton PD, Klinkhammer K, Salber J, Klee D, Möller M. Direct in vitro electrospinning with polymer melts. *Biomacromolecules*. 2006;7(3):686-690. doi:10.1021/bm050777q
138. Dalton PD, Joergensen NT, Groll J, Moeller M. Patterned melt electrospun substrates for tissue engineering. *Biomed Mater*. 2008;3(3). doi:10.1088/1748-6041/3/3/034109
139. Zhmayev E, Cho D, Joo YL. Nanofibers from gas-assisted polymer melt electrospinning. *Polymer (Guildf)*. 2010;51(18):4140-4144. doi:10.1016/j.polymer.2010.06.058
140. Detta N, Brown TD, Edin FK, et al. Melt electrospinning of polycaprolactone and its blends with poly(ethylene glycol). *Polym Int*. 2010;59(11):1558-1562. doi:10.1002/pi.2954
141. Karchin A, Simonovsky FI, Ratner BD, Sanders JE. Melt electrospinning of biodegradable polyurethane scaffolds. *Acta Biomater*. 2011;7(9):3277-3284. doi:10.1016/j.actbio.2011.05.017
142. Li X, Liu H, Wang J, Li C. Preparation and characterization of poly(??-caprolactone) nonwoven mats via melt electrospinning. *Polymer (Guildf)*. 2012;53(1):248-253. doi:10.1016/j.polymer.2011.11.008
143. Li X, Liu H, Wang J, Li C. Preparation and characterization of PLLA/nHA nonwoven mats via laser melt electrospinning. *Mater Lett*. 2012;73:103-106. doi:10.1016/j.matlet.2011.12.108
144. Dalton PD. Melt electrowriting with additive manufacturing principles. *Curr Opin Biomed Eng*. 2017;2:49-57. doi:10.1016/j.cobme.2017.05.007
145. Hutmacher DW, Dalton PD. Melt electrospinning. *Chem - An Asian J*. 2011;6(1):44-56. doi:10.1002/asia.201000436
146. Bas O, Catelas I, De-Juan-Pardo EM, Hutmacher DW. The quest for mechanically and biologically functional soft biomaterials via soft network composites. *Adv Drug Deliv Rev*. 2018;132:214-234. doi:10.1016/j.addr.2018.07.015
147. Li HY, Bubakir MM, Xia T, Zhong XF, Ding YM, Yang WM. Mass

production of ultra-fine fibre by melt electrospinning method using umbellate spinneret. *Mater Res Innov*. 2014;18(S4):S4-921-S4-925. doi:10.1179/1432891714Z.000000000877
148. Hochleitner G, Jüngst T, Brown TD, et al. Additive manufacturing of scaffolds with sub-micron filaments via melt electrospinning writing. *Biofabrication*. 2015;7(3):035002. doi:10.1088/1758-5090/7/3/035002
149. Zhao FW, Liu Y, Ding YM, Yan H, Xie PC, Yang WM. Effect of Plasticizer and Load on Melt Electrospinning of PLA. *Key Eng Mater*. 2012;501:32-36. doi:10.4028/www.scientific.net/KEM.501.32
150. Chen H, Li H, Ma X, He W, Tan J, Yang W. Large scaled fabrication of microfibers by air-suction assisted needleless melt electrospinning. *Fibers Polym*. 2016;17(4):576-581. doi:10.1007/s12221-016-5915-z
151. Li X, Liu Y, Peng H, Ma X, Fong H. Effects of hot airflow on macromolecular orientation and crystallinity of melt electrospun poly (L-lactic acid) fibers. *Mater Lett*. 2016;176:194-198. doi:10.1016/j.matlet.2016.04.070
152. McCann JT, Marquez M, Xia Y. Melt Coaxial Electrospinning: A Versatile Method for the Encapsulation\rof Solid Materials and Fabrication of Phase Change Nanofibers. *Nano Lett*. 2006;6(12):2868-2872.
153. Brown TD, Dalton PD, Hutmacher DW. Progress in Polymer Science Melt electrospinning today: An opportune time for an emerging polymer process. *Prog Polym Sci*. 2016;56:116-166. doi:10.1016/j.progpolymsci.2016.01.001
154. Zong X, Kim K, Fang D, Ran S, Hsiao BS, Chu B. Structure and process relationship of electrospun bioabsorbable nanofiber membranes. *Polymer (Guildf)*. 2002;43(16):4403-4412. doi:10.1016/S0032-3861(02)00275-6
155. Brown TD, Dalton PD, Hutmacher DW. Melt electrospinning today: An opportune time for an emerging polymer process. *Prog Polym Sci*. 2015;56:116-166. doi:10.1016/j.progpolymsci.2016.01.001
156. Ren J, Blackwood KA, Doustgani A, et al. Melt-electrospun polycaprolactone strontium-substituted bioactive glass scaffolds for bone regeneration. *J Biomed Mater Res - Part A*. 2014;102(9):3140-3153. doi:10.1002/jbm.a.34985
157. Yu S-X, Zheng J, Yan X, et al. Morphology control of PLA microfibers and spheres via melt electrospinning. *Mater Res Express*. 2018;5(4):045019. doi:10.1088/2053-1591/aab9f4
158. Doustgani A, Ahmadi E. Melt electrospinning process optimization of polylactic acid nanofibers. *J Ind Text*. 2016;45(4):626-634. doi:10.1177/1528083715610297
159. Qin Y, Cheng L, Zhang Y, et al. Efficient preparation of poly(lactic acid) nanofibers by melt differential electrospinning with addition of acetyl tributyl citrate. *J Appl Polym Sci*. 2018;135(31):42-45. doi:10.1002/app.46554
160. Li X, Zhang Y, Li H, Chen H, Ding Y, Yang W. Effect of oriented fiber membrane fabricated via needleless melt electrospinning on water filtration

efficiency. *Desalination*. 2014;344:266-273. doi:10.1016/j.desal.2014.04.003
161. Cao K, Liu Y. PLLA-PHB fiber membranes obtained by solvent-free electrospinning for short-time drug delivery. 2018:291-302.
162. Govinna ND, Keller T, Schick C, Cebe P. Melt-electrospinning of poly(ether ether ketone) fibers to avoid sulfonation. *Polymer (Guildf)*. 2019;171(February):50-57. doi:10.1016/j.polymer.2019.03.041
163. Ren J, Blackwood KA, Doustgani A, et al. Melt-electrospun polycaprolactone strontium-substituted bioactive glass scaffolds for bone regeneration. *J Biomed Mater Res - Part A*. 2014;102(9):3140-3153. doi:10.1002/jbm.a.34985
164. Lian H, Meng Z. Melt electrospinning of daunorubicin hydrochloride-loaded poly (ε-caprolactone) fibrous membrane for tumor therapy. *Bioact Mater*. 2017;2(2):1-5. doi:10.1016/j.bioactmat.2017.03.003
165. Nguyen NT, Kim JH, Jeong YH. Identification of sagging in melt-electrospinning of microfiber scaffolds. *Mater Sci Eng C*. 2019;103(May). doi:10.1016/j.msec.2019.109785
166. Brown TD, Dalton PD, Hutmacher DW. Melt electrospinning today: An opportune time for an emerging polymer process. *Prog Polym Sci*. 2015;56:116-166. doi:10.1016/j.progpolymsci.2016.01.001
167. Kamble P, Sadarani B, Majumdar A, Bhullar S. Nanofiber based drug delivery systems for skin: A promising therapeutic approach. *J Drug Deliv Sci Technol*. 2017;41:124-133. doi:10.1016/j.jddst.2017.07.003
168. Sun B, Long YZ, Zhang HD, et al. Advances in three-dimensional nanofibrous macrostructures via electrospinning. *Prog Polym Sci*. 2014;39(5):862-890. doi:10.1016/j.progpolymsci.2013.06.002
169. Zhang S, Liu H, Yin X, Yu J, Ding B. Anti-deformed Polyacrylonitrile/Polysulfone Composite Membrane with Binary Structures for Effective Air Filtration. *ACS Appl Mater Interfaces*. 2016;8(12):8086-8095. doi:10.1021/acsami.6b00359
170. Al-Attabi R, Dumée LF, Schütz JA, Morsi Y. Pore engineering towards highly efficient electrospun nanofibrous membranes for aerosol particle removal. *Sci Total Environ*. 2018;625:706-715. doi:10.1016/j.scitotenv.2017.12.342
171. Ngo TD, Kashani A, Imbalzano G, Nguyen KTQ, Hui D. Additive manufacturing (3D printing): A review of materials, methods, applications and challenges. *Compos Part B Eng*. 2018;143(December 2017):172-196. doi:10.1016/j.compositesb.2018.02.012
172. Shen Y, Xia S, Yao P, Hugh Gong R, Liu Q, Deng B. Structure regulation and properties of melt-electrospinning composite filter materials. *Fibers Polym*. 2017;18(8):1568-1579. doi:10.1007/s12221-017-7172-1
173. Sidaraviciute R, Buivydiene D, Krugly E, Valatka E, Martuzevicius D. A composite microfibre-supported short-nanofibre photocatalyst for environmental pollutant decomposition. *J Photochem Photobiol A Chem*.

2018. doi:10.1016/j.jphotochem.2018.09.017
174. Li Z, Xu Y, Fan L, Kang W, Cheng B. Fabrication of polyvinylidene fluoride tree-like nanofiber via one-step electrospinning. *Mater Des*. 2016;92:95-101. doi:10.1016/j.matdes.2015.12.037
175. Zhao X, Wang S, Yin X, Yu J, Ding B. Slip-Effect Functional Air Filter for Efficient Purification of PM 2.5. *Sci Rep*. 2016;6(July):1-11. doi:10.1038/srep35472
176. Balgis R, Kartikowati CW, Ogi T, et al. Synthesis and evaluation of straight and bead-free nanofibers for improved aerosol filtration. *Chem Eng Sci*. 2015;137:947-954. doi:10.1016/j.ces.2015.07.038
177. Buivydiene D, Dabasinskaite L, Krugly E, Kliucininkas L. Formation of PA12 fibres via melt electrospinning process: Parameter analysis and optimisation. *J Polym Eng*. 2019:2015-2017. doi:10.1515/polyeng-2019-0190
178. Schumacher S, Spiegelhoff D, Schneiderwind U, Finger H, Asbach C. Performance of New and Artificially Aged Electret Filters in Indoor Air Cleaners. *Chem Eng Technol*. 2018;41(1):27-34. doi:10.1002/ceat.201700105
179. Stephens B. Evaluating the sensitivity of the mass-based particle removal calculations for HVAC filters in ISO 16890 to assumptions for aerosol distributions. *Atmosphere (Basel)*. 2018;9(3). doi:10.3390/atmos9030085
180. Ismail N, Junior Maksoud F, Ghaddar N, Ghali K, Tehrani-Bagha A. A mathematical model to predict the effect of electrospinning processing parameters on the morphological characteristic of nano-fibrous web and associated filtration efficiency. *J Aerosol Sci*. 2017;113(June 2016):227-241. doi:10.1016/j.jaerosci.2017.08.013
181. Iregui A, Irusta L, Llorente O, et al. Electrospinning of cationically polymerized epoxy/polycaprolactone blends to obtain shape memory fibers (SMF). *Eur Polym J*. 2017;94(March):376-383. doi:10.1016/j.eurpolymj.2017.07.026
182. Park HK, Joo W, Gu BK, Ha MY, You SJ, Chun HJ. Collagen/poly(D,L-lactic-co-glycolic acid) composite fibrous scaffold prepared by independent nozzle control multi-electrospinning apparatus for dura repair. *J Ind Eng Chem*. 2018;66:430-437. doi:10.1016/j.jiec.2018.06.010
183. Beigmoradi R, Samimi A, Mohebbi-Kalhori D. Fabrication of polymeric nanofibrous mats with controllable structure and enhanced wetting behavior using one-step electrospinning. *Polymer (Guildf)*. 2018;143:271-280. doi:10.1016/j.polymer.2018.04.025
184. Li X, Yang W, Li H, et al. Water filtration properties of novel composite membranes combining solution electrospinning and needleless melt electrospinning methods. *J Appl Polym Sci*. 2015;132(10):1-8. doi:10.1002/app.41601
185. Ko J, Ahsani V, Yao S, Mohtaram N. Fabricating and controlling PCL electrospun microfibers using filament feeding melt electrospinning

technique. *J*. 2016. doi:10.1088/1361-6439/aa4fd9
186. Zeng J, Wang H, Lin Y, et al. Fabrication of microfluidic channels based on melt-electrospinning direct writing. *Microfluid Nanofluidics*. 2018;22(2):1-10. doi:10.1007/s10404-018-2043-7
187. Abolhasani MM, Shirvanimoghaddam K, Khayyam H, Moosavi SM, Zohdi N, Naebe M. Towards predicting the piezoelectricity and physiochemical properties of the electrospun P(VDF-TrFE) nanogenrators using an artificial neural network. *Polym Test*. 2018;66(January):178-188. doi:10.1016/j.polymertesting.2018.01.010
188. Senthil T, Anandhan S. Solution electrospinning of styrene-acrylonitrile random copolymer from dimethyl sulfoxide. *Int J Plast Technol*. 2013;17(2):123-138. doi:10.1007/s12588-013-9053-9
189. Liu Y, Li X, Ramakrishna S. Melt electrospinning in a parallel electric field. *J Polym Sci Part B Polym Phys*. 2014;52(14):946-952. doi:10.1002/polb.23511
190. Megelski S, Stephens JS, Bruce Chase D, Rabolt JF. Micro- and nanostructured surface morphology on electrospun polymer fibers. *Macromolecules*. 2002;35(22):8456-8466. doi:10.1021/ma020444a
191. Deitzel J., Kleinmeyer J, Harris D, Beck Tan N. The effect of processing variables on the morphology of electrospun nanofibers and textiles. *Polymer (Guildf)*. 2001;42(1):261-272. doi:10.1016/S0032-3861(00)00250-0
192. Thompson CJ, Chase GG, Yarin AL, Reneker DH. Effects of parameters on nanofiber diameter determined from electrospinning model. *Polymer (Guildf)*. 2007;48(23):6913-6922. doi:10.1016/j.polymer.2007.09.017
193. Jason Lyons, Christopher Li FK. Melt-electrospinning part I: processing parameters and geometric properties. *Polymer (Guildf)*. 2014;45(22):1-5. doi:10.1016/j.matlet.2016.04.070
194. Lian H, Meng Z. Melt electrospinning vs. solution electrospinning: A comparative study of drug-loaded poly (ε-caprolactone) fibres. *Mater Sci Eng C*. 2017;74:117-123. doi:10.1016/j.msec.2017.02.024
195. Karahaliloglu Z, Hacker C, Demirbilek M, Seide G, Denkbas EB, Gries T. Photocatalytic performance of melt-electrospun polypropylene fabric decorated with TiO2nanoparticles. *J Nanoparticle Res*. 2014;16(9). doi:10.1007/s11051-014-2615-8
196. Wang Q, Curtis CK, Thoppey NM, Bochinski J, Gorga R, Clarke L. Unconfined, melt edge electrospinning from multiple, spontaneous, self-organized polymer jets. *Mater Res Express*. 2014;1(4):45304. doi:10.1088/2053-1591/1/4/045304
197. Guo C, Zhou L, Lv J. Effects of expandable graphite and modified ammonium polyphosphate on the flame-retardant and mechanical properties of wood flour-polypropylene composites. *Polym Polym Compos*. 2013;21(7):449-456. doi:10.1002/app
198. Alazab M, Mitchell GR, Davis FJ, Mohan SD. Sustainable Electrospinning of

Nanoscale Fibres. *Procedia Manuf*. 2017;12(December 2016):66-78. doi:10.1016/j.promfg.2017.08.009
199. Shenoy A V., Saini DR, Nadkarni VM. Melt rheology of polymer blends from melt flow index. *Int J Polym Mater Polym Biomater*. 1984;10(3):213-235. doi:10.1080/00914038408080271
200. Cengiz F, Krucińska I, Gliścińska E, Chrzanowski M, Göktepe F. Comparative analysis of various electrospinning methods of nanofibre formation. *Fibres Text East Eur*. 2009;72(1):13-19.
201. Javier Macossay, Alexis Marruffo, Roman Rincon TE and AK. Effect of needle diameter on nanofiber diameter and thermal properties of electrospun poly(methyl methacrylate). *Polym Adv Technol*. 2007;(February):180–183. doi:10.1002/pat
202. Vaughn E, Ramachandran G. Fiberglass Vs . Synthetic Air Filtration Media. *INJ Fall*. 2002:41-53.
203. Kadam V V., Wang L, Padhye R. Electrospun nanofibre materials to filter air pollutants – A review. *J Ind Text*. 2018;47(8):2253-2280. doi:10.1177/1528083716676812
204. Zhang S, Shim WS, Kim J. Design of ultra-fine nonwovens via electrospinning of Nylon 6: Spinning parameters and filtration efficiency. *Mater Des*. 2009;30(9):3659-3666. doi:10.1016/j.matdes.2009.02.017
205. Huang SH, Chen CW, Kuo YM, Lai CY, McKay R, Chen CC. Factors affecting filter penetration and quality factor of particulate respirators. *Aerosol Air Qual Res*. 2013;13(1):162-171. doi:10.4209/aaqr.2012.07.0179
206. Zhang S, Liu H, Yin X, Li Z, Yu J, Ding B. Tailoring mechanically robust poly(m-phenylene isophthalamide) nanofiber/nets for ultrathin high-efficiency air filter. *Sci Rep*. 2017;7(January):1-11. doi:10.1038/srep40550
207. Frising T, Thomas D, Contal P, Bémer D, Leclerc D. Influence of filter fibre size distribution on filter efficiency calculations. *Chem Eng Res Des*. 2003;81(9):1179-1184. doi:10.1205/026387603770866353
208. Shou D, Fan J, Ye L, Zhang H, Qian X, Zhang Z. Inverse Problem of Air Filtration of Nanoparticles: Optimal Quality Factors of Fibrous Filters. *J Nanomater*. 2015;2015. doi:10.1155/2015/168392
209. Wang H, Xu Y, Wei Q. Preparation of bamboo-hat-shaped deposition of a poly(ethylene terephthalate) fiber web by melt-electrospinning. *Text Res J*. 2015;85(17):1838-1848. doi:10.1177/0040517515573414
210. Lee KW, Liu BYH. On the Minimum Efficiency and the Most Penetrating Particle Size for Fibrous Filters. *J Air Pollut Control Assoc*. 1980;30(4):377-381. doi:10.1080/00022470.1980.10464592
211. Boskovic L, Altman IS, Agranovski IE, Braddock RD, Myojo T, Choi M. Influence of particle shape on filtration processes. *Aerosol Sci Technol*. 2005;39(12):1184-1190. doi:10.1080/02786820500442410
212. Miaskiewicz-Peska E, Lebkowska M. Comparison of aerosol and bioaerosol

collection on air filters. *Aerobiologia (Bologna)*. 2012;28(2):185-193. doi:10.1007/s10453-011-9223-1

213. Boskovic L, Agranovski IE, Altman IS, Braddock RD. Filter efficiency as a function of nanoparticle velocity and shape. *J Aerosol Sci*. 2008;39(7):635-644. doi:10.1016/j.jaerosci.2008.03.003

214. Kang YO, Im JN, Park WH. Morphological and permeable properties of antibacterial double-layered composite nonwovens consisting of microfibers and nanofibers. *Compos Part B Eng*. 2015;75:256-263. doi:10.1016/j.compositesb.2015.01.029

Supplemented materials

Appendix 1. Technical properties of polymers used in melt electrospinning

Supplier				Evonik AG		Arkema		DSM
Product				Vestamid™		Rilsamid®	Pebax® RNEW	Arnitel®
Property	Test method	Unit		L1600	L1901	AMN 0 TLD	35R53 SP 01	3106
Polymer				Nylon 12		Natural polyamide resin	Polyether block resin	Thermoplastic Copolyester
Rheological properties								
Melt flow rate, MFR	230 °C; 2.16 kg	ISO 1133	g/10min	132	15	44	25	28
Molding shrinkage, normal		ISO 294-4, 2577	%	–	–	0.8	0.6	
Molding shrinkage, parallel		ISO 294-4, 2577	%	–	–	0.8	0.6	
Mechanical properties								
Tensile test		ISO 527-1						
Stress at yield		ISO 527-2	MPa	45	45	42	–	
Strain at yield			%	5	5	7	–	
Nominal strain at break			%	>50	>50	>50	>50	

Tensile modulus		ISO 527-1	MPa	1400	1400	1450	40	
Thermal properties								
Melting temperature	10°C/min	ISO 11357-1/-3	°C	178	178	178	135	
Temperature of deflection under load								
Method A	1.8 MPa	ISO 75-2	°C	50	50	55	–	
Method B	0.45 MPa		°C	110	110	135	–	
Vicat softening temperature		ISO 306						
Method A	10 N		°C	173	173	–	–	
Method B	50 N		°C	138	138	142	81	
Flammability acc. UL94	3.2 mm	IEC 60695		HB	HB	V-2	–	
	1.6 mm			HB	HB	HB	–	
Linear thermal expansion	23 – 55 °C	ISO 11359	$10^{-4} \cdot K^{-1}$	1.5	1.5	1.2	–	
Oxygen index		ISO 4589-1/-2	%	–	–	22	–	
Thermal degradation	10°C/min		°C	382	332	254	317	322
Electrical properties								
Relative permittivity	100 Hz	IEC 60250		3.1	3.8	4	–	
	1 MHz			2.9	2.5	3	–	

Dissipation factor	100 Hz	IEC 60250	10^{-4}	400	400	774	–	
	1 MHz		10^{-4}	300	300	290	–	
Electric strength	K20/P50	IEC 60243 -1	kV/mm	26	26	30	–	
Volume resistivity		IEC 60093	Ohm · m	$> 10^{13}$	$> 10^{13}$	10^{12}	–	
Surface resistivity		IEC 60093	Ohm · m	–	–	10^{14}	–	
Other properties								
Water absorption	saturation	ISO 62	%	1.5	1.5	1.8	1.3	
Moisture absorption	23 °C/50 % r.h.	ISO 62	%	0.7	0.7	0.7	0.5	
Viscosity number		ISO 307	ml/g	120	180	–	–	
Melting range	ISO 11357		°C	approx. 178	approx. 178	–	–	
Density	23 °C	ISO 1183	g/cm³	1.02	1.02	1.02	1.02	

Appendix 2. Fibre size parameters, morphologies and efficiencies of formed mats

Code	Average diameter, µm	Median, µm	Geometric Mean, µm	Quartile Range, µm	Min. diameter, µm	Max. diameter, µm	Morphology*	*e*PM$_1$ filtration efficiency, %	*e*PM$_1$ min
N1A	5.87±2.54	6.70	4.46	2.65	0.13	9.83	Normal	-	-
N2A	2.85±2.47	1.76	1.85	3.68	0.24	9.76	Disperse/Small	55	52
N3A	4.01±2.36	4.25	3.20	3.61	0.48	9.96	Disperse/Small	61	56
N4A	8.63±2.67	8.26	8.14	2.89	1.43	17.07	Normal	58	50
N5A	6.08±3.81	6.41	4.50	6.90	0.66	14.08	Disperse	80	79
N6A	5.10±2.81	4.18	4.47	1.80	0.74	15.01	Disperse/Small	63	62
N7A	5.72±3.47	5.17	4.48	5.61	0.84	14.53	Disperse	74	70
N8A	7.09±2.63	7.83	6.28	2.01	0.71	13.10	Suppressed whipping	-	-
N9A	3.92±2.06	3.84	3.29	2.83	0.37	10.86	Disperse/Small	56	53
N10A	7.18±4.34	5.79	6.20	3.37	2.49	23.25	Disperse/Thick	61	56
N11A	5.76±3.88	5.35	4.40	6.06	0.42	25.41	Normal/Few ribbons	58	57
N12A	6.35±5.29	3.89	4.43	7.39	0.37	21.29	Disperse	69	68
N13A	4.82±5.29	2.29	2.74	5.27	0.30	27.39	Disperse	63	60
N14A	5.58±3.77	4.88	4.06	6.81	0.48	14.26	Disperse/Small	77	75
Average	**5.64±3.77**	**5.04**	**4.47**	**4.35**	**0.69**	**16.13**	**Disperse (10/14)**	-	-
N1B	9.32±6.33	7.95	7.35	7.64	1.33	27.96	Disperse	-	-
N2B	7.69±5.37	7.76	5.39	9.64	0.36	20.25	Disperse	-	-
N3B	12.24±9.45	9.17	8.31	14.31	0.98	35.58	Disperse/Some ribbons	43	40
N4B	18.72±8.23	16.82	16.75	10.56	3.61	41.10	Disperse/Thick	-	-
N5B	9.33±5.86	9.72	6.80	7.91	0.17	30.29	Disperse	51	49
N6B	21.62±9.57	21.44	19.17	10.51	2.85	68.57	Disperse/Thick	-	-
N7B	7.57±6.73	4.58	4.50	11.32	0.27	28.64	Ribbon/Disperse/Thick	37	32
N8B	20.74±14.66	19.49	17.34	15.81	3.23	120.46	Disperse/Thick	-	-
N9B	9.64±5.25	8.52	8.51	4.93	1.54	37.62	Normal	16	14
N10B	21.97±12.06	20.03	18.78	15.89	3.26	54.17	Disperse/Thick	-	-
N11B	13.82±11.60	12.67	8.45	15.20	0.40	65.44	Ribbon/Disperse	-	-

Code	Average diameter, µm	Median, µm	Geometric Mean, µm	Quartile Range, µm	Min. diameter, µm	Max. diameter, µm	Morphology*	*e*PM$_1$ filtration efficiency, %	*e*PM$_1$ min
N12B	15.29±13.76	14.17	9.90	17.62	0.27	89.19	Disperse/Ribbon	20	14
N13B	4.47±4.68	3.27	2.48	3.63	0.17	19.99	Disperse /Ribbon/Thin	40	34
N14B	10.98±6.68	12.57	7.83	9.23	0.43	30.57	Disperse/Thick	40	38
Average	**14.0±9.07**	**12.69**	**10.94**	**11.78**	**1.52**	**51.61**	**Disperse (9/14)**	-	-
N1C	22.31±8.76	21.33	20.30	8.09	1.19	65.27	Parallel	-	-
N2C	5.93±1.38	5.83	5.74	1.65	1.56	8.96	Suppressed whipping	-	-
N3C	7.77±5.13	6.93	7.55	3.71	1.02	34.35	Disperse/Glued/ Ribbon	39	36
N4C	27.57±10.62	25.80	25.82	8.94	3.93	70.90	Thick/Normal	49	48
N5C	7.57±5.14	6.23	6.43	3.76	1.24	37.46	Normal/Glued	25	22
N6C	19.80±8.17	19.92	17.82	9.50	3.19	43.94	Normal	47	42
N7C	32.98±11.79	32.69	30.96	12.25	5.75	88.16	Ribbon/Normal/ Thick	-	-
N8C	22.12±11.96	19.62	18.25	15.53	1.52	50.59	Normal/Thick	30	29
N9C	8.89±4.77	9.96	7.06	7.94	0.86	18.64	Disperse	-	-
N10C	33.93±14.57	32.84	30.82	15.54	6.75	91.61	Parallel/Ribbon/Thick	45	43
N11C	17.89±8.10	17.84	15.48	7.61	0.53	47.98	Normal	29	28
N12C	22.20±10.79	22.03	18.91	8.37	0.56	80.51	Disperse	37	35
N13C	29.33±13.78	29.20	25.14	18.74	2.19	72.53	Parallel/Thick	22	15
N14C	20.54±7.95	21.36	18.37	9.53	2.37	40.62	Disperse	15	13
Average	**19.92±8.78**	**19.40**	**17.76**	**9.37**	**2.33**	**53.68**	**Normal (4/14)**	-	-
N1D	20.01±16.51	21.82	12.97	22.62	0.30	111.61	Disperse/Parallel	-	-
N2D	14.10±13.32	10.45	10.08	11.07	1.06	107.39	Disperse	-	-
N3D	14.45±11.00	8.93	10.33	17.75	0.54	43.47	Disperse	-	-
N4D	21.82±13.53	17.31	18.48	12.92	3.29	77.61	Parallel/Disperse/Thick	-	-
N5D	31.74±18.66	30.11	26.46	22.49	3.78	100.74	Ribbon/Disperse/Thick	12	11
N6D	22.94±9.77	25.76	19.48	12.88	1.47	42.91	Parallel/Thick	-	-
N7D	19.10±15.40	18.86	11.04	28.76	0.64	57.35	Disperse	-	-
N8D	15.49±12.05	12.01	10.27	15.63	0.34	52.17	Disperse	-	-

Code	Average diameter, µm	Median, µm	Geometric Mean, µm	Quartile Range, µm	Min. diameter, µm	Max. diameter, µm	Morphology*	*e*PM$_1$ filtration efficiency, %	*e*PM$_1$ min
N9D	6.57±8.50	2.99	3.39	7.17	0.23	80.23	Disperse/Thin	-	-
N10D	35.48±25.68	29.64	28.02	28.18	3.97	160.92	Parallel/Thick	-	-
N11D	26.32±21.53	21.16	16.43	33.81	0.71	80.21	Disperse/Thick	-	-
N12D	20.62±18.39	13.91	11.30	35.23	1.19	60.84	Disperse/Ribbon	-	-
N13D	24.08±21.76	18.89	13.49	37.06	0.25	117.29	Ribbon/Disperse/Thick	-	-
N14D	25.21±15.74	27.20	19.31	26.95	2.71	76.45	Parallel/Thick	-	-
Average	**21±15.85**	**18.50**	**15.07**	**22.32**	**1.46**	**83.51**	**Disperse (8/14)**	**-**	**-**
N6E	19.88±9.46	20.63	16.72	12.69	1.68	45.35	Parallel/Disperse	-	-
N9E	12.70±10.92	8.76	8.00	17.87	0.42	41.74	Disperse	-	-
N16E	9.36±5.79	9.91	6.97	9.74	0.69	26.05	Ribbon/Disperse/Small	35	30
N17E	16.04±10.74	15.84	11.74	16.98	0.67	58.91	Disperse	-	-
N18E	47.38±19.96	46.90	42.08	24.87	3.58	98.58	Parallel/Ribbon/Thick	15	12
N19E	35.99±19.36	32.30	31.79	22.02	7.84	116.97	Ribbon/Thick	20	17
N20E	38.96±19.51	37.46	34.64	22.87	9.74	113.84	Parallel/Ribbon/Thick	-	-
N21E	18.93±13.82	18.53	13.47	16.53	0.40	80.63	Disperse	-	-
N22E	7.08±6.08	4.62	4.72	9.62	0.69	24.97	Disperse	45	39
N23E	45.27±19.38	44.81	41.37	22.06	12.11	121.11	Parallel/Thick	25	23
N24E	31.67±23.26	31.25	25.86	16.66	2.86	204.77	Ribbon/Thick	-	-
N25E	27.71±16.38	23.67	22.83	21.17	3.75	79.30	Parallel/Thick	-	-
Average	**25.91±14.56**	**24.56**	**21.68**	**17.76**	**3.70**	**84.35**	**Parallel (5/12)**	**-**	**-**

* In case several morphologies were determined, the first one was dominant

Appendix 3. LIST OF SCIENTIFIC PUBLICATIONS

Publications injournals included into the list of *Web of Science* database

1. Buivydiene, Dalia; Dabasinskaite, Lauryna; Krugly, Edvinas; Kliucininkas, Linas. Formation of PA12 fibres via melt electrospinning process: parameter analysis and optimisation // Journal of polymer engineering. Berlin: Walter de Gruyter. ISSN 0334-6447. eISSN 2191-0340. 2020, vol. 40, iss. 1, p. 49-56. DOI: 10.1515/polyeng-2019-0190. [IF: 1.072; AIF: 3.469 (2018)];
2. Buivydiene, Dalia; Krugly, Edvinas; Ciuzas, Darius; Tichonovas, Martynas; Kliucininkas, Linas; Martuzevicius, Dainius. Formation and characterisation of air filter material printed by melt electrospinning // Journal of aerosol science. London: Elsevier. ISSN 0021-8502. eISSN 1879-1964. 2019, vol. 131, p. 48-63. DOI: 10.1016/j.jaerosci.2019.03.003. [IF: 2.240; AIF: 3.576 (2018)];
3. Buivydiene, Dalia; Todea, Ana-Maria; Asbach, Christof; Krugly, Edvinas; Martuzevicius, Dainius; Kliucininkas, Linas. A novel approach to multi-layered air filter formation: melt/solution electrospinning for micro/nano fibrous material – Submitted manuscript.

Conference Materials

Poster presentations

1. Buivydiene, D.; Krugly, E.; Todea, A.; Asbach, C.; Kliucininkas, L.; Martuzevicius, D. Novel air filtration materials via combined melt-solution electrospinning // ISESISIAQ 2019, Kaunas, Lithuania: joint meeting of the International Society of Exposure Science and the International Society of Indoor Air Quality and Climate, August 18-22, 2019: abstracts. [S.l.] : [s.n.]. 2019, SU-PO-72, TU-PO-10, p. 48. [FOR: T 004]
2. Martuzevicius, Dainius; Sidaraviciute, Ruta; Ciuzas, Darius; Buivydiene, Dalia; Krugly, Edvinas. The performance of a novel nanofibrous TiO 2 photocatalyst for the decomposition of toluene in air // Indoor air 2018: 15th conference of the International Society of Indoor Air Quality & Climate, July 22-27, 2018, Philadelphia, PA, USA. [S.l.] : [s.n.]. 2018, art. no. 462, p. 1-2. [FOR: T 004]
3. Buivydienė, D.; Krugly, E.; Kliučininkas, L.; Martuzevičius, D. Additive printing of fibre mats based on melt electrospinning from polymer filaments // Filtech: The filtration event, March 13–15, 2018, Cologne, Germany. [S.l.] : [s.n.], 2018, F06-02. eISBN 9783941655157. p. 1-7. [FOR: T 004]
4. Buivydienė, Dalia; Krugly, Edvinas; Kliučininkas, Linas; Martuzevičius, Dainius. Analysis of polymer fiber formation by melt electrospinning // Chemistry and chemical technology 2017: proceedings of the international conference, April 28, 2017, Kaunas. Kaunas: Kauno technologijos universitetas. ISSN 2538- 7359. 2017, p. 63. [FOR: N 003]

5. Buivydienė, Dalia; Krugly, Edvinas; Kliučininkas, Linas; Martuzevičius, Dainius. Factors affecting solvent-free electrospinning process for nanofibre production // Baltic polymer symposium 2016: Klaipeda, September 21-24, 2016 : programme and abstracts / Kaunas University of Technology, Vilnius University, Klaipeda University. Kaunas: Kaunas University of Technology, 2016. ISBN 9786090212356. p. 86. [FOR: T 005]
6. Buivydienė, Dalia; Kliučininkas, Linas. Review: biodegradable polymers and melt electrospinning method for nanofiber fabrication // Chemistry and chemical technology: international conference of the Lithuanian Society of Chemistry: Lithuanian Academy of Science, Vilnius, Lithuania, April 28-29, 2016: book of abstracts / Fizinių ir technologijos mokslų centras, Vilniaus universitetas, Lietuvos mokslų akademija, Kauno technologijos universitetas. [S.l.] : [s.n.], 2016. ISBN 9786099551135. p. 231. [FOR: T 005]

OTHER PUBLICATIONS

1. Sidaraviciute, Ruta; Buivydiene, Dalia; Krugly, Edvinas; Valatka, Eugenijus; Martuzevicius, Dainius. A composite microfibre-supported short-nanofibre photocatalyst for environmental pollutant decomposition // Journal of photochemistry and photobiology A: Chemistry. Amsterdam: Elsevier. ISSN 1010-6030. 2019, vol. 368, p. 7-14. DOI: 10.1016/j.jphotochem.2018.09.017.
2. [S1; NL] Jankūnaitė, Dalia; Tichonovas, Martynas; Buivydienė, Dalia; Radžiūnienė, Inga; Račys, Viktoras; Krugly, Edvinas. Removal of diclofenac, ketoprofen, and carbamazepine from simulated drinking water by advanced oxidation in a model reactor // Water, Air and Soil Pollution. Dordrecht : Springer. ISSN 0049-6979. eISSN 1573-2932. 2017, Vol. 228, iss. 9, article 353, p. 1-15. DOI: 10.1007/s11270-017-3517-z.
3. Matulevičius, Jonas; Kliučininkas, Linas; Prasauskas, Tadas; Buivydienė, Dalia; Martuzevičius, Dainius. The comparative study of aerosol filtration by electrospun polyamide, polyvinyl acetate, polyacrylonitrile and cellulose acetate nanofiber media // Journal of aerosol science. Oxford: Elsevier. ISSN 0021-8502. eISSN 1879-1964. 2016, vol. 92, p. 27-37. DOI: 10.1016/j.jaerosci.2015.10.006. [Science Citation Index Expanded (Web of Science); Current Contents / Engineering, Computing & Technology; Current Contents / Physical, Chemical & Earth Sciences]

SL344. 2020-05-12, 11,5 leidyb. apsk. l. Tiražas 14 egz.
Išleido Kauno technologijos universitetas, K. Donelaičio g. 73, 44249 Kaunas
Spausdino leidyklos „Technologija“ spaustuvė, Studentų g. 54, 51424 Kaunas